

## **Copyright Warning & Restrictions**

The copyright law of the United States (Title 17, United States Code) governs the making of photocopies or other reproductions of copyrighted material.

Under certain conditions specified in the law, libraries and archives are authorized to furnish a photocopy or other reproduction. One of these specified conditions is that the photocopy or reproduction is not to be “used for any purpose other than private study, scholarship, or research.” If a user makes a request for, or later uses, a photocopy or reproduction for purposes in excess of “fair use” that user may be liable for copyright infringement,

This institution reserves the right to refuse to accept a copying order if, in its judgment, fulfillment of the order would involve violation of copyright law.

**Please Note: The author retains the copyright while the New Jersey Institute of Technology reserves the right to distribute this thesis or dissertation**

Printing note: If you do not wish to print this page, then select “Pages from: first page # to: last page #” on the print dialog screen

The Van Houten library has removed some of the personal information and all signatures from the approval page and biographical sketches of theses and dissertations in order to protect the identity of NJIT graduates and faculty.

## **INFORMATION TO USERS**

**This manuscript has been reproduced from the microfilm master. UMI films the text directly from the original or copy submitted. Thus, some thesis and dissertation copies are in typewriter face, while others may be from any type of computer printer.**

**The quality of this reproduction is dependent upon the quality of the copy submitted. Broken or indistinct print, colored or poor quality illustrations and photographs, print bleedthrough, substandard margins, and improper alignment can adversely affect reproduction.**

**In the unlikely event that the author did not send UMI a complete manuscript and there are missing pages, these will be noted. Also, if unauthorized copyright material had to be removed, a note will indicate the deletion.**

**Oversize materials (e.g., maps, drawings, charts) are reproduced by sectioning the original, beginning at the upper left-hand corner and continuing from left to right in equal sections with small overlaps. Each original is also photographed in one exposure and is included in reduced form at the back of the book.**

**Photographs included in the original manuscript have been reproduced xerographically in this copy. Higher quality 6" x 9" black and white photographic prints are available for any photographs or illustrations appearing in this copy for an additional charge. Contact UMI directly to order.**

# **U·M·I**

University Microfilms International  
A Bell & Howell Information Company  
300 North Zeeb Road, Ann Arbor, MI 48106-1346 USA  
313/761-4700 800/521-0600

**Order Number 9120007**

**On local stresses and spring constants of a sphere-nozzle  
connection**

**Lyow, Ban-Li, Ph.D.**

**New Jersey Institute of Technology, 1991**

**U·M·I**  
300 N. Zeeb Rd.  
Ann Arbor, MI 48106

**NOTE TO USERS**

**THE ORIGINAL DOCUMENT RECEIVED BY U.M.I. CONTAINED PAGES  
WITH SLANTED AND POOR PRINT. PAGES WERE FILMED AS RECEIVED.**

**THIS REPRODUCTION IS THE BEST AVAILABLE COPY.**

On Local Stresses and Spring Constants of  
a Sphere-~~Nozzle~~ Connection

by  
Ban-Li Lyow

Dissertation submitted to the Faculty of Graduate School  
of New Jersey Institute of Technology in partial  
fulfillment of the requirements for the  
Degree of Doctor of Philosophy

1991

APPROVAL SHEET

Title of Dissertation : On Local Stresses and Spring Constants of  
a Sphere-Nozzle Connection

Name of Candidate : Ban-Li Lyow  
Doctor of Philosophy, 1991

Dissertation and  
Abstract Approved : \_\_\_\_\_ Date \_\_\_\_\_  
Benedict C. Sun  
Associate Professor, Department  
of Engineering Technology

Signatures of other members  
of the dissertation committee : \_\_\_\_\_ Date \_\_\_\_\_  


\_\_\_\_\_ Date \_\_\_\_\_  


\_\_\_\_\_ Date \_\_\_\_\_  


\_\_\_\_\_ Date \_\_\_\_\_  


## VITA

**Name** : Ban-Li Lyow

**Degree and Date to be Conferred** : Doctor of Philosophy, 1991

<b>Education</b>	<b>Dates</b>	<b>Degree</b>	<b>Date of Degree</b>
National Taipei Institute of Technology, Taiwan	1978-1981	BSME	June, 1981
New Jersey Institute of Technology, Newark, N.J.	1985-1987	MSME	May, 1987
New Jersey Institute of Technology, Newark, N.J.	1987-1991	Ph.D	January, 1991

Major: Mechanical Engineering

Presentation:

1. Lyow, B. L., Sun, B. C. and Koplik, B., "Finite Element Method to Determine the Localized Stresses and Spring Constant of a Spherical Shell with a Nozzle Attachment under Radial Loading", in Proceedings of the 1990 ASME Pressure Vessel and Piping Conference, Nashville, Tennessee, PVP-Vol. 194, pp. 1-8.
2. Lyow, B. L., Sun, B. C. and Koplik, B., (to be published), "On Local Stresses and Spring Constants of Sphere-Nozzle Connection due to Overturning Moment, Torsional Moment and Horizontal Shear Force by Finite Element Approach", ASME Pressure Vessel and Piping Conference, San Diego, California, 1991.
3. Sun, B. C., Sun, H. C., Lyow B. C., (to be published), "Computation of Principal Stresses and Stress Intensity of Nozzle on Cylindrical and Spherical Pressure Vessels", ASME Pressure Vessel and Piping Conference, San Diego, California, 1991.

## ABSTRACT

**Title of Dissertation** : On Local Stresses and Spring Constants  
of a Sphere–Nozzle Connection

**Ban–Li Lyow** : Doctor of Philosophy, 1991

**Dissertation directed by** : Dr. Benedict C. Sun  
Associate Professor, Department  
of Engineering Technology

This dissertation studies the local stresses and spring constants of a spherical shell with a nozzle attachment when it is under various loadings, namely radial force, overturning moment, horizontal shear force, and torsional moment. Because of the mathematical difficulty in modeling the nozzle-sphere configuration, particularly with nozzle opening, the finite element method (*ANSYS* package) is utilized in this study. The model used in this study is a quadrilateral thin shell element model when the  $\gamma_s$  (spherical radius/thickness) value is larger than 10. Otherwise the isoparametric solid element is used. The resulting stresses are basically biaxial state of stresses. It is observed that the local membrane and bending stresses are produced due to the radial force and the overturning moment as well as the shear force, and the local shear stresses are produced by both the torsional moment and the shear force. These individual stresses are presented as stress factors, which are functions of the dimensionless parameters,  $\beta$  (radius of nozzle/radius of sphere) and  $\gamma_s$ . They are reported in graphical plots.

The spring constants considered due to various loadings ( $K_y$  for radial force,  $K_{\phi_M}$  for overturnment moment,  $K_{\theta_T}$  for torsional moment,  $K_V$  for shear force) are also presented in this dissertation. Again, these spring constants are presented in normalized forms which are also functions of  $\beta$  and  $\gamma_s$ . Throughout the dissertation,

the  $\beta$  values considered are from 0.1 to 0.5 while the  $\gamma_s$  values are from 7 to 100. These values cover the range of the practical applications in pressure vessel design. In this work, the finite element method employed 22 elements along the juncture for the thin shell model, and 9 elements along the juncture with 4 elements across the thickness for the isoparametric model to ensure that the elements are small enough to provide convergence of the results. Stresses obtained from this study are in good agreement with the data extracted from Wichman's paper (W.R.C. bulletin 107,1968) and experimental results from other literature sources. The spring constants are in good agreement with data extracted from Batra & Sun's work and other theoretical results.

## ACKNOWLEDGEMENT

I wish to express my sincere gratitude and thanks to my dissertation adviser, Dr. Benedict C. Sun, for his valuable guidance and help throughout the period of this study. I would like to thank the members of the dissertation committee, Dr. Bernard Koplik, Dr. Harry Herman, Dr. Rong-Yaw Chen and Professor H. Kountouras for all the encouragement they have given to me.

I wish to express my gratitude to my parents, and brothers and sisters for the encouragement they have given me through the period. A special appreciation is extended to my wife, Eleanor, for all her patience and understanding during this study.

# Contents

<b>Nomenclature</b>	<b>viii</b>
<b>1 Introduction</b>	<b>1</b>
<b>2 Literature Survey</b>	<b>5</b>
<b>3 Theory of Loading Pattern</b>	<b>9</b>
3.1 Radial Load . . . . .	9
3.1.1 Derivation of Deflection . . . . .	9
3.1.2 Derivation of Membrane and Bending Forces . . . . .	15
3.2 Overturning Moment . . . . .	16
3.2.1 Derivation of Deflection . . . . .	16
3.2.2 Derivation of Membrane and Bending Forces . . . . .	24
3.3 Torsional Moment . . . . .	25
<b>4 Finite Element Method</b>	<b>31</b>
4.1 Finite Element Model . . . . .	31
4.1.1 Quadrilateral Shell Element-for Thin Shell . . . . .	31
4.1.2 Isoparametric Solid Element-for Thicker Shell . . . . .	33
4.2 Assumptions . . . . .	34
4.3 Geometrical Parameters . . . . .	34
4.4 Computational Model . . . . .	36

4.5	Boundary Conditions of the Model . . . . .	46
4.6	Loading Pattern . . . . .	50
4.6.1	Radial Force . . . . .	50
4.6.2	Overturning Moment . . . . .	52
4.6.3	Torsional Moment . . . . .	54
4.6.4	Horizontal Shear Force . . . . .	56
<b>5</b>	<b>Numerical Analysis</b>	<b>58</b>
5.1	Radial Force . . . . .	58
5.1.1	Local Stress . . . . .	58
5.1.2	Comparison of Normal Stresses due to Radial Load . . . . .	59
5.1.3	Radial Spring Constant . . . . .	60
5.1.4	Comparison of Radial Spring Constant . . . . .	61
5.2	Overturning Moment . . . . .	64
5.2.1	Local Stress . . . . .	64
5.2.2	Comparison of Normal Stresses due to Overturning Moment . . . . .	66
5.2.3	Rotational Spring Constant due to Overturning Moment . . . . .	69
5.2.4	Comparison of Rotational Spring Constant due to Overturning Moment . . . . .	71
5.3	Torsional Moment . . . . .	72
5.3.1	Local Stress . . . . .	72
5.3.2	Comparison of the Shear Stress . . . . .	72
5.3.3	Torsional Spring Constant . . . . .	74
5.3.4	Comparison of the Torsional Spring Constant . . . . .	74
5.4	Horizontal Shear Force . . . . .	77
5.4.1	Local Stress . . . . .	77

5.4.2	Comparison of Stresses . . . . .	79
5.4.3	Shear Spring Constant . . . . .	81
<b>6</b>	<b>Conclusion</b>	<b>82</b>
	<b>Appendix</b>	<b>103</b>
Appendix A	ANSYS Program . . . . .	103
Appendix A.1	Quadrilateral Shell Element Model due to Radial Force	103
Appendix A.2	Quadrilateral Shell Element Model due to Overturning Moment . . . . .	107
Appendix A.3	Quadrilateral Shell Element Model due to Torsional Moment . . . . .	113
Appendix A.4	Quadrilateral Shell Element Model due to Horizontal Shear Force . . . . .	119
Appendix A.5	Isoparametric Solid Element Model due to Radial Force	124
Appendix A.6	Isoparametric Solid Element Model due to Overturn- ing Moment . . . . .	132
Appendix A.7	Isoparametric Solid Element Model due to Torsional Moment . . . . .	141
Appendix A.8	Isoparametric Solid Element Model due to Horizontal Shear Force . . . . .	149
Appendix B	Kelvin Functions and their Derivatives . . . . .	157
Appendix C	Superposition of all Loads . . . . .	158

# List of Tables

4.1	Data Convergence of Quadrilateral Shell Element Model . . . . .	38
4.2	Data Convergence of Isoparametric Solid Element Model . . . . .	43
5.1	Comparison of Normal Stresses (Meridional and Circumferential) at the Outside Surface due to Radial Load with Bijlaard's work . . . .	62
5.2	Comparison of Normal Stresses (Meridional and Circumferential) at the Outside Surface due to Radial Load with Rily's Experimental Work	62
5.3	Comparison of $K_y$ with Batra's work (based on the Theoretical So- lution from Bijlaard) . . . . .	63
5.4	Comparison of Normal Stresses (Meridional and Circumferential) at the outside surface due to Overturning Moment with Bijlaard's The- oretical Solution . . . . .	67
5.5	Comparison of Normal Stresses (Meridional and Circumferential) at the Outside Surface due to Overturning Moment with Rily's Exper- imental Work . . . . .	67
5.6	Comparison of $K_{\phi_M}$ due to the Overturning Moment with Batra's Work (based on Bijlaard's Theoretical Solution) . . . . .	71
5.7	Comparison of Torsional Spring Constant with Pipe-Nozzle Connec- tion Solution from Chiou and Sun (when the nozzle is very small) .	75
5.8	Comparison of Torsional Spring Constant with Theoretical Solution	76

# List of Figures

1.1	Nozzle-Sphere Model Applied by Various Loads . . . . .	4
3.1	Position of Shell before and after Application of Radial Force . . . .	10
3.2	Shear Forces and Moments at the Juncture of Spherical Shell and Radial Nozzle due to Radial Force . . . . .	12
3.3	Overturning Moment Applied on the Nozzle-Sphere Model . . . . .	18
3.4	Deflections of Nozzle-Sphere Model due to a Bending Moment . . . .	19
3.5	Normal and Shear Forces Acting on the Spherical Shell at the Nozzle- Spherical Shell Juncture due to Overturning Moment . . . . .	21
3.6	Shear Stresses and Angular Displacement due to Torsional Moment .	27
4.1	Quadrilateral Shell Element . . . . .	32
4.2	Isoparametric Solid Element . . . . .	33
4.3	Shell Model . . . . .	35
4.4	Areas and Keypoints of Quadrilateral Shell Element Model . . . . .	37
4.5	Data Convergence curve of Quadrilateral Shell Element Model (for Meridional Stress of the Outer Surface) $\gamma_s = 20, \beta = 0.2, T = 0.4$ $in, P = 1000 lb$ . . . . .	39
4.6	Element Plot of Quadrilateral Shell Element Model . . . . .	40
4.7	Volumes and Keypoints of Isoparametric Solid Element Model . . .	42

4.8	Data Convergence Curve of Isoparametric Solid Element (for Meridional Stress of the Outer Surface) $\gamma_s = 7, \beta = 0.2, T = 0.4 \text{ inch}, P = 1000 \text{ lb}$ . . . . .	44
4.9	Element Plot of Isoparametric Solid Element Model . . . . .	45
4.10	Radial Force Pattern(quadrilateral shell element model) . . . . .	46
4.11	Overturning Moment Pattern for $M_Z$ (quadrilateral shell element model) . . . . .	47
4.12	Torsional Moment Pattern(quadrilateral shell element model) . . . . .	48
4.13	Horizontal Shear Force Patern for $V_Z$ (quadrilateral shell element model) . . . . .	49
4.14	Radial Force Pattern (isoparametr solid element model) . . . . .	51
4.15	Overturning Moment Pattern for $M_Z$ (isoparametric solid element model) . . . . .	53
4.16	Torsional Moment Pattern(isoparametric solid element model) . . . . .	55
4.17	Horizontal Shear Force Pattern(isoparametric solid element model) . . . . .	57
5.1	Superposition of Various External Loads Applied on the Model . . . . .	65
5.2	Comparison of Normal Stresses due to Overturning Moment between Finite Element Method and Experimental Method ( $\gamma_s=120, \text{beta}=0.5, M=18000 \text{ in} - \text{lb}$ ) . . . . .	68
5.3	Angular Displacement by Overturning Moment . . . . .	70
5.4	Comparison of Shear Stress due to Torsional Moment with Theoretical Solution . . . . .	73
5.5	Comparison of Shear Stress due to Horizontal Shear Force with the Theoretical Solution . . . . .	80
6.1	Circumferential Bending Stress Factor due to Radial Force $P$ . . . . .	85
6.2	Meridional Bending Stress Factor due to Radial Force $P$ . . . . .	86

6.3	Circumferential Membrane Stress Factor due to Radial Force $P$ . . . .	87
6.4	Meridional Membrane Stress Factor due to Radial Force $P$ . . . . .	88
6.5	Circumferential Bending Stress Factor due to Overturning Moment $M_X$ or $M_Z$ . . . . .	89
6.6	Meridional Bending Stress Factor due to Overturning Moment $M_X$ or $M_Z$ . . . . .	90
6.7	Circumferential Membrane Stress Factor due to Overturning Moment $M_X$ or $M_Z$ . . . . .	91
6.8	Meridional Membrane Stress Factor due to Overturning Moment $M_X$ or $M_Z$ . . . . .	92
6.9	Shear Stress Factor due to Torsional Moment $M_T$ . . . . .	93
6.10	Circumferential Bending Stress Factor due to Horizontal Shear Force $V_X$ or $V_Z$ . . . . .	94
6.11	Meridional Bending Stress Factor due to Horizontal Shear Force $V_X$ or $V_Z$ . . . . .	95
6.12	Circumferential Membrane Stress Factor due to Horizontal Shear Force $V_X$ or $V_Z$ . . . . .	96
6.13	Meridional Membrane Stress Factor due to Horizontal Shear Force $V_X$ or $V_Z$ . . . . .	97
6.14	Shear Stress Factor due to Horizontal Shear Force $V_X$ or $V_Z$ . . . . .	98
6.15	Normalized Radial Spring Constant due to Radial Force $P$ . . . . .	99
6.16	Normalized Rotational Spring Constsnt due to Overturning Moment $M_X$ or $M_Z$ . . . . .	100
6.17	Normalized Torsional Spring Constant due to Torsional Moment $M_T$	101
6.18	Normalized Shear Spring Constant due to Horizontal Shear Force $V_X$ or $V_Z$ . . . . .	102

# Nomenclature

$D = Et^3/[12(1 - \mu^2)] =$  Flexural Rigidity of spherical shell, *in-lb*

$E =$  modulus of elasticity, *psi*

$F =$  stress function for radial force or overturning moment

$K_y =$  spring constant by radial force in the  $y$  direction, *lb/in*

$K_{\phi_M} =$  rotational spring constant by overturning moment, *in-lb/rad*

$K_{\theta_T} =$  torsional spring constant by torsional moment, *in-lb/rad*

$K_V =$  shear spring constant by horizontal shear force, *lb/in*

$K_{c,m} =$  circumferential membrane stress coefficient

*psi/lb* for external force, *psi/in-lb* for external moment

$K_{c,b} =$  circumferential bending stress coefficient

*psi/lb* for external force, *psi/in-lb* for external moment

$K_{m,m} =$  meridional membrane stress coefficient

*psi/lb* for external force, *psi/in-lb* for external moment

$K_{m,b} =$  meridional bending stress coefficient

*psi/lb* for external force, *psi/in-lb* for external moment

$K_{c_o} =$  circumferential stress coefficient at the outside surface

*psi/lb* for external force, *psi/in-lb* for external moment

$K_{c_i} =$  circumferential stress coefficient at the inside surface

*psi/lb* for external force, *psi/in-lb* for external moment

$K_{m_o} =$  meridional stress coefficient at the outside surface

*psi/lb* for external force, *psi/in-lb* for external moment

$K_{mi}$  = meridional stress coefficient at the inside surface

*psi/lb* for external force, *psi/in-lb* for external moment

$l$  =  $[R^2t^2/(12(1 - \mu^2))]^{1/4}$ , *in*

$M_B$  = overturning moment for theoretical method, *in-lb*

$M_X$  = overturning moment, *in-lb*

$M_Z$  = overturning moment, *in-lb*

$M_T$  = torsional moment, *in-lb*

$M_x$  = Radial moment acting per unit width upon a normal section of the spherical shell, *in-lb/in*

$M_y$  = Tangential moment acting per unit width upon a meridional section of the spherical shell, *in-lb/in*

$M_{xy}$  = Twisting moment in cylindrical shell or spherical shell, *in-lb/in*

$N_x$  = Radial membrane force, acting per unit width upon a normal section of the spherical shell, *lb/in*

$N_y$  = Tangential membrane force, acting per unit width upon a meridional section of the spherical shell, *lb/in*

$P$  = total radial force, *lb*

$p_i$  = internal pressure, *psi*

$Q_x$  = Transverse shear force in cross section of the cylindrical shell (nozzle),  
*lb/in*

$Q_{xv}$  = Equivalent transverse shear force for the cylindrical shell in section upon which  $Q_x$  acts, *lb/in*

$R_m$  = mean radius of sphere, *in*

$r_m$  = mean radius of nozzle, *in*

$s$  =  $\frac{r}{l} = 1.81784(\frac{r}{R_m})(\frac{R_m}{T})^{1/2}$

- $T$  = thickness of sphere, *in*  
 $t$  = thickness of nozzle, *in*  
 $T_x$  = Axial membrane force in the cylindrical shell, *lb/in*  
 $T_y$  = Tangential membrane force in the cylindrical shell, *lb/in*  
 $u$  =  $\frac{r_m}{t} = 1.81784(\frac{r_m}{R_m})(\frac{R_m}{T})^{1/2}$   
 $v$  = radial deflection of nozzle under radial force, *in*  
 $V_x$  = horizontal shear force in *x* direction, *lb*  
 $V_z$  = horizontal shear force in *z* direction, *lb*  
 $w$  = radial deflection of spherical shell under radial force, *in*  
 $\phi$  = stress function for torsional moment  
 $\phi_M$  = angular displacement by overturning moment, *rad*  
 $\gamma_n$  =  $\frac{r_m}{t}$  (for nozzle)  
 $\gamma_s$  =  $\frac{R_m}{T}$  (for sphere)  
 $\mu$  = Poisson's ratio  
 $\rho$  =  $\frac{t}{T}$   
 $\sigma_{co}$  = circumferential stress at the outside surface, *psi*  
 $\sigma_{ci}$  = circumferential stress at the inside surface, *psi*  
 $\sigma_{mo}$  = meridional stress at the outside surface, *psi*  
 $\sigma_{mi}$  = meridional stress at the inside surface, *psi*  
 $\sigma_c$  = circumferential stress, *psi*  
 $\sigma_m$  = meridional stress, *psi*  
 $\theta_T$  = angular displacement by torsional moment, *rad*

# Chapter 1

## Introduction

It is known that there exists highly localized stresses at the juncture of nozzles in pressure vessels under external loadings. In the last several decades, theoretical approaches to find the local stresses around the nozzle-sphere connection have resulted in several approximate methods. It is known that classical mathematical solutions have serious limitations due to the unusual geometries and boundary conditions present in practical cases. In the past, various numerical procedures, such as the shallow shell theorem, have been formulated to deal with special geometric shapes, but their applicability is highly limited. Although experimental approaches such as strain gauge testing and photoelastic methods have provided some practical indication of the stress distribution at the juncture of the nozzle-sphere model, these methods are both time consuming and costly. In addition, the results from experimental method are affected by set-up technique and system calibration. The local stresses and displacements due to the external loadings can best be evaluated with the help of sophisticated computer programs such as *ANSYS*, [1], [2]. Such programs use the finite element approach to describe the real geometries and loading conditions.

In this dissertation, the finite element method simulates the real nozzle-sphere

geometry at the juncture; Four different loading conditions are studied: radial load  $P$ , overturning moment  $M_X$  or  $M_Z$ , horizontal shear force  $V_X$  or  $V_Z$ , and torsional moment  $M_T$ . The radial load and overturning moment are applied on the top of the nozzle, and the horizontal shear force and torsional moment are applied at the juncture, as shown in the Figure 1.1. The radial load  $P$  is applied uniformly downward through the thickness of the nozzle onto the juncture. The overturning moment  $M_X$  and  $M_Z$  are simulated by a cosine functional distribution of nodal force. The nodal force for  $M_X$  is antisymmetrical with respect to the  $x$  axis, while, the nodal force for  $M_Z$  is antisymmetric with respect to the  $z$  axis. In the  $V_X$  and  $V_Z$  model, nodal forces are uniformly distributed in the  $x$  and  $z$  directions respectively. In  $M_T$  model, the nodal forces, which are tangent to the juncture of the model, are applied uniformly.

This dissertation studies the local stresses and the spring constants at the nozzle-sphere connection. The localized stresses are an important component in the A.S.M.E. Pressure Vessel and Boiler Code Class I pressure vessel and piping equations. The spring constants are very important in piping system analysis. Since the thin shell model is considered in this study, the resulting stresses due to various loadings are basically in a biaxial state of stress. That is, the radial loading, the overturning moment and shear force yield membrane and bending stresses in both the circumferential and meridional directions, and shear force and torsional moment yield the shear stresses. For each external load, the membrane and bending stress factors, in both the circumferential and meridional directions, are plotted separately in terms of  $\gamma$ , and  $\beta$ . The spring constants due to various loading ( $K_y$  for radial loading,  $K_{\phi_M}$  for overturnment moment,  $K_{\theta_T}$  for torsional moment,  $K_V$  for shear force) are also presented in normalized forms in this study. The radial spring constant is defined as the radial load, in pounds, which would yield one

inch of deflection in the  $y$  direction. The shear spring constant is defined as the shear force, in pounds, which would yield one inch displacement in the  $x$  (or  $z$ ) direction. The rotational spring constants are defined as the moment, in  $in-lb$ , which would yield one radian of angular rotation with respect to its axis. These individual stress factors and normalized spring constants are presented as a function of the dimensionless parameters,  $\beta$  (nozzle radius/sphere radius) and  $\gamma_s$  (sphere radius/sphere thickness), and are presented in graphical plots. Since  $\gamma_s$  of 10 is often considered as a lower bound for the applicability of thin-shell theory [3], the quadrilateral thin shell element model will be used when  $\gamma_s$  is larger than 10. If the  $\gamma_s$  is less than 10, the 3-D isoparametric solid element model will be applied. In this dissertation,  $\beta$  ranges from 0.1 to 0.5 and  $\gamma_s$  ranges from 7 to 100. These ranges cover the practical applications in pressure vessel design. Since the purpose of this dissertation is to study the spring constants and the local stresses in the shell region, it is assumed that the nozzle has the same thickness as the shell and that the nozzle becomes relatively rigid and hence the resulting nozzle strain is negligible [4], [5].

The literature survey is given in the Chapter 2. Chapter 3 discusses the theoretical background of the model utilized in this study. Chapter 4 introduces geometrical parameters, boundary conditions, and loading patterns. Chapter 5 discusses the details of the numerical analysis used in the model for radial loading, overturning moment, horizontal shear force, and torsional moment respectively. In this Chapter, the local stress factors and normalized spring constants are derived. The conclusions are presented in the Chapter 6. Appendix A gives the ANSYS program and Appendix B gives the mathematical equation for the Kelvin functions and their derivatives. Appendix C tabulates and computes the stress factors and determines the resulting stresses.

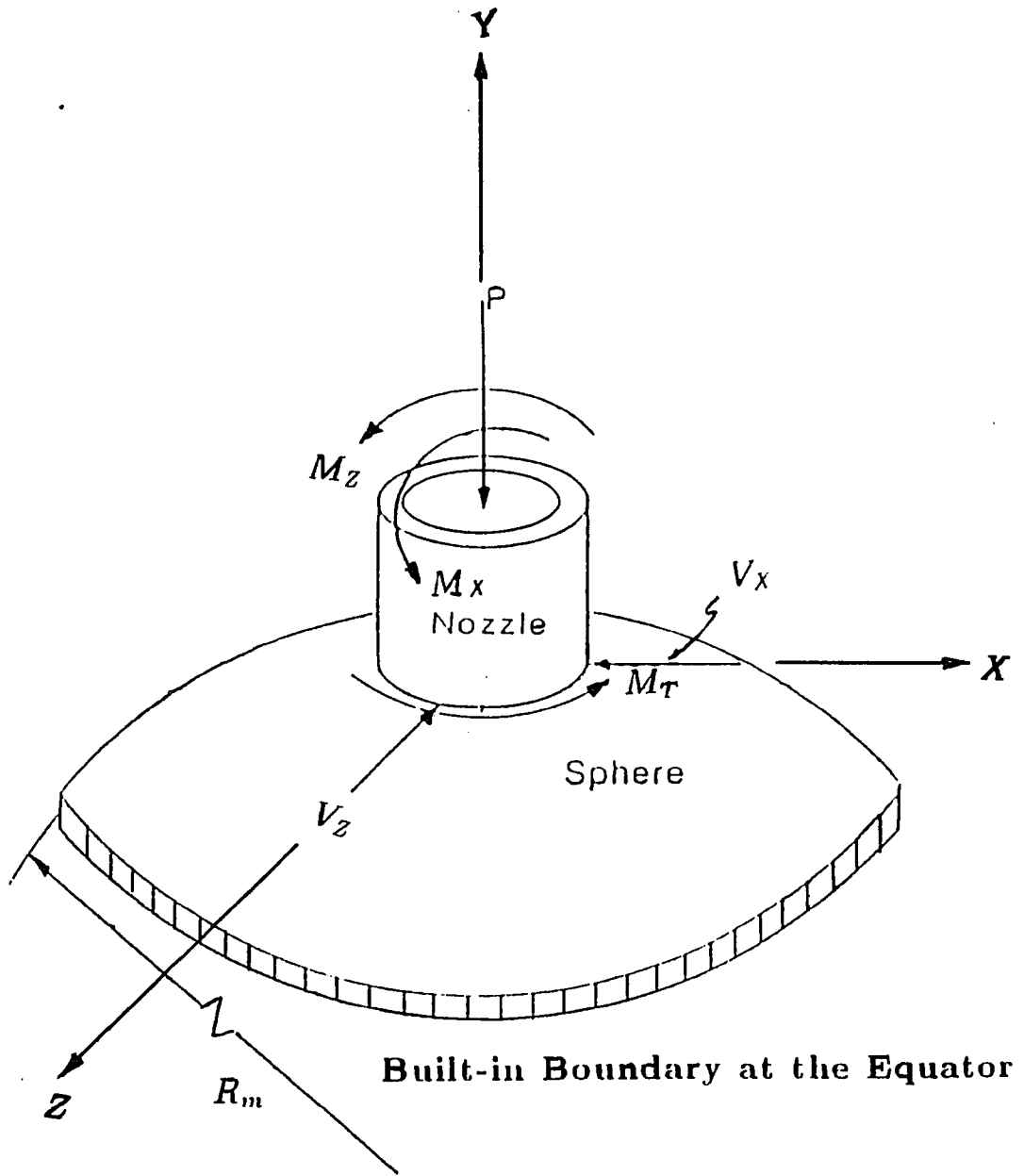


Figure 1.1: Nozzle-Sphere Model Applied by Various Loads

# Chapter 2

## Literature Survey

Bijlaard was among the first to use Bessel functions to solve the governing differential equations of spherical pressure vessels under external loading [6], [7], [8], [9], [10], and [11]. He [7] [8] was the first to apply a radial load and external moments on top of the rigid cylindrical insert and determine the localized stresses and displacements at the structure. His analysis used the shallow shell theory. The influence of the internal pressure was also considered.

He extended his study of stresses due to local loads on spherical vessels by considering the more realistic case of a spherical vessel with an inserted tube subjected to a radial load [9].

Bijlaard also investigated the case of an external moment acting on an inserted pipe [10]. The continuity conditions between the vessel and the pipe were established in order to determine the constants in the general solutions for the deflections and the stress functions in the spherical vessel.

Bijlaard later suggested a simple design method [11], from which one could compute the stresses in a spherical vessel from radial loads and external moments transferred by a pipe. The method takes into account the pipe radius and thickness, as well as the effect of a reinforcing pad on the vessel.

Penny & Leckie [12] [13] studied the effect of a bending moment and shear

force on a nozzle-sphere connection. They utilized the asymptotic solutions developed by Havers to derive the stresses. Their model had no opening, and the external force and moment were applied on the top of the sphere.

Later, Batra and Sun [14][15] utilized the deflection solution from Bijlaard to obtain the radial spring constant and rotational spring constant in terms of the geometric parameters. However, these previous studies dealt with a regional loading on a closed sphere to simulate the nozzle-sphere geometry. Due to the mathematical difficulty, there was no analytical solution presented when the nozzle opening was taken into account. These studies did not solve the real problem of the nozzle-sphere connection. Furthermore, their solutions have convergence difficulties, especially when the shell is relatively thick and the nozzle radius is relatively large.

Parakash and Rao [16] studied the problem of a circular elastic inclusion in a thin pressurized spherical shell. Using Reisser's differential equations, which governed the behavior of a thin shallow spherical shell, the solution regions were obtained in terms of Bessel and Hankel functions. Results were presented in nondimensional form which greatly facilitated the design of spherical shells containing a rigid or an elastic inclusion.

Waters [17] derived a stress analysis of the sphere-cylinder structure that treats the two components with a minimum of overlap at their juncture. He presented a computational procedure that employed three geometrical parameters to calculate the critical stresses over a wide range of sizes and proportions. All those results are based on an internal pressure of 1 *psi* and a mean sphere diameter of 1 *inch*; values for other pressures and sizes were in direct proportion.

An experimental investigation by Dally [18] obtained information concerning the effect of the external loadings in cylindrical nozzle connections on spherical shells. This experiment, which was performed to verify Bijlaard's theory, was for

a  $\beta$  value of approximately 0.1 and for  $\gamma_s$  values of approximately 18.5, 40, 46 respectively. These parameters were well within Bijlaard's limit.

Subsequently, Riley [19] at the IIT Research Institute, tested one steel model for PVRC(Pressure Vessel Research Council), with a  $\gamma_s$  value of 118 and a  $\beta$  value of 0.5.

Witt et al. [20] used strain gauges to test the principal stresses at the inner and outer surfaces of the juncture with no fillet. These models were subjected to internal pressure, axial thrust and moment loading on the nozzle. In this study the nozzle protruded through the vessel. Six different spherical shell-nozzle combinations, without pressure, were tested. Each nozzle was loaded by a radial load and an external moment.

Calladine [21] proposed a plastic design approach to the solution of the problem of design of reinforcement for openings in thin spherical pressure vessels. The essence of the approach is to adjust the thickness and shape of the vessel in the vicinity of the opening so that the full limit pressure of the vessel may be carried with relatively little bending action. Bailey and Hicks [22] used the mathematical method based on shallow theory to show how the principal stresses along the juncture were effected by increasing the cylinder insert thickness when all other dimensions were kept constants.

Taylor et al., [5] described the 3-D elastic model for the determination of the stresses around the cylindrical shell loaded by internal pressure. Several sizes and shapes of reinforcement were tested to study the effects of certain variables and to determine an optimum design. The results were tabulated in the forms of stress concentrated factors. Distribution of the principal stresses on the surfaces of the models were included.

Chao [23] utilized a double Fourier series for the stress analysis of spherical

vessels with pressure loads applied over a rectangular region. The calculations were for complete spheres with pressure loadings over a rectangular region rather than for a loaded attachment. This approach ignored the stiffness of the lug. Brooks [24] [25] used the Green's function to develop the stresses and spring constant for a rectangular attachment to a thin spherical vessel, loaded by a radial force or an overturning moment.

# Chapter 3

## Theory of Loading Pattern

### 3.1 Radial Load

#### 3.1.1 Derivation of Deflection

Two given governing simultaneous equations for the shallow spherical shell loaded by a radial force  $P$  are given by [26].

$$\nabla^4 F - \left(\frac{TE}{R_m}\right) \nabla^2 w = 0 \quad (3.1)$$

$$\nabla^4 w + \left(\frac{1}{R_m D}\right) \nabla^2 F = \frac{P}{D} \quad (3.2)$$

where  $T$ ,  $R_m$  are shown in Figure 3.1

The solutions of the above two simultaneous differential equations are given by:

$$w = C_3 kers + C_4 keis \quad (3.3)$$

$$F = \left[\frac{ET^3}{\sqrt{12(1-\mu^2)}}\right](C_3 keis - C_4 kers + C_{12} \ln s) \quad (3.4)$$

where

$$C_{12} = -(\sqrt{3(1-\mu^2)}) \frac{PR_m}{ET^2\pi}$$
$$s = \frac{r_m}{l} = 1.81784 \left(\frac{r_m}{R_m}\right) \left(\frac{R_m}{T}\right)^{1/2}$$

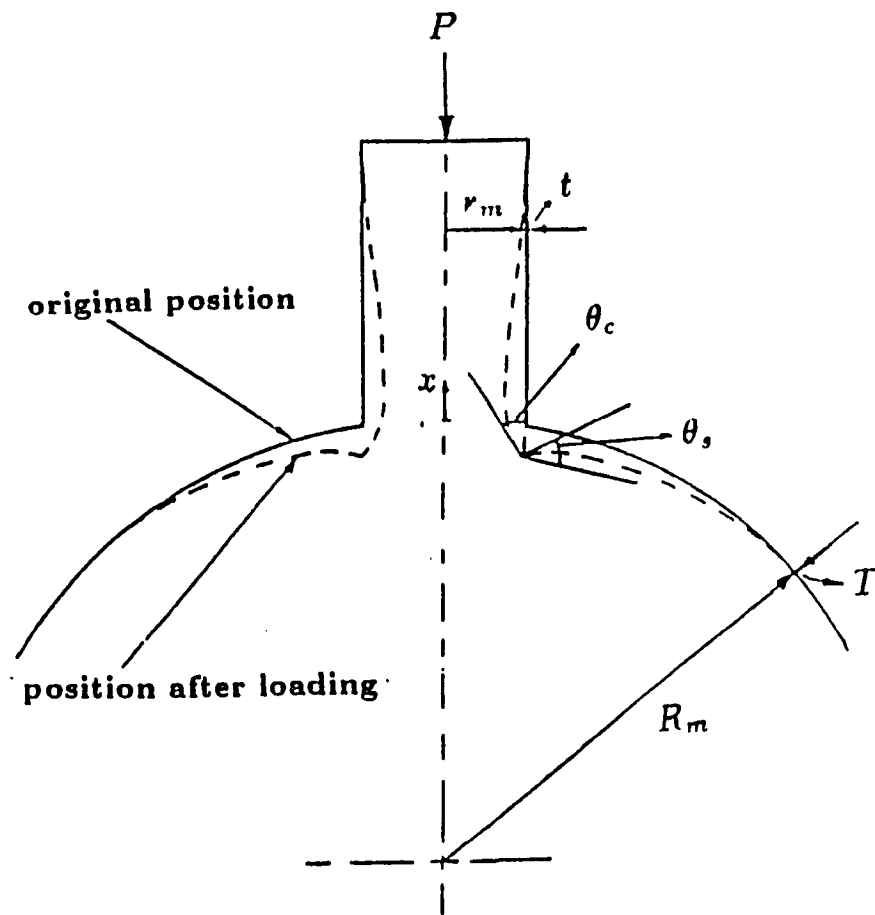


Figure 3.1: Position of Shell before and after Application of Radial Force

F is a stress function, from which the membrane forces are determined as

$$N_x = \frac{1}{r} \frac{\partial F}{\partial r} + \frac{1}{r^2} \frac{\partial^2 F}{\partial r^2} \quad (3.5)$$

$$N_y = \frac{\partial^2 F}{\partial r^2} \quad (3.6)$$

And the radial moment  $M_x$  and tangential moment  $M_y$  are given as follows:

$$M_x = -D \left[ \frac{\partial^2 w}{\partial r^2} + \nu \left( \frac{1}{r} \frac{\partial w}{\partial r} + \frac{1}{r^2} \frac{\partial^2 w}{\partial \theta^2} \right) \right] \quad (3.7)$$

$$M_y = -D \left[ \frac{1}{r} \frac{\partial w}{\partial r} + \frac{1}{r^2} \frac{\partial^2 w}{\partial \theta^2} + \nu \frac{\partial^2 w}{\partial r^2} \right] \quad (3.8)$$

$C_3$  and  $C_4$  have to be determined from the two boundary conditions at  $r = r_m$ , as indicated in Figure 3.2.

B.C.1: The angle of rotation of sphere and nozzle at the juncture are equal.

That is

$$(\theta_s)_{r=r_m} = (\theta_c)_{x=0} \quad (3.9)$$

B.C.2: the circumferential strain of nozzle and sphere at the juncture are equal. That is

$$(\epsilon_{cs})_{r=r_m} = (\epsilon_{cc})_{x=0} \quad (3.10)$$

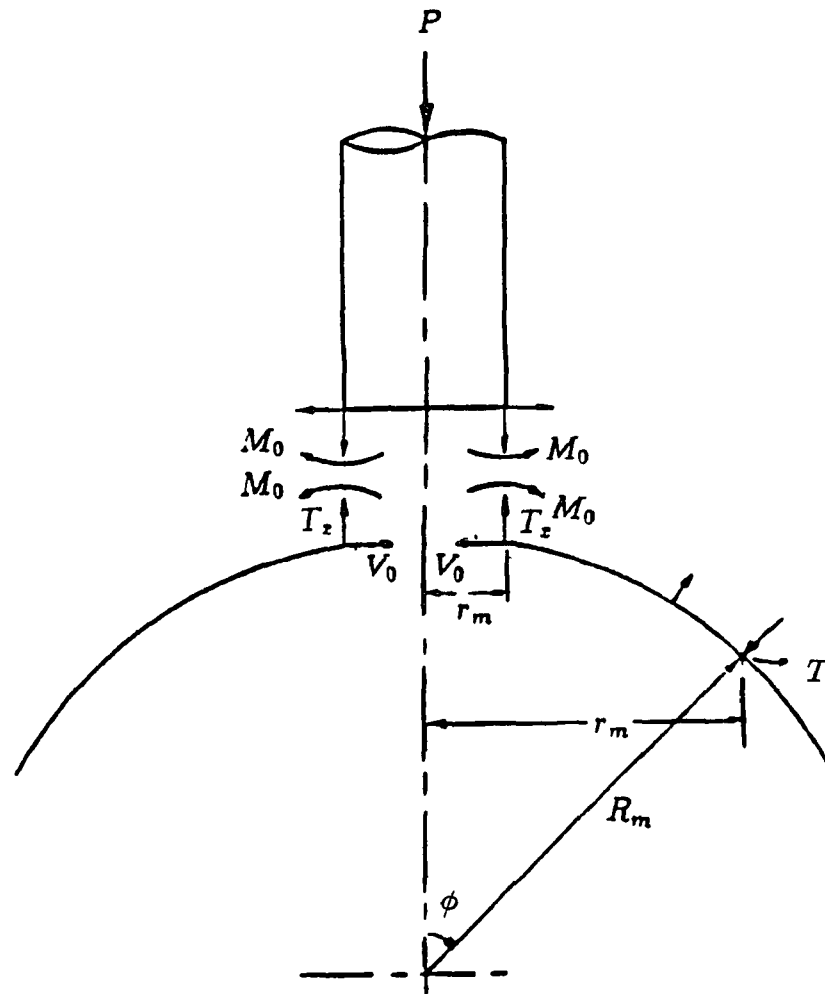


Figure 3.2: Shear Forces and Moments at the Juncture of Spherical Shell and Radial Nozzle due to Radial Force

From Eq.(3.3) and Figure 3.2, the slope  $\theta_s$  of the spherical shell with respect to its original position and due to its deflection is given by

$$\begin{aligned}
(\theta_s)_{r=r_m} &= \left(\frac{dw}{dr}\right)_{r=r_m} \\
&= \left(\frac{dw}{ds}\right)_{r=r_m} \left(\frac{ds}{dr}\right)_{r=r_m} \\
&= \left(\frac{C_3ker's + C_4kei's}{l}\right)_{r=r_m} \\
&= \frac{C_3ker'u + C_4kei'u}{l}
\end{aligned} \tag{3.11}$$

where at  $r = r_m$ ,  $s = r_m/l = u$

Also from Eq.(280) of [27], the angle of rotation at  $x = 0$  is given by:

$$(\theta_c)_{x=0} = -\frac{dv}{dx} = \frac{1}{2\beta_0^2 N} (2\beta_0 M_0 + V_0) \tag{3.12}$$

where

$$\begin{aligned}
N &= \frac{Et^3}{12(1-\mu^2)} \\
\beta_0^4 &= \frac{3(1-\mu^2)}{r_m^2 t^2}
\end{aligned}$$

$M_0$ =Bending moment ( $M_x$ ) in the cylindrical shell at  $x = 0$

$V_0$ =Transverse shear ( $V_x$ ) in the cylindrical shell at  $x = 0$

Due to the continuity of the boundary, the bending moment  $M_0$  and transverse shear  $V_0$  of the nozzle at  $x = 0$  must equal those of the spherical shell at  $r = r_m$  respectively, which is given from [9]

$$M_0 = \frac{-ET^2}{R_m \sqrt{12(1-\mu^2)}} \left[ C_3(keiu + (1-\mu)\frac{ker'u}{u}) - C_4(keru - \frac{(1-\mu)kei'u}{u}) \right] \tag{3.13}$$

$$V_0 = \frac{ET}{R_m u} \left[ (1+\eta)(C_3kei'u - C_4ker'u) + \frac{(1-\eta)C_{12}}{u} \right] \tag{3.14}$$

The strain  $\epsilon_s$  in the spherical shell at  $r = r_m$  is given by [8]

$$(\epsilon_{cs})_{r=r_m} = \frac{N_y - N_x \mu}{ET} \tag{3.15}$$

Substituting Eqs. (3.3), (3.4), (3.5) and (3.6) into the Eq.(3.15), one obtains

$$(\epsilon_{cs})_{r=r_m} = [C_3(keru - \frac{kei'u}{u}) + C_4(keiu + \frac{ker'u}{u}) - \frac{C_{12}}{u^2} - \mu(C_3 \frac{kei'u}{u} - C_4 \frac{ker'u}{u} + \frac{C_{12}}{u^2})] / R_m \quad (3.16)$$

The radial deflection of the nozzle at  $x = 0$  due to  $M_0$  and  $V_0$  is given by (279) of [27]

$$(v)_{y=0} = \frac{\beta_0 M_0 + V_0}{2\beta_0^3 N} \quad (3.17)$$

$$(\epsilon_{cc})_{x=0} = v/r_m = \frac{\beta_0 M_0 + V_0}{2\beta_0^3 N r_m} \quad (3.18)$$

And the radial force  $P$  produces a stress  $\sigma_x = -P/(2r_m t \pi)$  and causes a circumferential strain  $\epsilon_{cc} = P\mu/(2r_m t E \pi)$

From Eqs.(3.17) and (3.18) above one obtains the total circumferential strain at  $x = 0$

$$(\epsilon_{cc})_{x=0} = \frac{\beta_0 M_0 + V_0}{2\beta_0^3 N r_m} + \frac{P\mu}{2r_m t E \pi} \quad (3.19)$$

Substituting Eqs.(3.11), (3.12), (3.13), (3.14), (3.16), and (3.19) into boundary conditions (1) and (2), then  $C_3$  and  $C_4$  are found to be:

$$C_3 = \left[ \frac{A_4 6(1 - \mu^2)(1 - \eta)\gamma_n \rho}{A_2 \sqrt[4]{12(1 - \mu^2)u^2 \pi}} - \frac{\sqrt{12(1 - \mu^2)}}{2u^2 \pi} (1 + \mu + \sqrt[4]{48(1 - \mu^2)}(1 - \eta)\rho\sqrt{\gamma_n}) + \frac{\mu\rho^2}{2\gamma_n \pi} \right] \times \frac{A_2 P R_m}{(A_2 A_3 - A_1 A_4) E T^2} \quad (3.20)$$

$$C_4 = -\frac{1}{A_2} \left[ A_1 C_3 + \frac{6(1 - \mu^2)(1 - \eta) P R_m \gamma_n \rho}{\pi \sqrt[4]{12(1 - \mu^2)u^2 E T^2}} \right] \quad (3.21)$$

where  $A_1, A_2, A_3, A_4$  are given as follows :

$$A_1 = \frac{\sqrt[4]{12(1 - \mu^2)}}{u} \left[ \frac{\gamma_n}{\rho} ker'u - \gamma_n \rho (1 + \eta) kei'u \right] + \rho^2 \sqrt{2\gamma_n} \left[ keiu + ker'u \frac{1 - \mu}{u} \right] \quad (3.22)$$

$$A_2 = \frac{\sqrt[4]{12(1-\mu^2)}}{u} \left[ \frac{\gamma_n}{\rho} kei'u + \gamma_n \rho (1+\eta) ker'u \right] - \rho^2 \sqrt{2\gamma_n} \left[ keru - (1-\mu) \frac{kei'u}{u} \right] \quad (3.23)$$

$$A_3 = keru - (1+\mu) \frac{kei'u}{u} + \rho^2 \left[ keiu + (1-\mu) \frac{ker'u}{u} \right] - \sqrt[4]{48(1-\mu^2)} \rho \sqrt{\gamma_n} kei'u \frac{1+\eta}{u} \quad (3.24)$$

$$A_4 = keiu + ker'u \frac{1+\mu}{u} - \rho^2 \left[ keru - kei'u \frac{1-\mu}{u} \right] + \sqrt[4]{48(1-\mu^2)} \rho \sqrt{\gamma_n} ker'u \frac{1+\eta}{u} \quad (3.25)$$

### 3.1.2 Derivation of Membrane and Bending Forces

Since the model is axisymmetrical, all derivatives of Eqs.(3.5), (3.6), (3.7), and (3.8) with respect to  $\theta$  are zero. One obtains bending stress and membrane stress in both circumferential and meridional directions as:

$$M_m = M_x = \frac{ET^2}{R_m [12(1-\nu^2)]^{1/2}} \left\{ C_3 \left[ keis - \frac{1-\nu}{s} ker's \right] - C_4 \left[ kers - \frac{1-\nu}{s} kei's \right] \right\} \quad (3.26)$$

$$M_c = M_y = \frac{ET^2}{R_m [12(1-\nu^2)]^{1/2}} \left\{ C_3 \left[ \nu keis - \frac{1-\nu}{s} ker's \right] - C_4 \left[ \nu kers + \frac{1-\nu}{s} kei's \right] \right\} \quad (3.27)$$

$$N_m = N_x = \frac{ET}{R_m s} (C_3 kei's - C_4 ker's + C_{12} s^{-1}) \quad (3.28)$$

$$N_c = N_y = \frac{ET}{R_m} \left[ C_3 \left( kers - \frac{kei's}{s} \right) + C_4 \left( keis + \frac{ker's}{s} \right) - \frac{C_{12}}{s^2} \right] \quad (3.29)$$

## 3.2 Overturning Moment

### 3.2.1 Derivation of Deflection

The deformation of a spherical vessel is determined by the solutions of the Eqs.(51) and (52) of [8] which are given as:

$$w_v = (C_3 k e r' s + C_4 k e i' s) \cos \theta \quad (3.30)$$

$$F = \frac{ET^2}{[12(1 - \mu^2)]^{1/2}} (C_3 k e i' s - C_4 k e r' s + \frac{C_{12}}{s}) \cos \theta \quad (3.31)$$

where

$w_v$  = Radial deflection of the spherical pressure vessel

$\theta$  = Polar coordinate for the cylindrical and spherical shell, in radians, as shown in the Figure 3.3. The deflections of the cylindrical shell in the axial, tangential and radial directions are given by [10].

$$u_1 = [e^{-\alpha_1 x} (H_5 \cos \beta_1 x + H_6 \sin \beta_1 x) - \frac{M_B}{\pi r_m t E} \frac{x}{r_m} - H_3 r_m] \cos \theta \quad (3.32)$$

$$v_1 = [e^{-\alpha_1 x} (H_7 \cos \beta_1 x + H_8 \sin \beta_1 x) - \frac{M_B}{\pi 2 r_m t E} \frac{x^2}{r_m^2} - H_3 x - H_4] \sin \theta \quad (3.33)$$

$$w_1 = [e^{-\alpha_1 x} (H_1 \cos \beta_1 x + H_2 \sin \beta_1 x) - \frac{M_B}{2 \pi r_m t E} (\frac{x^2}{r_m^2} + 2\mu) + H_3 x + H_4] \cos \theta \quad (3.34)$$

All of the unknown constants can be obtained by applying the boundary continuity conditions between the sphere and nozzle. Those boundary conditions are given below :

It is assumed that the cross section of the nozzle remains circular and its radius does not change. In addition, it is assumed that plane cross section remains plane after loading. Hence, the boundary conditions are:

B.C.1:

$$(w_1)_{x=0} = 0 \quad (3.35)$$

B.C.2

$$(u_1)_{x=0} = 0 \quad (3.36)$$

Since the shell is subjected to the overturning moment, one has from [26]:

B.C.3:

$$C_{12} = \frac{[3(1 - \mu^2)]^{1/2} R_m M_B}{\pi E T^2 l} \quad (3.37)$$

From Figure 3.3, the compatibility of rotation at the juncture of the shell and nozzle requires:

B.C.4:

$$\left(\frac{w_v}{r_m} - \frac{\partial w_v}{\partial r}\right)_{r=r_m} = \left(\frac{\partial w_1}{\partial x}\right)_{x=0} \quad (3.38)$$

The rotation of the spherical shell at  $r = r_m$  and that of the nozzle at  $x = 0$  should be equal. This leads to:

B.C.5:

$$(\epsilon_{\theta v})_{r=r_m} = (\epsilon_{\theta})_{x=0} \quad (3.39)$$

Also, since at the juncture, the bending moment  $M_x$  in the walls of nozzle and shell should be equal, one arrives at the condition:

B.C.6:

$$(M_{xv})_{r=r_m} = (M_x)_{x=0} \quad (3.40)$$

The shear force  $Q_x$  in the nozzle at  $x = 0$  has to be in equilibrium with the horizontal components of the force in the shell at  $r = r_m$ .

$$N_x \cos \phi_0 + Q_{xv} \sin \phi_0 = Q_x \quad (3.41)$$

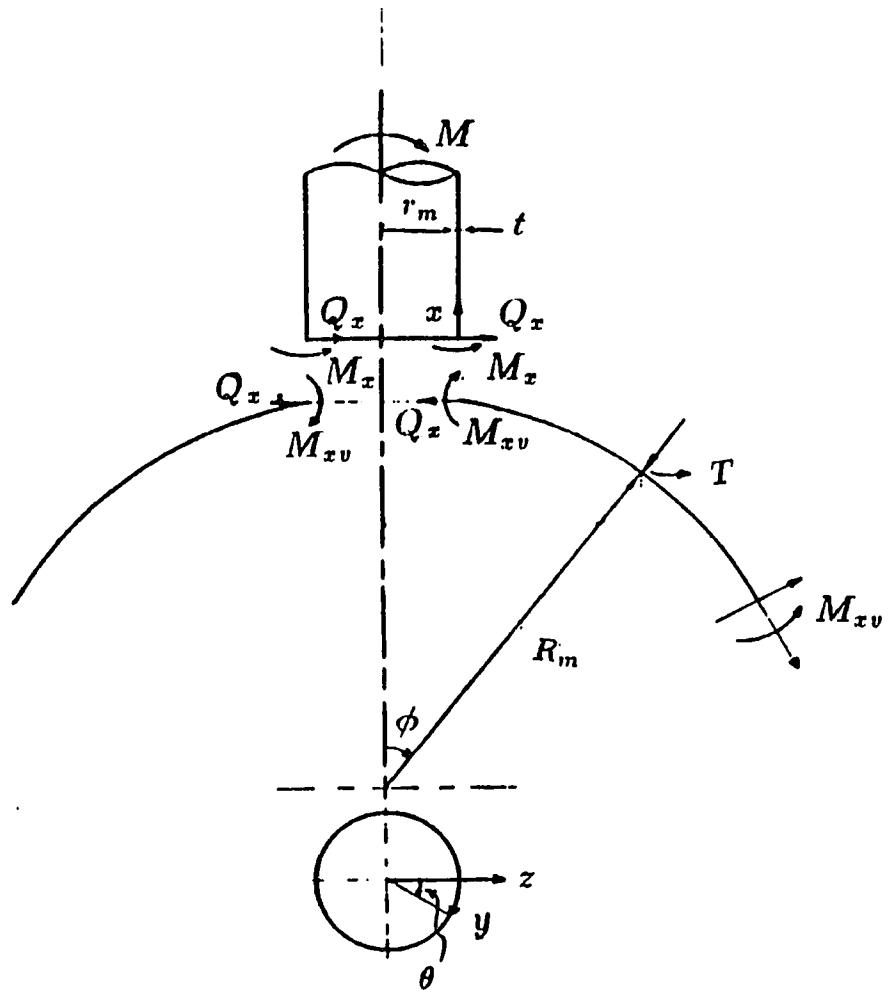


Figure 3.3: Overturning Moment Applied on the Nozzle-Sphere Model

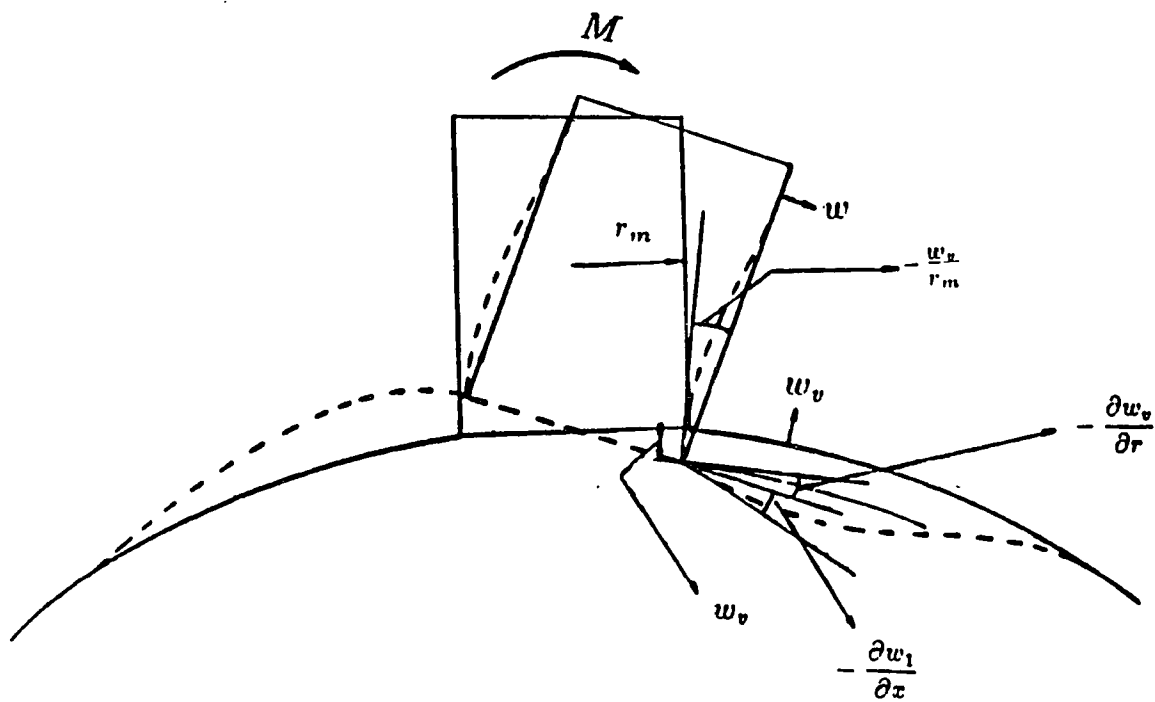


Figure 3.4: Deflections of Nozzle-Sphere Model due to a Bending Moment

From Figure 3.4 and Figure 3.5, one notes that  $Q_{zv}$  and  $Q_x$  are the equivalent transverse shear forces for the shell and nozzle, respectively, including the effects of the twisting moments. Since  $\phi_0$  is assumed to be small, this condition reduces to:

B.C.7:

$$\left[ \left(1 - \frac{r_m^2}{2R_m^2}\right) N_x + \frac{r_m}{R_m} Q_{zv} \right] = (Q_x)_{x=0} \quad (3.42)$$

From B.C.1 and Eq. (3.34), one obtains

$$H_4 = -H_1 - \frac{\mu M_B}{\pi r_m t E} \quad (3.43)$$

from B.C.2 and Eq. (3.32), one obtains

$$H_3 = \frac{H_5}{r_m} \quad (3.44)$$

Using the remaining conditions, the constants  $C_3$ ,  $C_4$ ,  $H_1$  and  $H_2$  can be found from Eq.(54), (59), (61), and (68) of [10]. Those equations are numbered as Eq. (3.45), (3.46), (3.47), and (3.48), which are given below.

$$D_1 C_3 + D_2 C_4 - \left[ \alpha_1 - \left( \frac{L_1}{r_m} \right) \right] H_1 - \left[ \beta_1 + \left( \frac{L_2}{r_m} \right) \right] H_2 = 0 \quad (3.45)$$

$$\begin{aligned} D_3 C_3 + D_4 C_4 - \frac{(1 + L_3) \gamma_n [12(1 - \mu^2)]^{1/2}}{\rho u^2} H_1 - \frac{L_4 \gamma_n [12(1 - \mu^2)]^{1/2}}{\rho u^2} H_2 \\ = \frac{1}{\pi u} \left[ \frac{\mu \rho^2}{\gamma_n} - \frac{(1 + \mu) [12(1 - \mu^2)]^{1/2}}{u^2} \right] \frac{R_m M_B}{ET^2 l} \end{aligned} \quad (3.46)$$

$$D_5 C_3 + D_6 C_4 - D_7 H_1 + D_8 H_2 = \frac{(2 - \mu^2)}{12(1 - \mu^2) \pi} \frac{R_m M_B}{ET^2 l} \quad (3.47)$$

$$D_9 C_3 + D_{10} C_4 + D_{11} H_1 - D_{12} H_2 = (1 - \eta) \frac{[12(1 - \mu^2)]^{1/2}}{\pi u^3} \frac{R_m M_B}{ET^2 l} \quad (3.48)$$

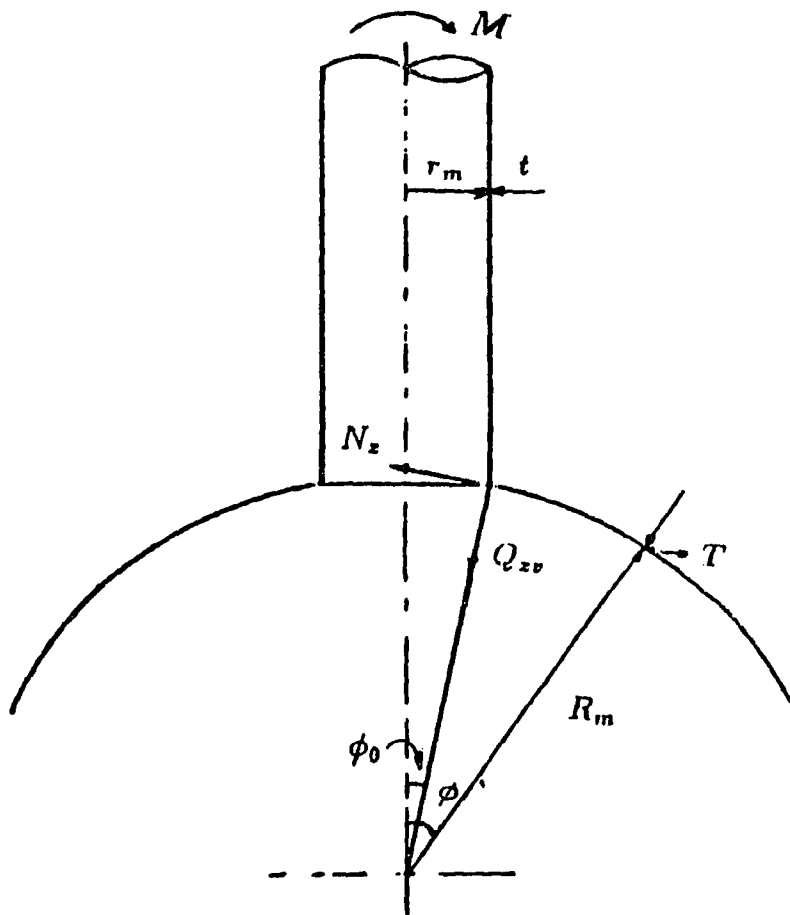


Figure 3.5: Normal and Shear Forces Acting on the Spherical Shell at the Nozzle-Spherical Shell Junction due to Overturning Moment

Where the constants  $D_1$  to  $D_{12}$  are given below:

$$D_1 = \left(\frac{u}{r_m}\right)[keiu + \left(\frac{2}{u}\right)ker'u] \quad (3.49)$$

$$D_2 = \left(\frac{u}{r_m}\right)\left[\frac{2}{u}kei'u - keru\right] \quad (3.50)$$

$$D_3 = -\frac{(1+\mu)}{u}keru + ker'u + \frac{2(1+\mu)}{u^2}kei'u \quad (3.51)$$

$$D_4 = -\frac{(1+\mu)}{u}keiu + kei'u - \frac{2(1+\mu)}{u^2}ker'u \quad (3.52)$$

$$D_5 = \frac{\gamma_n^2 u}{[12(1-\mu^2)]^{1/2}} \left[ \frac{1-\mu}{u} keiu + \frac{2(1-\mu)}{u^2} ker'u - kei'u \right] \quad (3.53)$$

$$D_6 = \frac{\gamma_n^2 u}{[12(1-\mu^2)]^{1/2}} \left[ -\frac{1-\mu}{u} keru + \frac{2(1-\mu)}{u^2} kei'u + ker'u \right] \quad (3.54)$$

$$D_7 = \frac{\gamma_n^2 r_m^2}{\rho^3 u [12(1-\mu^2)]^{1/2}} \left[ \alpha_1^2 - \beta_1^2 - \frac{\mu}{r_m^2} (1+L^3) + \frac{l}{r_m} (\alpha_1 L_1 + \beta_1 L_2) \right] \quad (3.55)$$

$$D_8 = \frac{\gamma_n^2 r_m^2}{\rho^3 u [12(1-\mu^2)]^{1/2}} \left[ 2\alpha_1 \beta_1 + \frac{\mu}{r_m^2} L_4 - \frac{l}{r_m} (\alpha_1 L_2 - \beta_1 L_1) \right] \quad (3.56)$$

$$D_9 = \frac{1-\eta}{u} \left( keru - \frac{2kei'u}{u} \right) - \frac{u^3 \rho^2}{12(1-\mu^2) \gamma_n^2} \left[ \frac{(1-\mu)keiu}{u^2} - keru + \frac{kei'u}{u} + \frac{2(1-\mu)ker'u}{u^3} \right] \quad (3.57)$$

$$D_{10} = \frac{1-\eta}{u} \left( keiu + \frac{2ker'u}{u} \right) + \frac{u^3 \rho^2}{12(1-\mu^2) \gamma_n^2} \left[ \frac{(1-\mu)keru}{u^2} + keiu + \frac{ker'u}{u} - \frac{2(1-\mu)kei'u}{u^3} \right] \quad (3.58)$$

$$D_{11} = \frac{r_m^3}{u^2 \rho^2 \gamma_n [12(1 - \mu^2)]^{1/2}} \left[ \alpha_1 (\alpha_1^2 - 3\beta_1^2) - \frac{(2 - \mu)}{r_m^2} \alpha_1 + \frac{(3 - \mu)}{2r_m^2} (-\alpha_1 L_3 - \beta_1 L_4) \right. \\ \left. + \frac{1}{r_m} ((\alpha_1^2 - \beta_1^2)L_1 + 2\alpha_1 \beta_1 L_2) + \frac{(1 - \mu)}{2r_m^3} L_1 \right] \quad (3.59)$$

$$D_{12} = \frac{r_m^3}{u^2 \rho^2 \gamma_n [12(1 - \mu^2)]^{1/2}} \left[ \beta_1 (3\alpha_1^2 - \beta_1^2) - \frac{(2 - \mu)}{r_m^2} \beta_1 - \frac{(3 - \mu)}{2r_m^2} (-\alpha_1 L_4 + \beta_1 L_3) \right. \\ \left. - \frac{1}{r_m} ((\alpha_1^2 - \beta_1^2)L_2 - 2\alpha_1 \beta_1 L_1) - \frac{(1 - \mu)}{2r_m^3} L_2 \right] \quad (3.60)$$

Where  $\alpha_1$  and  $\beta_1$  are given by Eq.(11) of [10]:

$$\alpha_1 = \frac{1}{r_m} \left[ 1 - \frac{1}{2\mu} + (3(1 - \mu^2)\gamma_n^2 + 1 - \frac{3}{4\mu^2})^{1/2} \right]^{1/2} \quad (3.61)$$

$$\beta_1 = \frac{1}{r_m} \left[ -(1 - \frac{1}{2\mu}) + (3(1 - \mu^2)\gamma_n^2 + 1 - \frac{3}{4\mu^2})^{1/2} \right]^{1/2} \quad (3.62)$$

The constants  $L_1$  to  $L_4$  are given by:

$$L_1 = \frac{K_1}{K_5} \quad (3.63)$$

$$L_2 = \frac{K_2}{K_5} \quad (3.64)$$

$$L_3 = \frac{K_3}{K_5} \quad (3.65)$$

$$L_4 = \frac{K_4}{K_5} \quad (3.66)$$

and constants  $K_1$  to  $K_5$  are given by:

$$K_1 = r_m \alpha_1 [(1 - \mu)(1 - 3\mu(1 + \mu + \mu^2)) - 12(1 - \mu^4)\gamma_n^2]$$

$$+ (2(1 - \mu))(2 + 3\mu + 3\mu^2) + 24\mu(1 - \mu^2)\gamma_n^2 r_m^2 \beta_1^2] \quad (3.67)$$

$$K_2 = -r_m \beta_1 [(1 - \mu)(1 - 3\mu(1 + \mu + \mu^2)) - 12(1 - \mu^4)\gamma_n^2 \\ - (2(1 - \mu)(2 + 2\mu + 3\mu^2) + 24\mu(1 - \mu^2)\gamma_n^2) r_m^2 \alpha_1^2] \quad (3.68)$$

$$K_3 = (1 - \mu)(3 + \mu)(1 - 3\mu^2) + 12(1 - 2\mu - \mu^2)(1 - \mu^2)\gamma_n^2 \quad (3.69)$$

$$K_4 = 2[(4 + 9\mu + 3\mu^2)(1 - \mu) + 12(2 + \mu)(1 - \mu^2)\gamma_n^2] r_m^2 \alpha_1 \beta_1 \quad (3.70)$$

$$K_5 = [12(1 - \mu^2)\gamma_n^2 + (1 - \mu)(1 + 3\mu)]^2 \quad (3.71)$$

The solution for deflection of the spherical shell due to bending moment  $M$  is given by Eq(3.30) in which  $C_3$  and  $C_4$  can be obtained by using Eq.(3.45) to Eq.(3.60)

### 3.2.2 Derivation of Membrane and Bending Forces

Substituting Eqs.(3.30) into Eqs.(3.5), (3.6), (3.7), and(3.8), one can obtain bending stress and membrane stress in both meridional and circumferential directions, as follows:

$$M_m = M_x = \frac{ET^2}{R_m [12(1 - \nu^2)]^{1/2}} \times (C_3 G_1 + C_4 G_2) \cos \theta \quad (3.72)$$

$$M_c = M_y = \frac{ET^2}{R_m [12(1 - \nu^2)]^{1/2}} \times (-C_3 G_3 + C_4 G_4) \cos \theta \quad (3.73)$$

$$N_m = N_x = G_6 \left( \frac{ET}{R_s} \right) \cos \theta \quad (3.74)$$

$$N_c = N_y = G_7 \left( \frac{ET}{R_m} \right) \cos \theta \quad (3.75)$$

where

$$C_3 = \frac{2kei'u - ukeru}{G_5} \frac{M_B R_m}{ET^2 l}$$

$$C_4 = \frac{-C_3(2ker'u + ukeiu)}{2kei'u - ukeru}$$

$$G_1 = (1 - \mu) \frac{keis}{s} + \frac{2(1 - \mu)}{s^2} ker's - kei's$$

$$G_2 = -(1 - \mu) \frac{kers}{s} + 2(1 - \mu) \frac{kei's}{s^2} + ker's$$

$$G_3 = (1 - \mu) \frac{keis}{s} + \frac{2(1 - \mu)}{s^2} ker's + \mu kei's$$

$$G_4 = (1 - \mu) \frac{kers}{s} - 2(1 - \mu) \frac{kei's}{s^2} + \mu ker's$$

$$G_5 = \pi u(1 + \mu)[u^2(ker^2u + kei^2u) + 4(ker'^2u + kei^2u)$$

$$+ 4u(ker'u keiu - keru kei'u)] - \pi u^4(keruker'u + keiukei'u)$$

$$G_6 = C_3(kers - \frac{2kei's}{s}) + C_4(keis + \frac{2ker's}{s} + \frac{2C_{12}}{s^2})$$

$$G_7 = C_3(-\frac{kers}{s} + 2\frac{kei's}{s^2} + ker's) \frac{2C_{12}}{s^3} - C_4(\frac{keis}{s} + \frac{2ker's}{s^2} - kei's)$$

### 3.3 Torsional Moment

It is assumed that a shaft in the form of a half spherical shell with fixed boundary at its equator is subjected to a torsional moment at the juncture of the half sphere and nozzle as shown in the Figure 3.6. The axis of the nozzle is taken as the  $y$  axis and  $r$  and  $\theta$  are used to define the position of an element in the plane of the cross section. The components of displacement in the radial, tangential and  $y$  directions

are denoted by  $u$ ,  $v$ , and  $w$  respectively. The expressions for the strain components are given below:

$$\begin{aligned} \epsilon_\theta &= \frac{v}{r} + \frac{\partial v}{r \partial \theta} & \epsilon_r &= \frac{\partial u}{\partial r} & \epsilon_y &= \frac{\partial w}{\partial y} \\ \gamma_{r\theta} &= \frac{\partial u}{r \partial \theta} + \frac{\partial v}{\partial y} - \frac{v}{r} & \gamma_{ry} &= \frac{\partial u}{\partial y} + \frac{\partial w}{\partial r} & \gamma_{y\theta} &= \frac{\partial v}{\partial y} + \frac{\partial w}{r \partial \theta} \end{aligned} \quad (3.76)$$

The differential equations of equilibrium are:

$$\begin{aligned} \frac{\partial \sigma_r}{\partial r} + \frac{1}{r} \frac{\partial \tau_{r\theta}}{\partial \theta} + \frac{\partial \tau_{ry}}{\partial y} + \frac{\sigma_r - \sigma_\theta}{r} &= 0 \\ \frac{\partial \tau_{ry}}{\partial r} + \frac{1}{r} \frac{\partial \tau_{\theta y}}{\partial \theta} \frac{\partial \sigma_y}{\partial y} + \frac{\tau_{ry}}{r} &= 0 \end{aligned} \quad (3.77)$$

$$\frac{\partial \tau_{r\theta}}{\partial r} + \frac{1}{r} \frac{\partial \sigma_\theta}{\partial r} + \frac{\partial \tau_{\theta y}}{\partial y} + \frac{2\tau_{r\theta}}{r} = 0$$

In the application of these equations to the torsional problem the *semi-inverse method* is used with the assumptions that  $u$  and  $w$  are zero. That is, during twist, the particles move only in the tangential direction. Substituting  $u = w = 0$  into Eq.(3.76) and noting that from symmetry, the displacement  $v$  does not depend on the angle  $\theta$ , one finds that

$$\begin{aligned} \epsilon_r &= \epsilon_\theta = \epsilon_y = \gamma_{ry} = 0 \\ \gamma_{r\theta} &= \frac{\partial v}{\partial r} - \frac{v}{r} \\ \gamma_{\theta y} &= \frac{\partial v}{\partial y} \end{aligned} \quad (3.78)$$

the third of Eq.(3.77) gives:

$$\frac{\partial \tau_{r\theta}}{\partial r} + \frac{\partial \tau_{\theta y}}{\partial y} + \frac{2\tau_{r\theta}}{r} = 0 \quad (3.79)$$

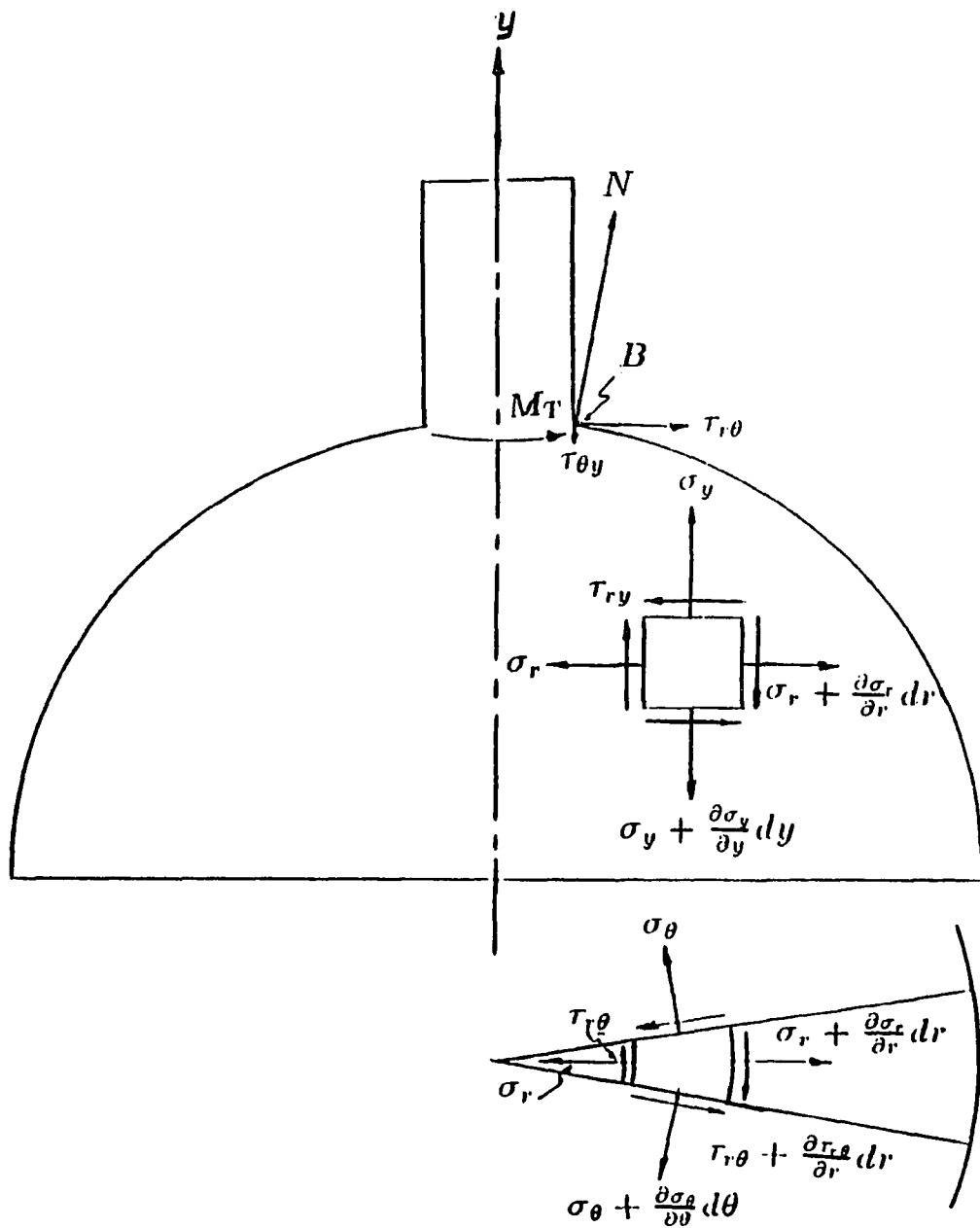


Figure 3.6: Shear Stresses and Angular Displacement due to Torsional Moment

Eq.(3.79) can be written in the form

$$\frac{\partial}{\partial r}(r^2 \tau_{r\theta}) + \frac{\partial}{\partial y}(r^2 \tau_{\theta y}) = 0 \quad (3.80)$$

It is seen that this equation is satisfied by using a stress function  $\phi$  of  $r$  and  $y$ , such that

$$\begin{aligned} r^2 \tau_{r\theta} &= -\frac{\partial \phi}{\partial y} \\ r^2 \tau_{\theta y} &= \frac{\partial \phi}{\partial r} \end{aligned} \quad (3.81)$$

To satisfy the compatability conditions, it is necessary to recognize that  $\tau_{r\theta}$  and  $\tau_{\theta y}$  are functions of the displacement  $v$ . From Eqs.(3.78) and (3.81) one finds

$$\tau_{r\theta} = -\frac{1}{r^2} \frac{\partial \phi}{\partial y} \quad (3.82)$$

$$\tau_{\theta y} = \frac{1}{r^2} \frac{\partial \phi}{\partial r} \quad (3.83)$$

From these equaions it follows that

$$\frac{\partial}{\partial r} \left( \frac{1}{r^3} \frac{\partial \phi}{\partial r} \right) + \frac{\partial}{\partial y} \left( \frac{1}{r^3} \frac{\partial \phi}{\partial y} \right) = 0 \quad (3.84)$$

or

$$\frac{\partial^2 \phi}{\partial r^2} - \frac{3}{r} \frac{\partial \phi}{\partial r} + \frac{\partial^2 \phi}{\partial y^2} = 0 \quad (3.85)$$

From the condition that the lateral surface of the nozzle is free from external forces, one concludes that at any point  $B$  on the boundary of an axial section, the total shearing stress must be in the tangential direction of the boundary and its projection on the normal  $N$  on the boundary must be zero. Hence

$$\tau_{r\theta} \frac{ds}{dy} - \tau_{\theta y} \frac{dr}{ds} = 0 \quad (3.86)$$

Substituting from Eq.(3.81), one finds that

$$\frac{\partial \phi}{\partial y} \frac{dy}{ds} + \frac{\partial \phi}{\partial r} \frac{dr}{ds} = 0 \quad (3.87)$$

$$M_T = \int_{r_i}^{r_o} 2\pi r^2 \tau_{\theta y} dr = 2\pi(\phi_{r_o} - \phi_{r_i}) \quad (3.88)$$

One defines  $\theta_T = v/r$  as the angle of rotation of an elemental ring of radius  $r$  on the cross section of the nozzle. Eq.(3.83) can be written in the form:

$$Gr^3 \frac{\partial \theta_T}{\partial r} = -\frac{\partial \phi}{\partial y} \quad (3.89)$$

$$Gr^3 \frac{\partial \theta_T}{\partial y} = \frac{\partial \phi}{\partial r}$$

from which

$$\frac{\partial^2 \theta_T}{\partial r^2} + \frac{3}{r} \frac{\partial \theta_T}{\partial r} + \frac{\partial^2 \theta_T}{\partial y^2} = 0 \quad (3.90)$$

In the spherical shaft model, the equation can be indicated as follows:

$$r^2 + y^2 = C \quad (3.91)$$

where  $C$  is constant at the boundary of the axial section and equals  $R^2$ . Any function of this constant will satisfy Eq.(3.83). In order to also satisfy Eq.(3.90), one utilizes

$$\phi = c[(r^2 + y^2) + a(r^2 + y^2)^3] \quad (3.92)$$

where  $c$  and  $a$  are arbitrary constants. Substituting Eq.(3.92) into Eq.(3.85), we obtain

$$a = \frac{1}{9(r^2 + y^2)^2} \quad (3.93)$$

$$M_T = 2\pi[\phi(r_o) - \phi(r_i)] \quad (3.94)$$

or

$$M_T = 2\pi c(R_o^2 + aR_o^4 - R_i^2 - aR_i^4) \quad (3.95)$$

then

$$c = \frac{M_T}{2\pi(R_o^2 + aR_o^4 - R_i^2 - aR_i^4)} \quad (3.96)$$

From Eq.(3.81), one obtains

$$\tau_{r\theta} = \frac{-c}{r^2} [2y + 6ay(r^2 + y^2)] \quad (3.97)$$

Substituting  $\phi$  into Eq.(3.89) and integrating with respect to  $r$  gives the twisting angle  $\theta_T$ .

$$\theta_T = \frac{-c}{G} \left[ \frac{-y}{r^2} + \frac{3r^2 y}{9(r^2 + y^2)} + \frac{12y^3 \ln r}{9(r^2 + y^2)} - \frac{3y^5}{9r^2(r^2 + y^2)} \right] \quad (3.98)$$

# Chapter 4

## Finite Element Method

### 4.1 Finite Element Model

In this dissertation, the ANSYS finite element software [1][2] is used for the parametric studies. The finite element mesh is developed by using the quadrilateral shell element model (STIF 63) for thin shells, and isoparametric solid element (STIF 45) for thicker shells. The node and element generator, PREP7 is used in generating the mesh.

#### 4.1.1 Quadrilateral Shell Element-for Thin Shell

This element has both bending and membrane capabilities. Both in-plane and normal loads are permitted. The element has six degrees of freedom at each node: three in translations and three in rotations. The quadrilateral shell has options for variable thicknesses, elastic foundation supports, concentrated pressure loadings and large rotations.

The geometry, nodal point locations, and the coordinate system for this element are shown in Figure 4.1. The element is defined by four nodal points (I, J, K, L). It can accommodate four different thicknesses, one elastic foundation stiffness, one material direction angle, and the orthotropic material properties. The material  $x$ -direction corresponds to the element  $x$ -direction, which may be rotated an angle  $\theta$  (in degrees) from the IJ side of the element. Since the model for this study has

uniform thickness, only TK(1) is used.

An assemblage of flat shell elements can produce a good approximation to a curved shell surface provided that each flat element does not extend over more than a 15 deg arc. Shear deflection is not included in this thin-shell element. The four nodal points defining the element should lie in an exact flat plane; however, a small out-of-plane tolerance is permitted so that the element may have a slightly warped shape.

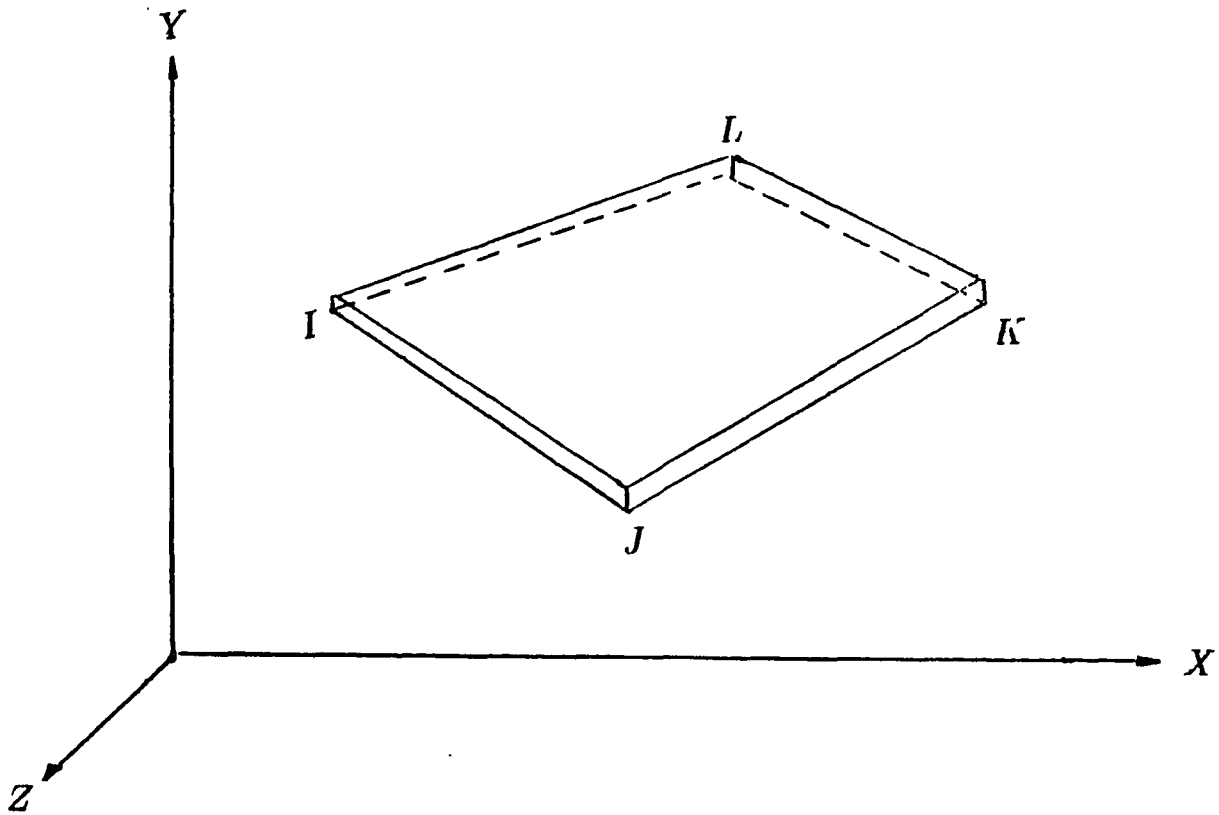


Figure 4.1: Quadrilateral Shell Element

### 4.1.2 Isoparametric Solid Element-for Thicker Shell

This element is defined by eight nodal points having three degrees of freedom at each node: translations in the nodal  $x$ ,  $y$ , and  $z$  directions. The geometry, nodal point locations, face numbers, and the coordinate system for this element are shown in Figure 4.2. The element must be defined by eight nodal points. Zero volume elements are not allowed.

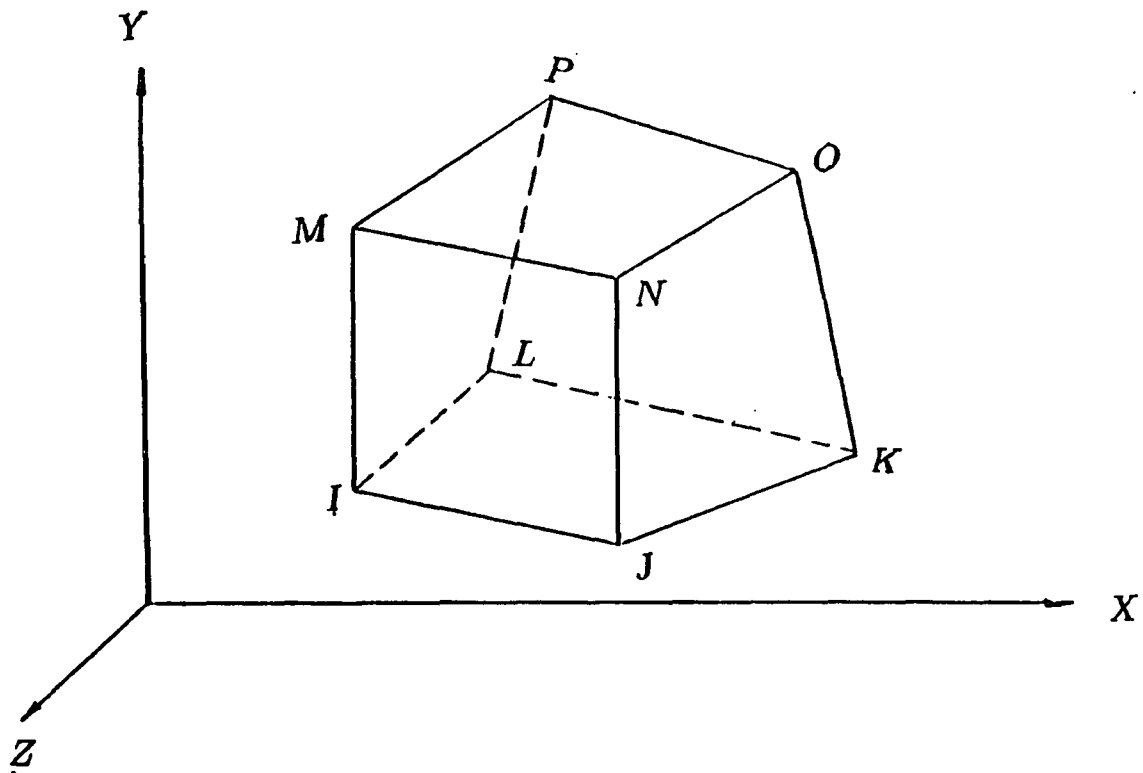


Figure 4.2: Isoparametric Solid Element

## 4.2 Assumptions

For the analysis of this model, the following assumptions are used:

- The material is assumed to be homogeneous, isotropic, and within the elastic range.
- The internal pressure is not taken into account.
- The thickness of the nozzle is the same as the thickness of the sphere.
- The model is a hemisphere with a nozzle on the top, and with a fixed boundary at the equator, as shown in Figure 4.3.
- Modulus of elasticity of  $3 \times 10^6$  *psi* and a Poisson's ratio of 0.3 are assumed.

## 4.3 Geometrical Parameters

Since the thickness of the nozzle is assumed to be identical with the spherical shell, only two geometric parameters,  $\gamma_s$  and  $\beta$ , are needed to analyze the model.  $\gamma_s$  is defined as the ratio of the spherical radius to the thickness of the shell.  $\beta$  is defined as the ratio of the nozzle radius to the sphere radius. For each given  $\beta$  value (0.1, 0.2, 0.3, 0.4, 0.5), the  $\gamma_s$  values of 7, 10, 15, 20, 25, 30, 40, 50, 75, 100 are used to analyze the nozzle-sphere model under various loadings. Hence, fifty runs are executed for each loading case. In this study, a  $\beta$  value of 0.5 is the upper bound for the practical applications. If  $\beta$  is greater than 0.5, the fixed boundary at the equator may significantly affect the outcome of the analysis. Although a shell thickness of 0.4 inch is used for this study, this value has been used to normalize the results. Hence the results on stress factors and the normalized spring constants can be applied to shells with different thicknesses.

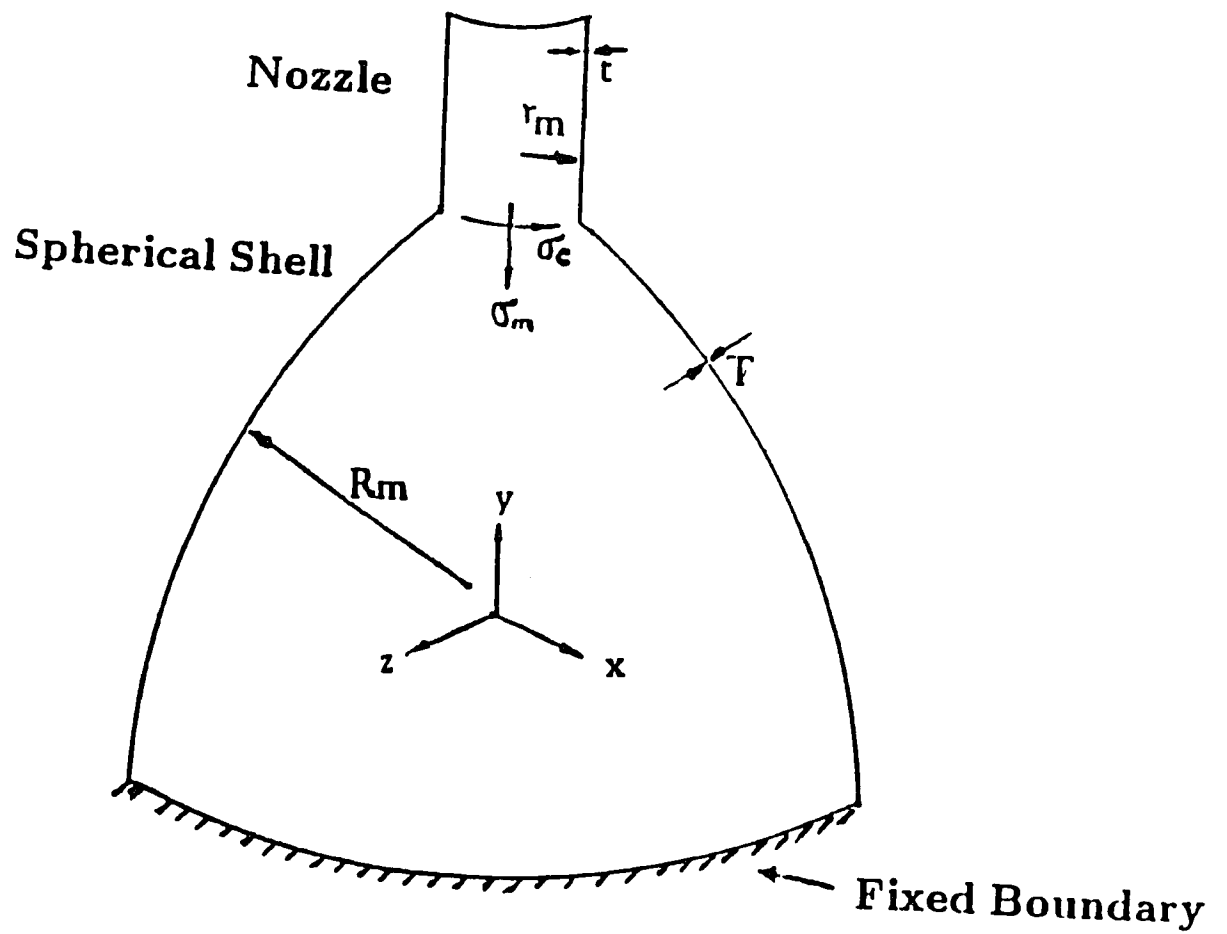


Figure 4.3: Shell Model

## 4.4 Computational Model

Due to the symmetry of the loading and the geometry of the nozzle-sphere configuration, 1/4 of the complete geometry is used as the computational model as shown in Figure 4.4. In the *ANSYS* finite element package, the subroutine PREP7 is used to generate the geometry. In order to obtain a smooth stress profile, five to six elements were modelled throughout the intersection area. In order to optimize the computing time, a wave-front reduction method was implemented through the element reordering.

For quadrilateral shell element model, 15 key points are used to divide the model into eight areas, A1 to A8, as shown in Figure 4.4. Areas A1 to A4 are generated with the spherical coordinate system, and areas A5 to A8 are generated with the cylindrical coordinate system. The element type STIF63 is utilized to generate this quadrilateral shell model which is rectangular or square in shape with 4 nodes at the corners. Smaller sized elements are generated in areas A3 to A6, where greater stress gradients exist.

Since the top boundary of the nozzle, which is circular in shape, is described by line segments between node points, the number of nodes used is very important in simulating the true geometry. To study the convergence of the results, 4 trial models with 10, 15, 22 and 26 elements, respectively, on the top boundary of the nozzle were used. The deviation of resulting stresses for each model is shown in Table 4.1 and Figure 4.5. It shows Model 3, with 22 elements, to be the most optimum one as it presents very good convergence. Therefore, this model is adopted for all the computations in this dissertation. The completely meshed model is shown in Figure 4.6.

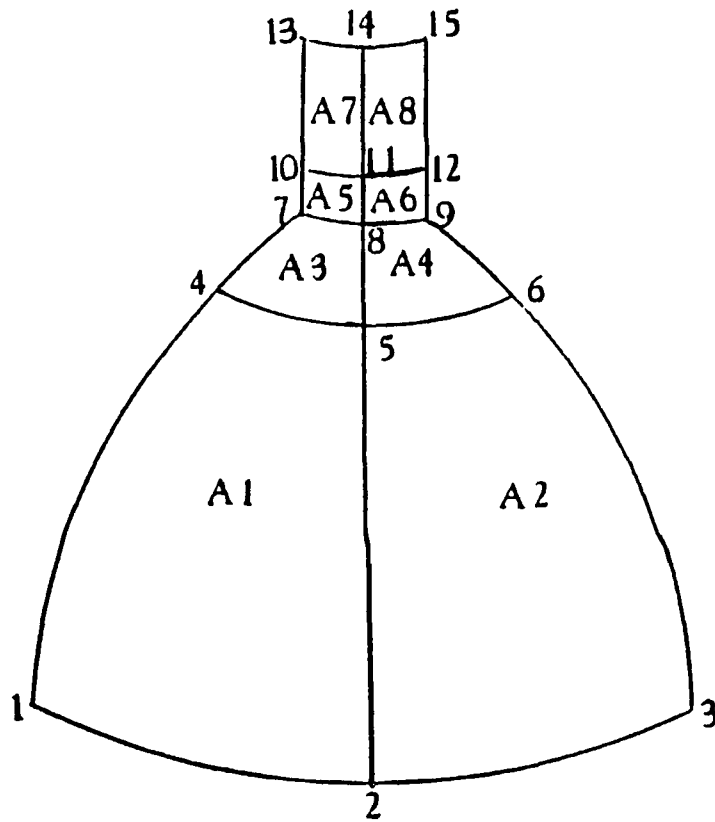


**Figure 4.4: Areas and Keypoints of Quadrilateral Shell Element Model**

$T = t = 0.4\text{in}$ $\gamma_r = 20 \beta = 0.2$	$\sigma_{co}$ psi	$\sigma_{mo}$ psi	Maximum Deviation
Model 1 10 elements	992.8	1710	0.23%
Model 2 15 elements	997.8	1714	0.13%
Model 3 22 elements	1005	1740	0.099%
Model 4 26 elements	1005	1740	0%

(Total Radial Force =  $1000/b$  upward)

Table 4.1: Data Convergence of Quadrilateral Shell Element Model

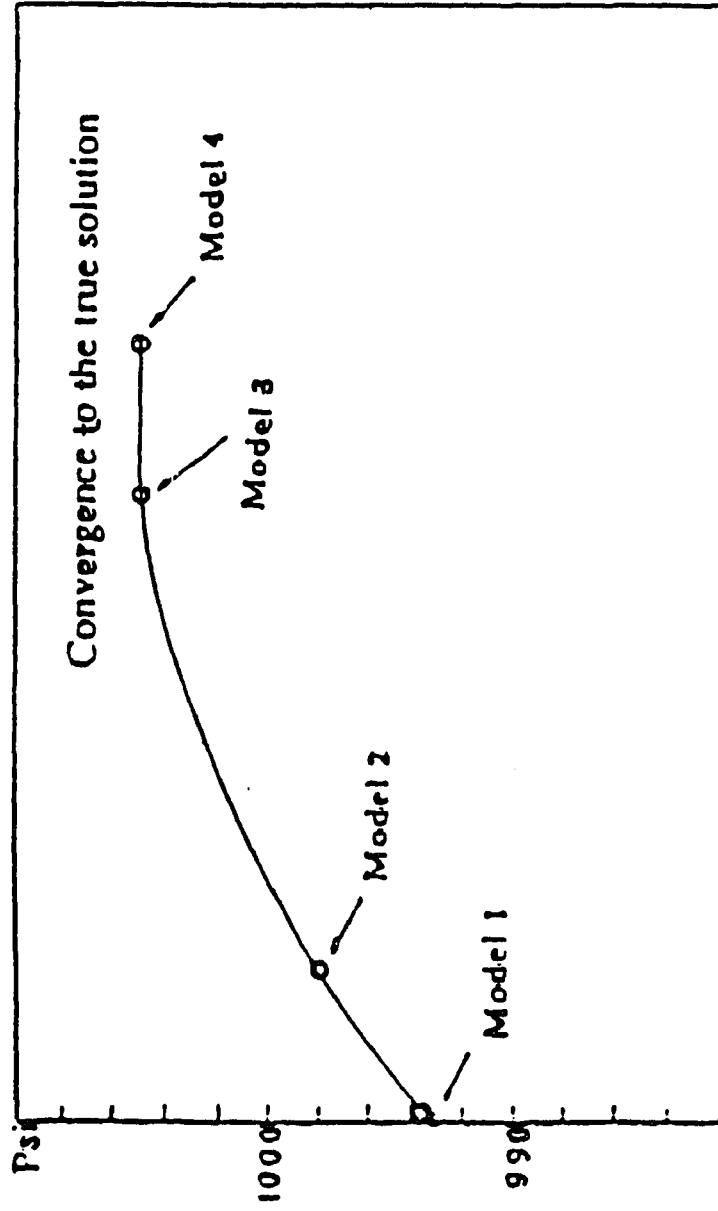


Figure 4.5: Data Convergence curve of Quadrilateral Shell Element Model (for Meridional Stress of the Outer Surface)  $\gamma_s = 20, \beta = 0.2, T = 0.4 \text{ in}, P = 1000 \text{ lb}$

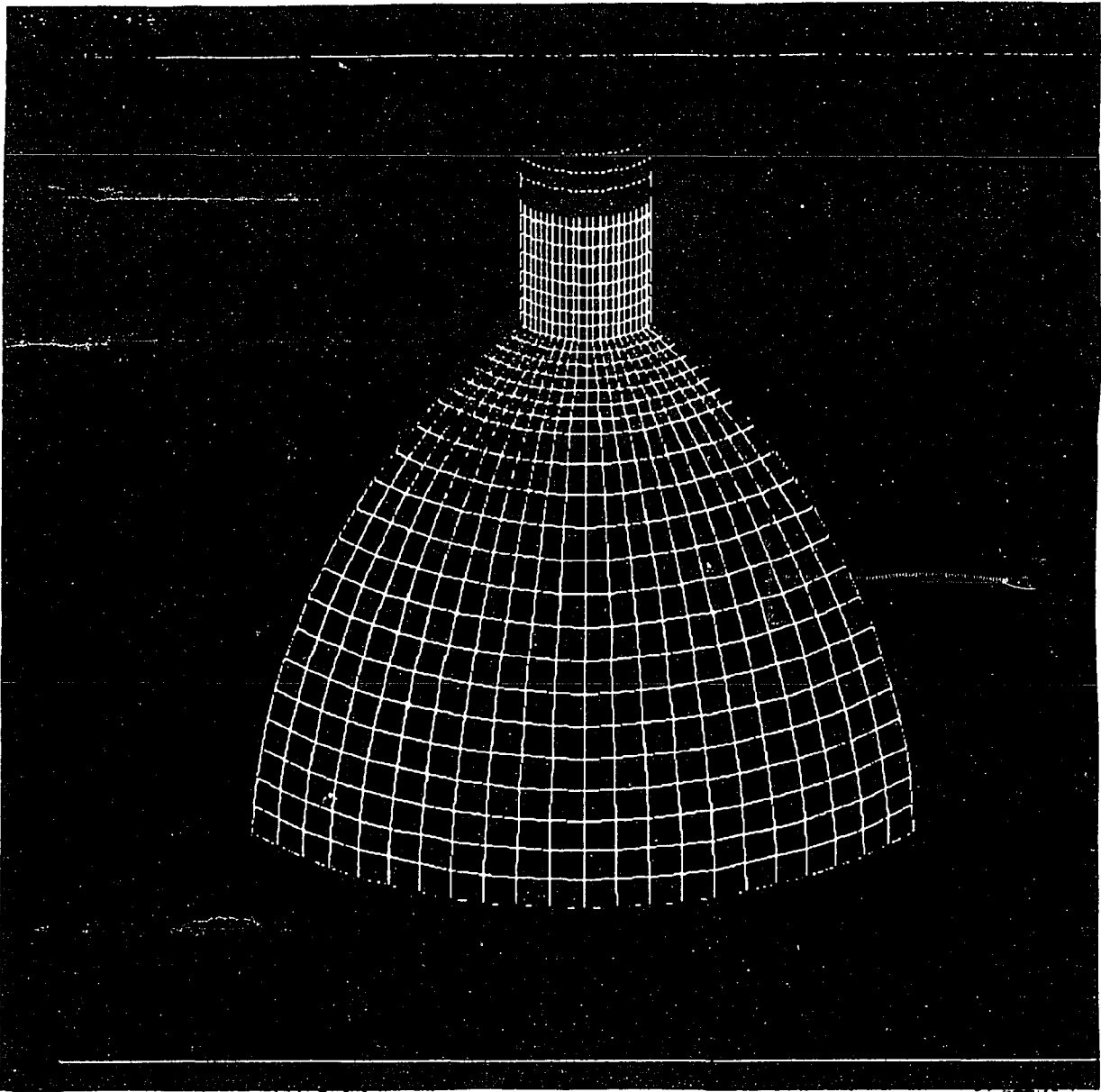


Figure 4.6: Element Plot of Quadrilateral Shell Element Model

For the isoparametric solid element model, there are 10 nodes on the circumference of each quarter with five nodes across the thickness. First, 20 key points are used to divide the whole model into 4 volumes as shown in Figure 4.7. Volumes V1 and V2 are generated with a spherical coordinate system, and volumes V3 and V4 are generated with a cylindrical coordinate system. The element type STIF45 is utilized to generate this isoparametric solid model with 8 nodes at the corners. Smaller sized elements are generated in volumes V2 and V3, where greater stress gradients exist. When  $\gamma_s$  is smaller than 10, the thickness becomes a significant factor for the finite element mesh. Five trial models have been employed as shown in the Table 4.2. Model 1 to Model 4 has 9 elements along the circumference and has 1, 2, 3, or 4 elements across the thickness respectively. Model 5 has 18 elements along the circumference and 4 elements across the thickness. The deviation of resulting stresses for each model as shown in the Table 4.2 and Figure 4.8. It shows the model 4 with 9 elements along the circumference and 4 elements across the thickness to be the most optimum model as it presents very good convergence. Therefore this model is adopted for computations with the isoparametric solid element model. The completely meshed model is shown in Figure 4.9.

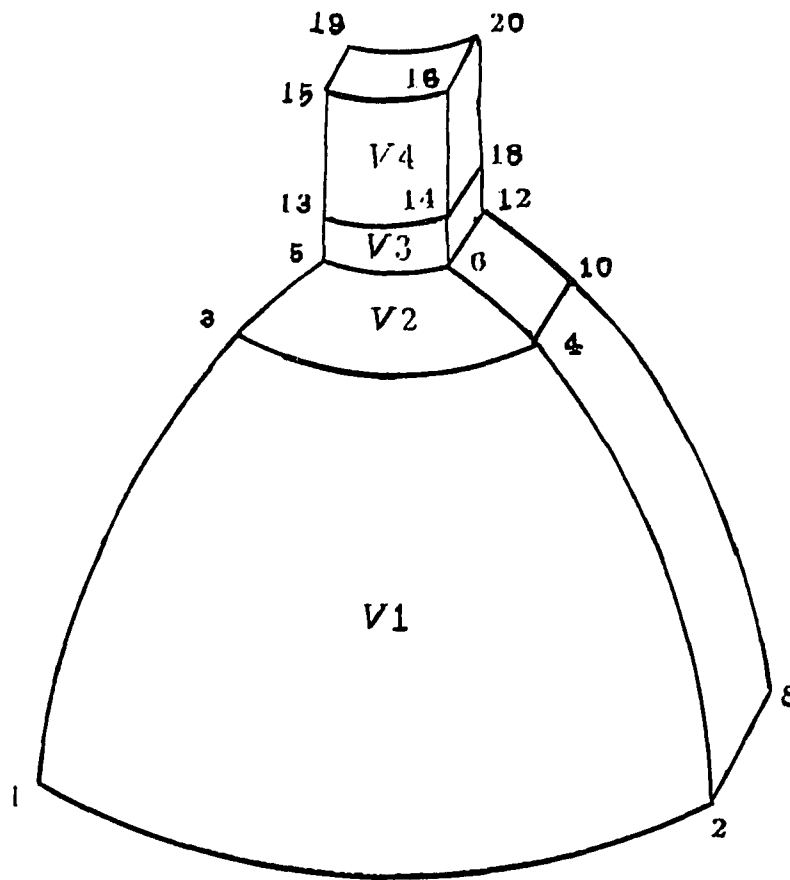


Figure 4.7: Volumes and Keypoints of Isoparametric Solid Element Model

$T = t = 0.4 \text{ in}$ $\gamma_s = 7 \beta = 0.2$	$\sigma_{co}$ Psi	$\sigma_{mo}$ Psi	Maximum Deviation
Model 1	1444	3109	0.65%
Model 2	1472	3170	0.32%
Model 3	1497	3223	0.25%
Model 4	1510	3252	0.15%
Model 5	1512	3257	0.07%

(Total Radial Force = 1000lb upward)

Table 4.2: Data Convergence of Isoparametric Solid Element Model

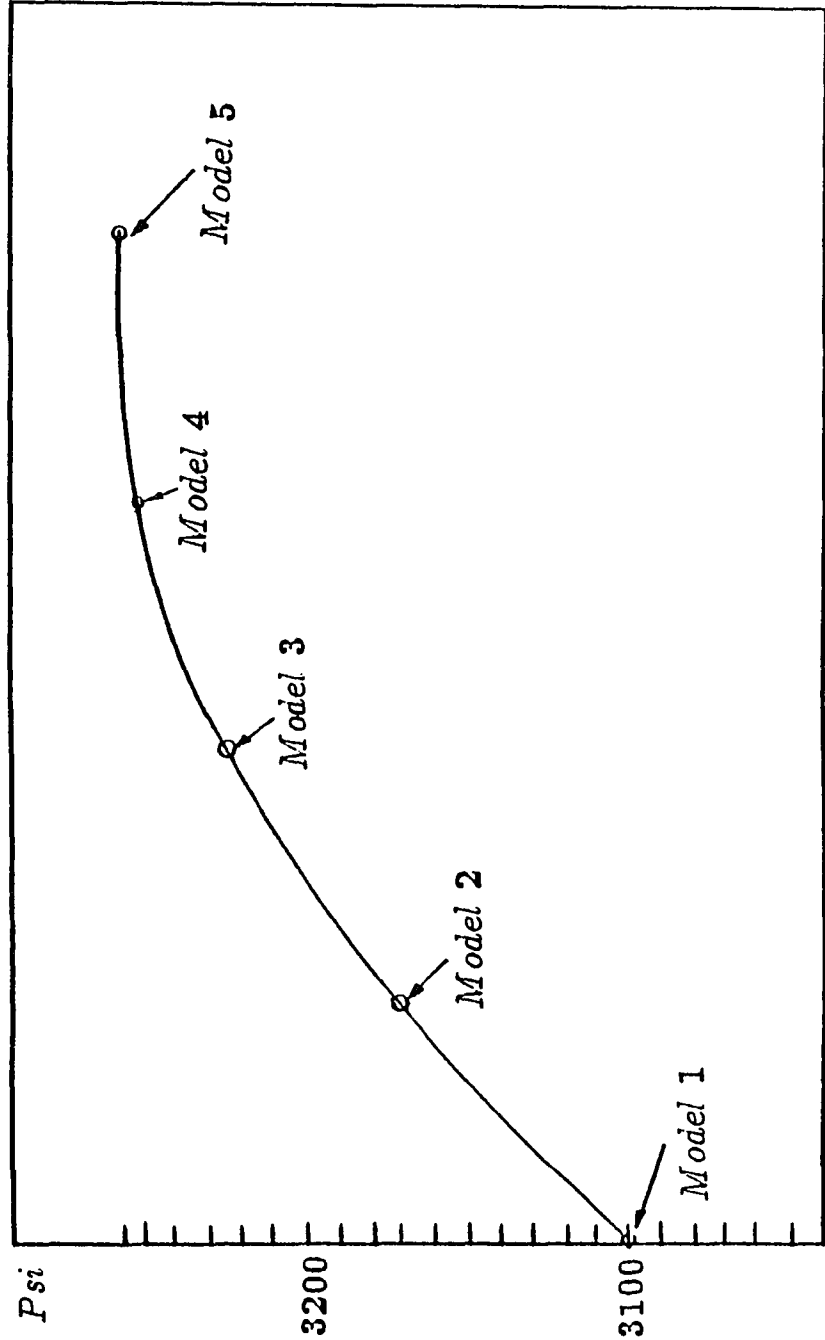


Figure 4.8: Data Convergence Curve of Isoparametric Solid Element (for Meridional Stress of the Outer Surface)  $\gamma_s = 7$ ,  $\beta = 0.2$ ,  $T = 0.4$  inch,  $P = 1000$  lb

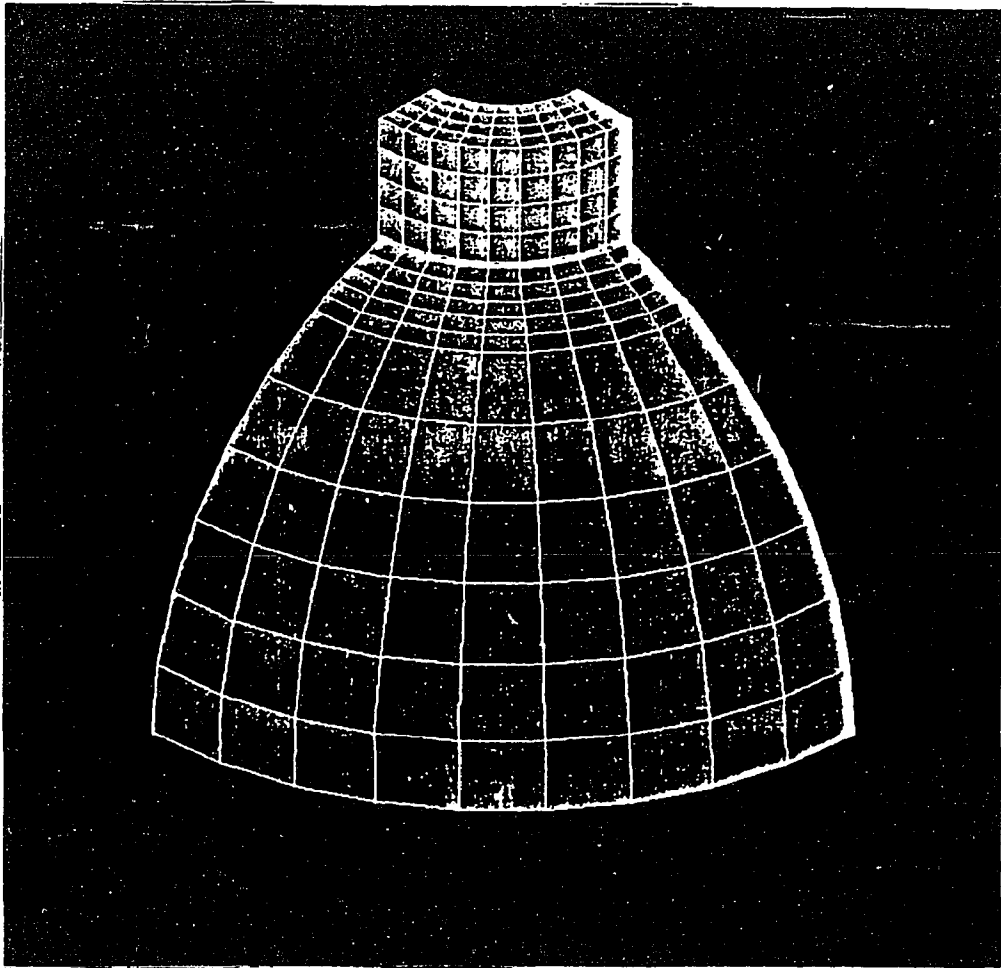


Figure 4.9: Element Plot of Isoparametric Solid Element Model

## 4.5 Boundary Conditions of the Model

Since the nozzle-sphere juncture is symmetrical with the  $xy$  and  $yz$  planes, a quarter portion of the hemisphere is needed as the computational model by setting constraints along the symmetrical planes.

1. Radial Force  $P$ : The radial load  $P$  is simulated by a uniformly distributed nodal force applied on the top of the nozzle as shown in Figure 4.10. All of the nodal displacements are specified as:

- On the  $xy$  plane, the displacement in the  $z$  direction, and rotation about the  $x$  and  $y$  axes are constrained.
- On the  $yz$  plane, the displacement in the  $x$  direction, and rotation about the  $z$  and  $y$  axes are constrained.

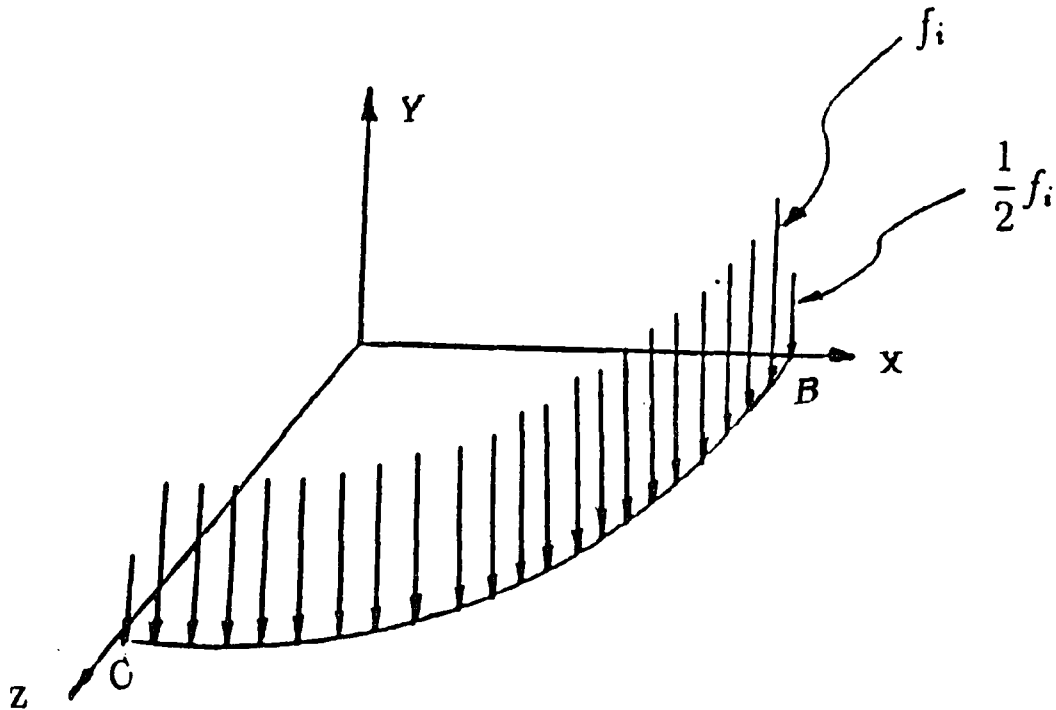


Figure 4.10: Radial Force Pattern (quadrilateral shell element model)

2. Overturning Moment  $M_x$  or  $M_z$ : The typical overturning moment,  $M_z$ , for example, is simulated by linearly distributed forces as shown in Figure 4.11.

For  $M_z$ , all of the nodal displacements are specified as:

- On the  $xy$  plane, the displacement in the  $z$  direction, and the rotation about  $x$  and  $y$  axes are constrained.
- On the  $yz$  plane, the displacement in the  $y$  and  $z$  directions, and the rotation about  $x$  axes are constrained.

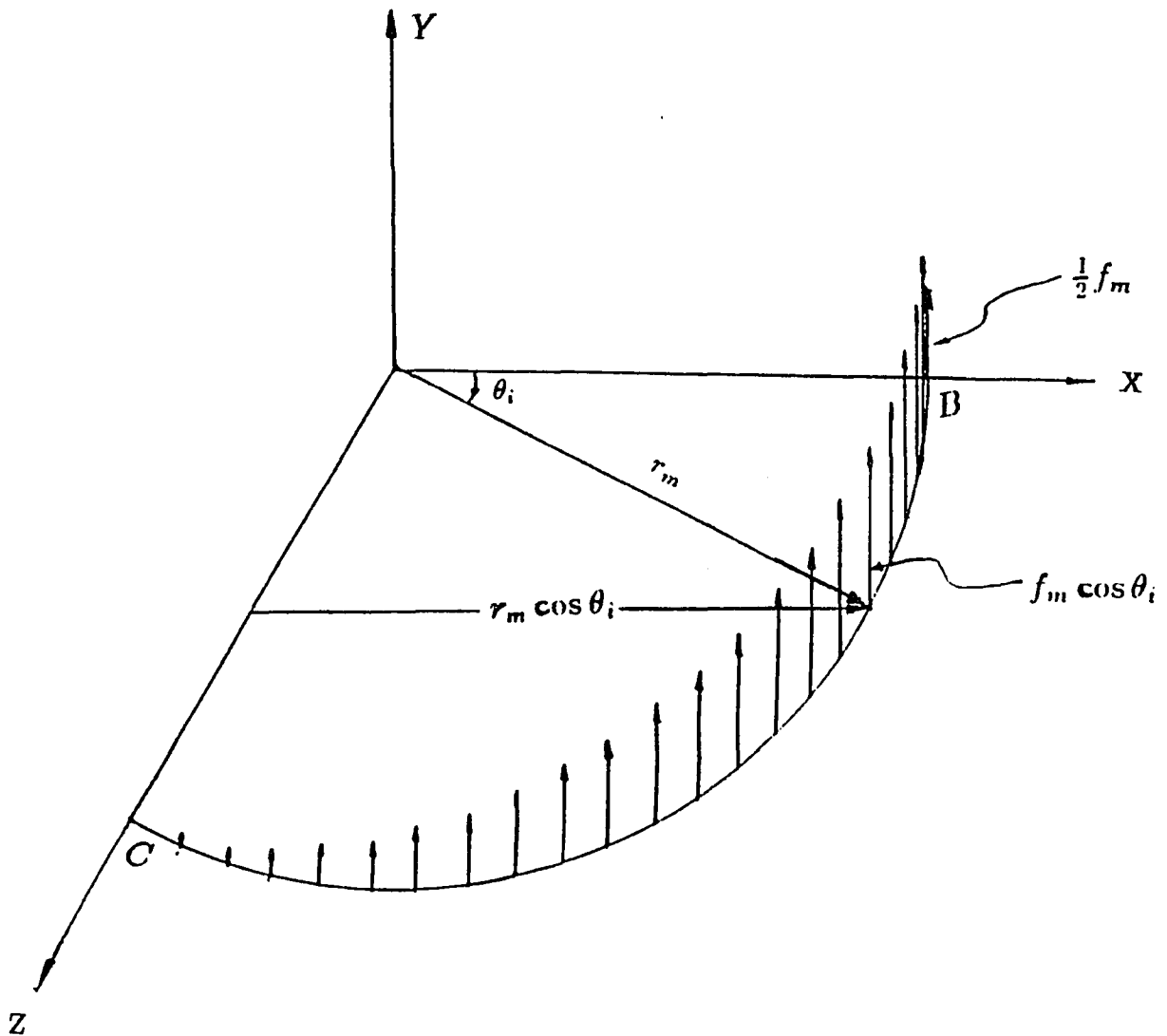


Figure 4.11: Overturning Moment Pattern for  $M_z$  (quadrilateral shell element model)

3. Torsional Moment  $M_T$ : The torsional moment is simulated by uniformly distributed nodal forces tangent to the nozzle-sphere juncture of the model as shown in Figure 4.12. All of the nodal displacements are specified as:

- On the  $xy$  plane, the displacement in the  $x$  and  $y$  direction, and the rotation about  $z$  axis are constrained.
- On the  $yz$  plane, the displacement in the  $y$  and  $z$  direction, and the rotation about  $x$  axis are constrained.

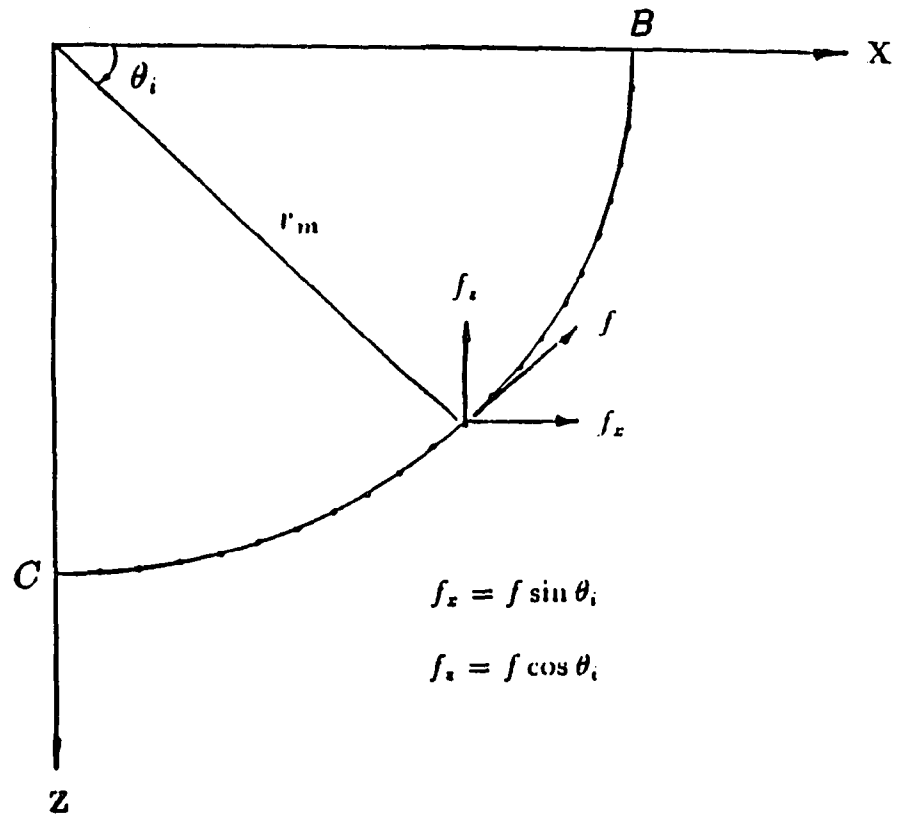


Figure 4.12: Torsional Moment Pattern (quadrilateral shell element model)

4. Horizontal shear force  $V_X$  or  $V_Z$ : The typical shear force,  $V_Z$ , is simulated by the uniformly distributed nodal forces in the negative  $z$  direction as shown in Figure 4.13. All of the nodal displacements are specified as:

- On the  $xy$  plane, the displacement in the  $x$  and  $y$  direction, and the rotation about the  $z$  axis are constrained.
- On the  $yz$  plane, the displacement in the  $x$  direction, and the rotation about  $y$  and  $z$  axes are constrained.

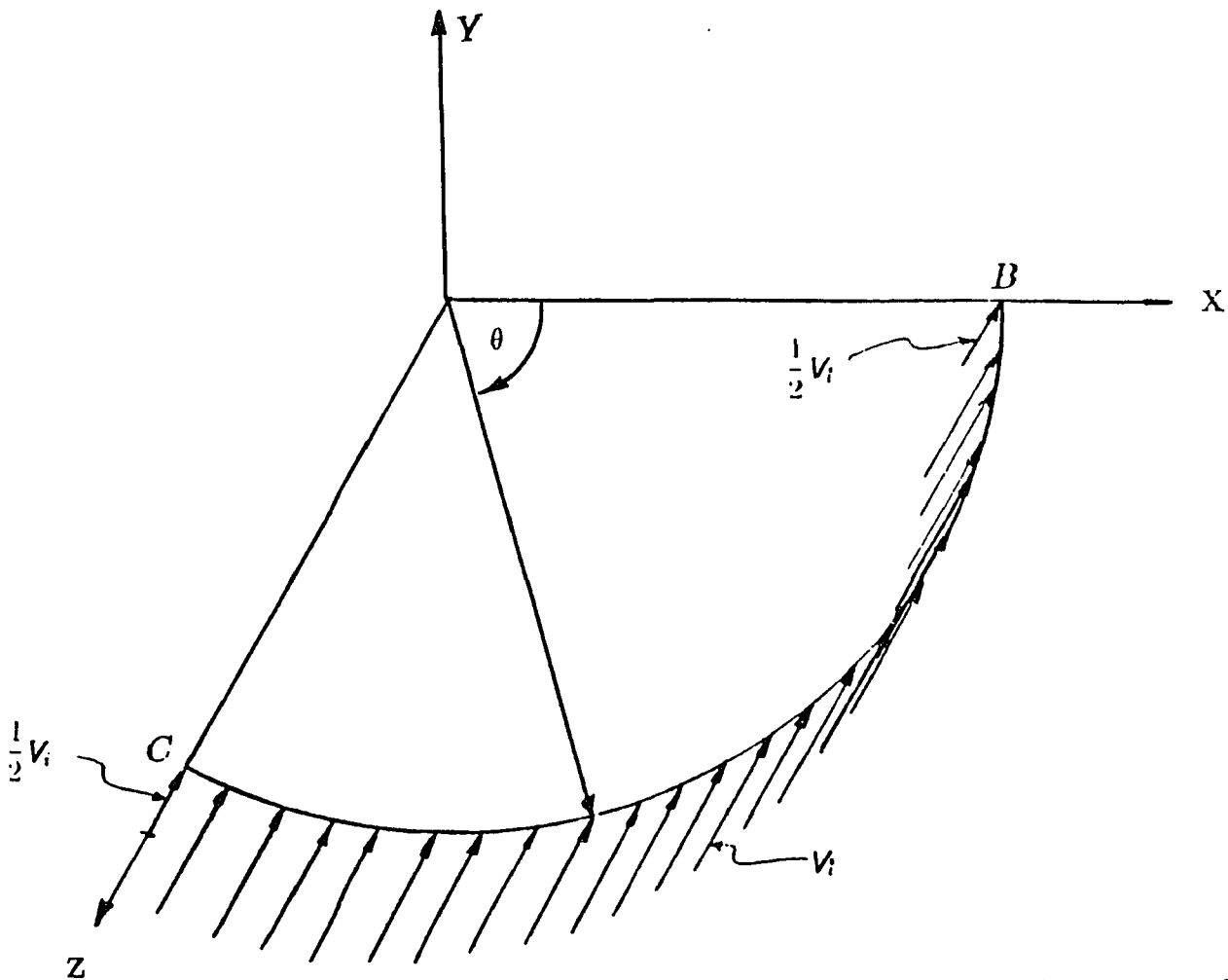


Figure 4.13: Horizontal Shear Force Pattern for  $V_Z$  (quadrilateral shell element model)

## 4.6 Loading Pattern

In this dissertation, the given model is subjected to various loading: radial force, overturning moment, torsional moment and horizontal shear force. All of the external loads are applied in the form of nodal force. Radial nodal force and overturning moment are applied on the top of the nozzle. However, torsional moment and horizontal shear force are applied at the outside surface of the nozzle-sphere juncture. It is assumed that the resulting stresses and strains are within the elastic range of the material, and the resulting stresses and displacements may be normalized by the input force or moment value.

### 4.6.1 Radial Force

In the quadrilateral shell model, the distributed radial load is applied downward (negative  $y$  direction) on to the top of the nozzle. In the isoparametric solid element model, the distributed load is applied equally on the top of the nozzle across the thickness and along the circumference. Since the  $xy$  and  $yz$  planes are symmetric planes, the nodal loads applied directly on these boundary planes are half of the loads applied elsewhere.

For the quadrilateral shell element model as shown in Figure 4.10, the nodal force is:

$$f_i = \frac{P/4}{22} \quad (4.1)$$

For the isoparameter solid element model as shown in Figure 4.14, the nodal force is:

$$f_i = \frac{P/4}{5 \times 9} \quad (4.2)$$

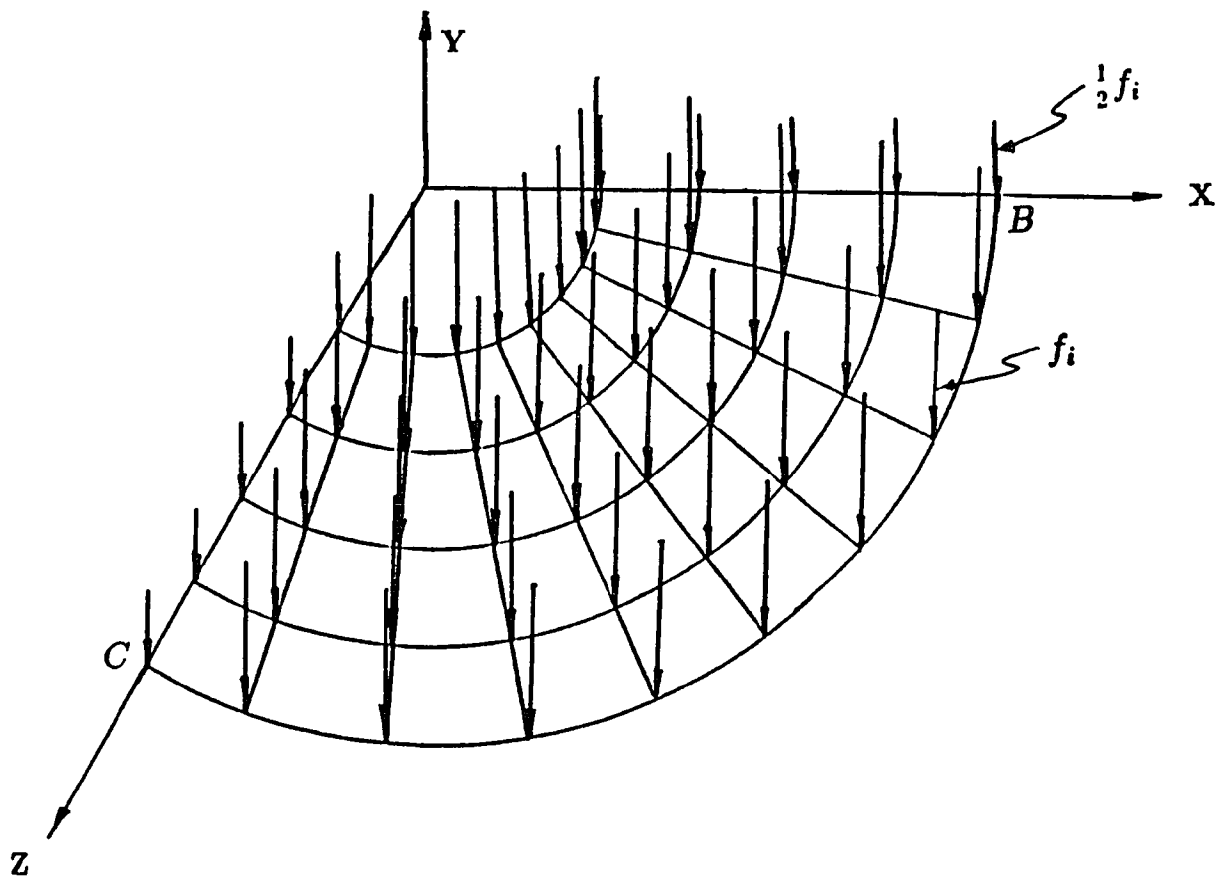


Figure 4.14: Radial Force Pattern (isoparametr solid element model)

## 4.6.2 Overturning Moment

For quadrilateral shell element model:

In the quadrilateral shell element model, there are 22 elements in the circumferential direction as shown in Figure 4.11. The nodal forces in the shell model are distributed by cosine functional relationships, with the nodal force applied on the  $z$  axis being zero.

$$\frac{M_z}{4} = \sum_{i=1}^{22} (f_m \cos \theta_i r_m \cos \theta_i) + \frac{1}{2} f_m r_m \quad (4.3)$$

For isoparametric solid element model:

The nodal forces are again assumed to be a cosine function distribution in the circumferential direction and a linear distribution across the thickness, i.e., those nodal forces are proportional to the distance from the symmetric axis as shown in Figure 4.15. Due to the symmetry condition on the  $xy$  plane, those nodes located on that plane are half of the nodal forces applied elsewhere. There are no nodal forces applied on the  $z$  axis. The equations describing overturning moment are:

$$\frac{M_z}{4} = \sum_{i=1}^9 (f \cos \theta_i r \cos \theta_i) + \frac{1}{2} f r \quad (4.4)$$

where  $\theta_i = 90i/22$ , and

$$f r \cos^2 \theta_i = \cos^2 \theta [f_i (r_m - \frac{1}{2}t) + f_{im} (r_m - \frac{1}{4}t) + f_m r_m + f_{mo} (r_m + \frac{1}{4}t) + f_o (r_m + \frac{1}{2}t)]$$

where

$$f_i = \frac{r_m - \frac{1}{2}t}{r_m} f_m$$

$$f_{im} = \frac{r_m - \frac{1}{4}t}{r_m} f_m$$

$$f_{mo} = \frac{r_m + \frac{1}{4}t}{r_m} f_m$$

$$f_o = \frac{r_m + \frac{1}{2}t}{r_m} f_m$$

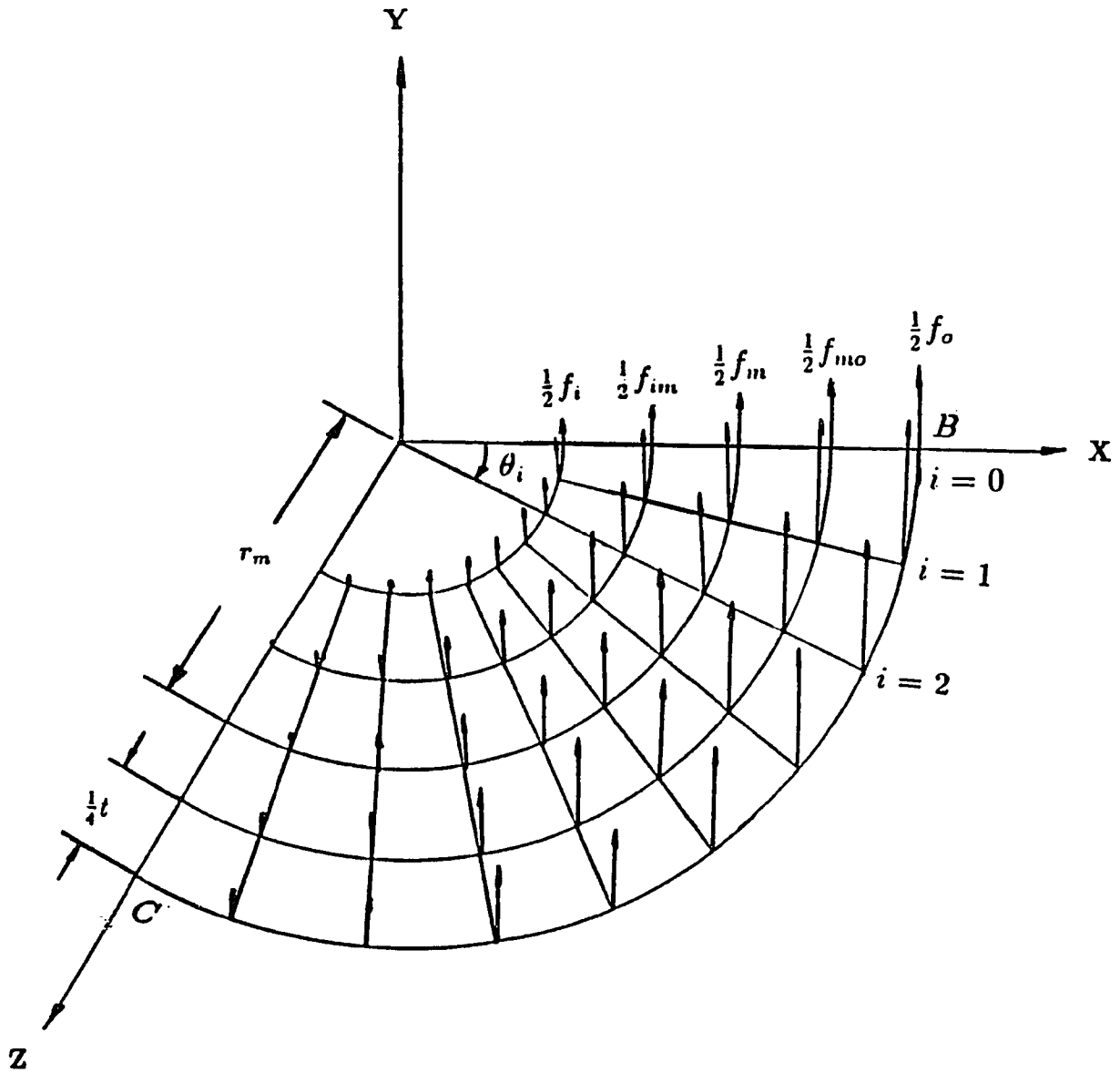


Figure 4.15: Overturning Moment Pattern for  $M_z$ (isoparametric solid element model)

### 4.6.3 Torsional Moment

The tangential forces are applied at each node on the outside surface of the nozzle-sphere intersection. In the quadrilateral shell element model as shown in Figure 4.12 and isoparametric solid element model as shown in Figure 4.16, the nodal force applied at the symmetric plane is half of the normal value applied elsewhere.

For the quadrilateral shell element model the torsional moment is given by:

$$\frac{T}{4} = \sum_{i=1}^{21} (f_x r_m \sin \theta_i + f_z r_m \cos \theta_i) + \frac{1}{2} (f_x r_m + f_z r_m) \quad (4.5)$$

where

$$\theta_i = \frac{90i}{22}$$

$$f_x = f \sin \theta_i$$

$$f_z = f \cos \theta_i$$

$$i = 1, 2, 3, \dots, 22$$

$\theta_i$  is the angular position of the node at the intersection of the model.

For isoparametric solid element model the torsional moment is given by:

$$\frac{T}{4} = \sum_{i=1}^8 (f_x r_o \sin \theta_i + f_z r_o \cos \theta_i) + \frac{1}{2} (f_x r_o + f_z r_o) \quad (4.6)$$

where

$$\theta_i = \frac{90i}{9}$$

$$f_x = f \sin \theta_i$$

$$f_z = f \cos \theta_i$$

$$i = 1, 2, 3, \dots, 9$$

$\theta_i$  is the angular position of the node at the intersection of the model.

$$i = 1, 2, 3, \dots, 9$$

$\theta_i$  is the angular position of the node at the intersection of the model.

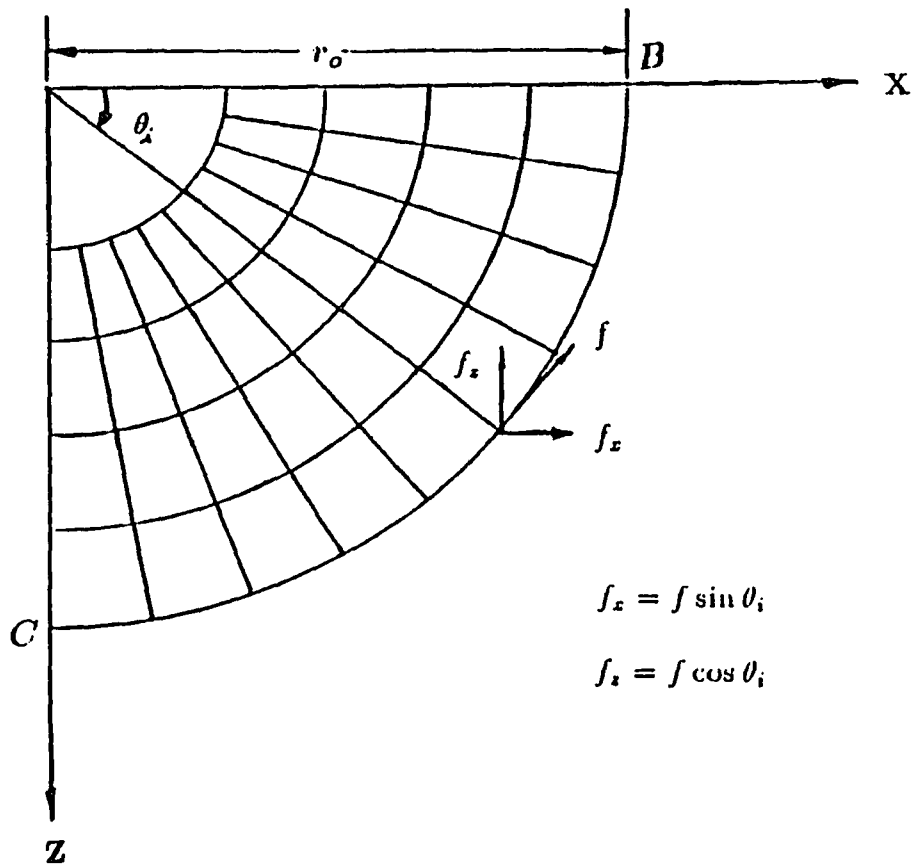


Figure 4.16: Torsional Moment Pattern(isoparametric solid element model)

#### 4.6.4 Horizontal Shear Force

The equal nodal forces are applied at each node on the outside surface of the sphere-nozzle intersection. In the quadrilateral shell element model as shown in Figure 4.13 and the isoparametric solid element model as shown in Figure 4.17, the nodal force applied at the symmetric plane is half of the normal value applied on the nodes elsewhere.

For quadrilateral shell element model:

$$V_i = \frac{V/4}{22} \quad (4.7)$$

For isoparametric solid element model:

$$V_i = \frac{V/4}{9} \quad (4.8)$$

where  $V_i$  is nodal shear force and  $V$  is total shear force

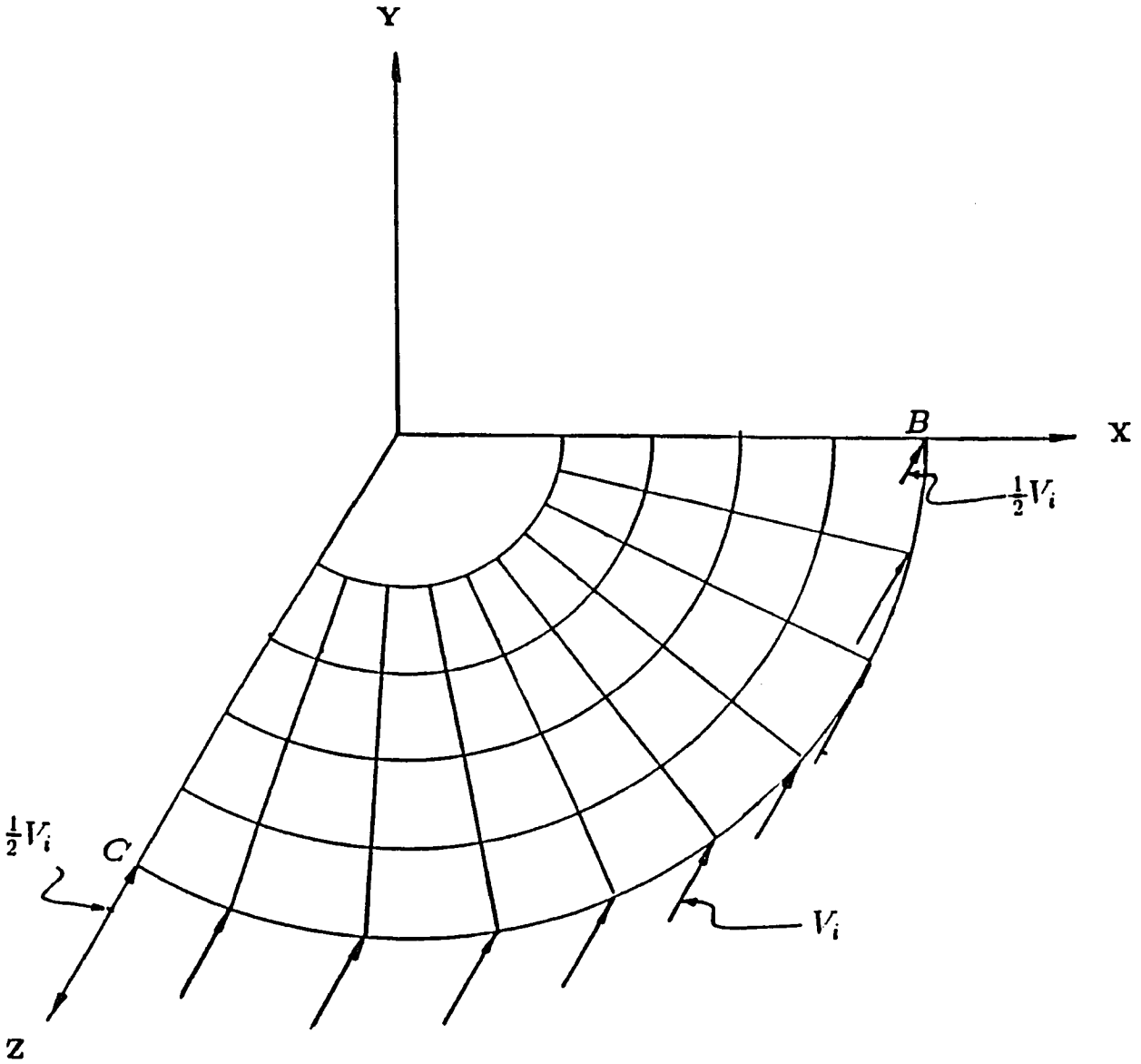


Figure 4.17: Horizontal Shear Force Pattern (isoparametric solid element model)

# Chapter 5

## Numerical Analysis

### 5.1 Radial Force

#### 5.1.1 Local Stress

The numerical results show a biaxial state of stress in the circumferential and meridional directions as shown in Figure 4.3. In this study the uniformly distributed nodal loads are acting downward onto the shell. This distribution causes an uniform compressive membrane stress across the thickness of the juncture. In addition, a local bending stress occurs that it is tensile on the inside surface of the sphere and compressive on the outside surface. The stress coefficient,  $K$ , *psi* per unit radial load, is defined to describe these normal stresses. The circumferential stress is thus given by:

$$\sigma_c = K_c \cdot P \quad (5.1)$$

where  $K_c$  has both membrane and bending components, i.e.

$$K_c = K_{c,m} \pm K_{c,b} \quad (5.2)$$

where the "+" sign is used for the outside surface of the sphere, and the "-" sign is used for the inside surface of the sphere as shown in Appendix C. The second subscript  $m$  stands for membrane and  $b$  stands for bending, respectively. The meridional stress is given by:

$$\sigma_m = K_m \cdot P \quad (5.3)$$

where again,

$$K_m = K_{m,m} \pm K_{m,b} \quad (5.4)$$

From Eqs. (28), (31), (32), (38), and (39) of Bijlaard's paper [8], and from Section 2 of WRC bulletin 107 [28], one also may define:

$$K_{c,b} \cdot T^2 = H_1 \quad (5.5)$$

$$K_{m,b} \cdot T^2 = H_2 \quad (5.6)$$

where  $H_1$  and  $H_2$  are dimensionless parameters. Again, from Eqs. (28), (31), (32), (40), (41) of Bijlaard's paper [8], and from Section 2 of WRC bulletin 107 [28], one may define:

$$K_{c,m} \cdot T^2 = H_3 \quad (5.7)$$

$$K_{m,m} \cdot T^2 = H_4 \quad (5.8)$$

where  $H_3$  and  $H_4$  are also dimensionless parameters. Therefore from Eqs. (5.5), (5.6), (5.7), and (5.8),  $K_{c,b}T^2$ ,  $K_{m,b}T^2$ ,  $K_{c,m}T^2$ , and  $K_{m,m}T^2$  are defined as stress factors due to radial load. For each  $\gamma_s$  value (7, 10, 15, 20, 25, 30, 40, 50, 75,100), the values of,  $K_{c,b}T^2$ ,  $K_{m,b}T^2$ ,  $K_{c,m}T^2$ ,  $K_{m,m}T^2$ , are plotted as functions of  $\beta$  as shown in Figures 6.1-6.4.

### 5.1.2 Comparison of Normal Stresses due to Radial Load

Bijlaard's work on spherical shells was based on the shallow shell theory [26], where the upper limit of  $\beta$  is about 0.3, and the shell is thin (for example,  $\gamma_s$  is larger than

27.5).

In order to compare and verify the stress results from this study with Wichman's work [28], which was based on the Bijlaard's method [9], 3 special models with various  $\beta$  and  $\gamma$  values are used, as shown in Table 5.1. In these three models the stresses in both the meridional and circumferential directions are in excellent agreement with Wichman's.

A fourth model (with  $\gamma_s = 120$  and  $\beta = 0.5$ ) is compared with the experimental results given by W. F. Riley [19], as shown in Table 5.2. Again stress results from the finite element method are in excellent agreement with Riley's although his model had a fillet at the juncture. However, Witt [20] reported that the fillet at the juncture does not contribute significantly to the stress results.

### 5.1.3 Radial Spring Constant

Again, the geometrical parameters  $\gamma_s$  and  $\beta$  are used to evaluate the radial spring constant,  $K_y$ . In theory, the  $y$ -deflection,  $\delta_y$ , is uniformly distributed across the thickness at the juncture. In reality, there are small deviations in  $\delta_y$  between the outside and inside surfaces of the juncture. The average value for  $\delta_y$  has been used to define the spring constant.

From Equations, (31), (32), and (34) in [8], one obtains

$$\frac{\delta_y ET^2}{R_m P} = H_5 \quad (5.9)$$

where  $H_5$  is an arbitrary constant. Then the radial spring constant is defined as

$$K_y = \frac{P}{\delta_y} \quad (5.10)$$

Combining Eq. (5.9) and Eq. (5.10), yields,

$$\frac{K_y}{ET} = \frac{1}{H_s \gamma_s} \quad (5.11)$$

where

$$\gamma_s = \frac{R_m}{T} \quad (5.12)$$

From Eq.(5.11), one observes that  $K_y/ET$  is a normalized radial spring constant. For various  $\gamma_s$  values,  $K_y/ET$  is plotted as a function of  $\beta$  in Figure 6.15.

#### 5.1.4 Comparison of Radial Spring Constant

In Batra & Sun's work [14] which is based on the solution of the governing differential equation given by Reisner [26], the radial spring constant,  $K_R$ , is defined as radial force per unit displacement toward the center of the sphere. Though the deflection in the negative  $y$  direction is theoretically different from radial deflection, that difference is very small and hence it is acceptable to replace  $K_R$  with  $K_y$  when describing the radial spring constant of the model. For  $K_y$ , several special cases of  $\gamma_s$  and  $\beta$  combinations are computed for the purpose of comparing the spring constant results with those of Batra and & Sun's work. These comparisons are shown in Table 5.3. It is noted that, as expected, the finite element method yields a more flexible spring constant than Batra & Sun's work. Since they utilized the differential equation solution from Bijlaard, the sphere was a closed shell without an opening. Naturally, a closed shell is stiffer than one with an opening. One further notes that the disagreement between the the results progressively decreases as the  $\beta$  values decrease; i.e. the discrepancy will be smaller when the opening is small. Thus the radial spring constant results from this dissertation is considered as reasonable.

	Finite Element method		Bijlaard's Method	
	$\sigma_{mo}$ Psi	$\sigma_{co}$ Psi	$\sigma_{mo}$ Psi	$\sigma_{co}$ Psi
$T = t = 0.4in$ All Models				
Model A $\gamma_s = 25 \beta = 0.2$	1537	926.6	1497.5	887.5
Model B $\gamma_s = 50 \beta = 0.1$	2046	1294	2262.5	1300
Model C $\gamma_s = 75 \beta = 0.2$	817	598.6	906.25	582.5

(Total Radial Force = 1000lb upward)

Table 5.1: Comparison of Normal Stresses (Meridional and Circumferential) at the Outside Surface due to Radial Load with Bijlaard's work [9]

	Experimental Method (Strain Gage)		Finite Element Method	
	$\sigma_{mo}$ Psi	$\sigma_{co}$ Psi	$\sigma_{mo}$ Psi	$\sigma_{co}$ Psi
$T = t = 0.1in$				
Model D $\gamma_s = 120 \beta = 0.5$	20700	16600	20700	15900

(Total Radial Force = 6000lb upward)

Table 5.2: Comparison of Normal Stresses (Meridional and Circumferential) at the Outside Surface due to Radial Load with Rily's Experimental Work [19]

	Finite Element Method lb/in	Batra & Sun Work lb/in
$T = 0.4 \text{ in}$ $\gamma_s = 25 \beta = 0.2$	$3.71 \times 10^6$	$4.00 \times 10^6$
$T = 0.4 \text{ in}$ $\gamma_s = 50 \beta = 0.1$	$1.39 \times 10^6$	$1.50 \times 10^6$
$T = 0.2 \text{ in}$ $\gamma_s = 50 \beta = 0.1$	$6.94 \times 10^5$	$7.50 \times 10^5$
$T = 1 \text{ in}$ $\gamma_s = 150 \beta = 0.033$	$7.81 \times 10^5$	$8.87 \times 10^5$
$T = 0.4 \text{ in}$ $\gamma_s = 75 \beta = 0.2$	$2.06 \times 10^6$	$2.28 \times 10^6$

Table 5.3: Comparison of  $K_y$  with Batra & Sun's Work [14] (based on the Theoretical Solution from Bijlaard)

## 5.2 Overturning Moment

### 5.2.1 Local Stress

Again, numerical results show a biaxial state of stresses in circumferential and meridional directions. Each stress has two components, the membrane stress and bending stress. Referring to Figure 4.3, the moment  $M_Z$  causes a tensile membrane stress across the thickness of the juncture at point  $B$ . Also, local bending stress occurs at point  $B$  that is tensile at the outside of the juncture  $B_U$  and compressive at the inside  $B_L$  as shown in Figure 5.1. Using the stress coefficient,  $K$ , *psi* per unit overturning moment, to define these normal stresses, the circumferential stress is given by:

$$\sigma_c = K_c \cdot M_Z \quad (5.13)$$

where  $K_c$  has both membrane and bending components, i.e.

$$K_c = K_{c,m} \pm K_{c,b} \quad (5.14)$$

the "+" sign is used for the outside surface, and the "-" sign is used for the inside surface as shown in Appendix C. The subscript  $m$  stands for membrane, and  $b$  stands for bending, respectively. The meridional stress is given by:

$$\sigma_m = K_m \cdot M_Z \quad (5.15)$$

where again,

$$K_m = K_{m,m} \pm K_{m,b} \quad (5.16)$$

From Eqs. (68), (69), (70), and (71) of Bijlaard's paper [10], and from Section 2 of WRC bulletin 107 [28], one may also define

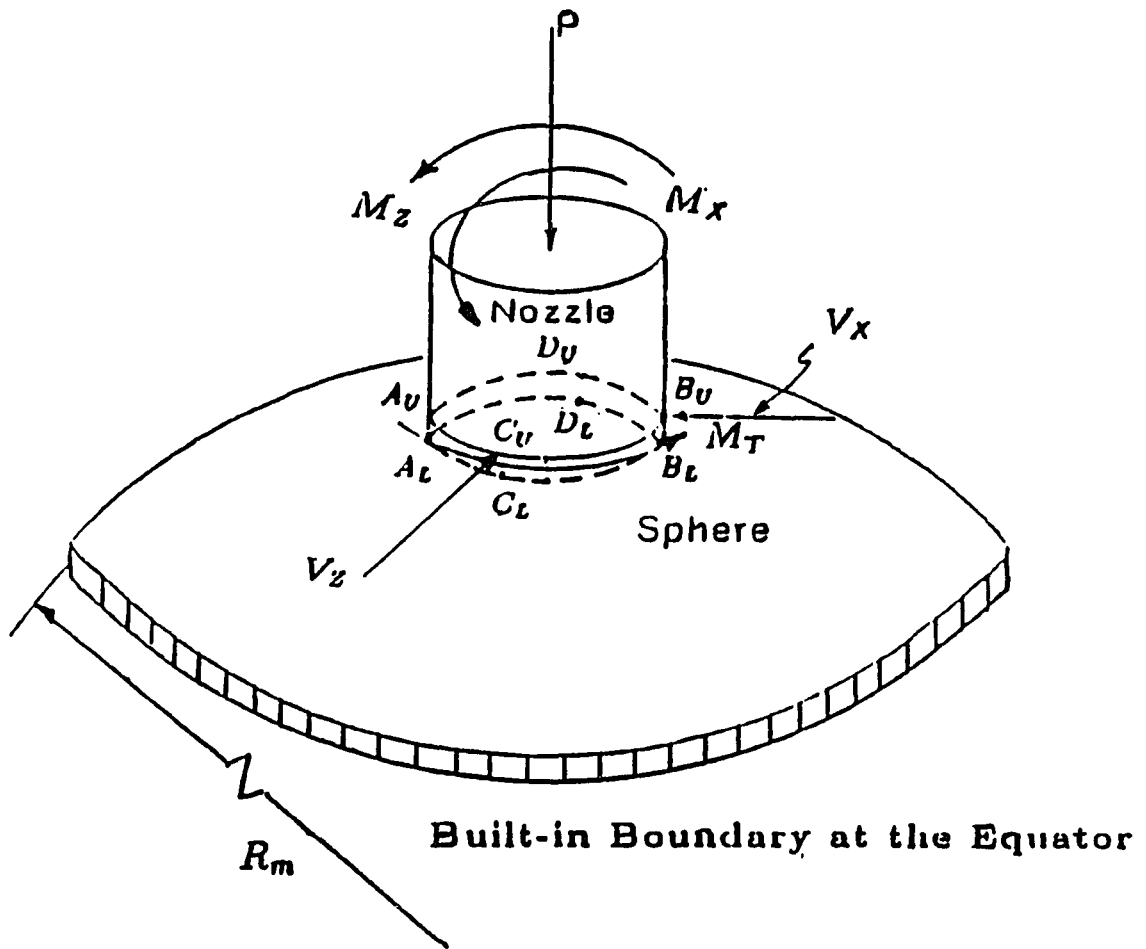


**Figure 5.1: Superposition of Various External Loads Applied on the Model**

$$K_{c,b} \cdot T^3 = H_6 \quad (5.17)$$

$$K_{m,b} \cdot T^3 = H_7 \quad (5.18)$$

where  $H_6$  and  $H_7$  are dimensionless parameters. From Eqs. (68), (69), (72), and (73) of Bijlaard's paper [10], and from Section 2 of WRC bulletin 107 [28], one may define

$$K_{c,m} \cdot T^3 = H_8 \quad (5.19)$$

$$K_{m,m} \cdot T^3 = H_9 \quad (5.20)$$

where  $H_8$  and  $H_9$  are also dimensionless parameters.  $K_{c,b}T^3$ ,  $K_{m,b}T^3$ ,  $K_{c,m}T^3$ , and  $K_{m,m}T^3$  are stress factors. They are plotted against  $\gamma_s$  and  $\beta$  as shown in Figures 6.5-6.8.

### 5.2.2 Comparison of Normal Stresses due to Overturning Moment

As illustrated in the discussion of radial load, normal stress results from three models due to Bijlaard are compared to the normal stress results from the finite element method due to an overturning moment. These comparisons, which exhibit excellent agreement, are shown in Table 5.4.

In addition, Riley's experimental results [19] with  $\gamma_s = 120$  and  $\beta = 0.5$  are compared with results from this study as shown in Table 5.5 and Figure 5.2. Again these stresses are in excellent agreement.

	Bijlaard's method		Finite Element Method	
	$\sigma_{mo}$ Psi	$\sigma_{co}$ Psi	$\sigma_{mo}$ Psi	$\sigma_{co}$ Psi
$T = t = 0.4in$				
Model a $\gamma_s = 25 \beta = 0.2$	1829	1021	2050	1049
Model b $\gamma_s = 50 \beta = 0.1$	2568	1257	2433	1207
Model c $\gamma_s = 75 \beta = 0.2$	1283	797	1215	774

(Total overturning moment = 18000 *in-lb*)

Table 5.4: Comparison of Normal Stresses (Meridional and Circumferential) at the outside surface due to Overturning Moment with Bijlaard's Theoretical Solution

	Experimental Method (Strain Gage)		Finite Element Method	
	$\sigma_{mo}$ Psi	$\sigma_{co}$ Psi	$\sigma_{mo}$ Psi	$\sigma_{co}$ Psi
$T = t = 0.1in$				
Model d $\gamma_s = 120 \beta = 0.5$	23500	15500	20576	15258

(Total overturning moment = 18000 *in-lb*)

Table 5.5: Comparison of Normal Stresses (Meridional and Circumferential) at the Outside Surface due to Overturning Moment with Rily's Experimental Work

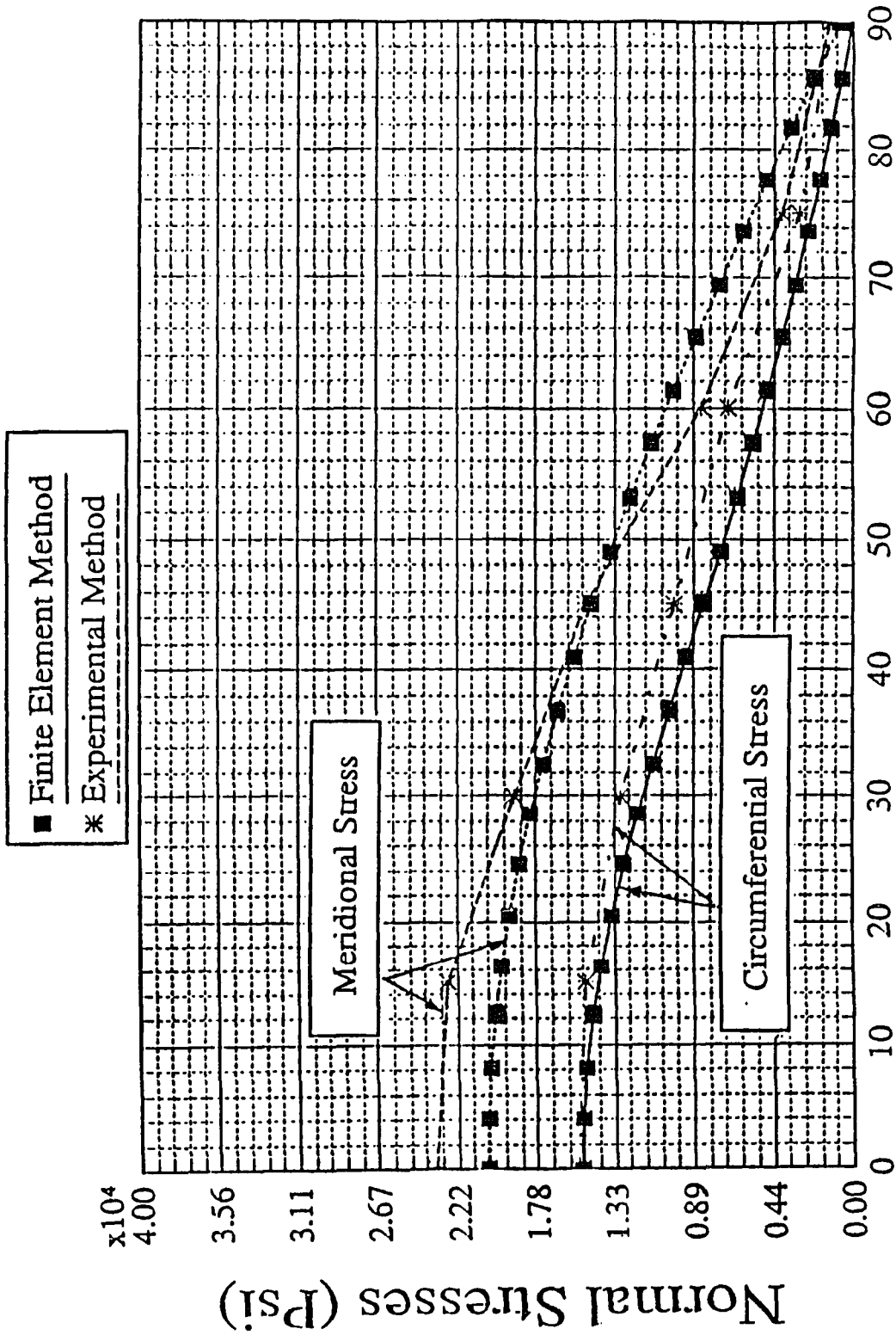


Figure 5.2 - Comparison of Normal Stresses due to Overturning Moment between Finite Element Method and Experiment Method ( $\gamma=120, \beta=0.5$ ) [19]

### 5.2.3 Rotational Spring Constant due to Overturning Moment

Computation results have shown that there are small deviations in  $\phi_M$  between the outside and inside surfaces of the juncture at point  $B$  (Figure 3.4). The average value for  $\phi_M$  has been used to define the spring constant. From Equations. (48), (68), and (69) of Bijlaard [10], one obtains

$$\frac{\delta_w ET^2}{M_Z \sqrt{\gamma_s} \cos \theta} = H_{10} \quad (5.21)$$

where  $H_{10}$  is dimensionless. The rotational spring constant is defined as

$$K_{\phi_M} = \frac{M_Z}{\phi_M} \quad (5.22)$$

where  $\phi_M$  is shown in the Figure 5.3, and

$$\phi_M = \frac{\delta_w}{r_m} \quad (5.23)$$

Combining Eq. (5.23) and Eq. (5.22), yields,

$$\frac{K_{\phi_M}}{ET^3} = \frac{\beta \sqrt{\gamma_s}}{H_5} \quad (5.24)$$

where

$$\gamma_s = \frac{R_m}{T} \quad (5.25)$$

From Eq.(5.24), one selects  $K_{\phi_M}/ET^3$  as a normalized rotational spring constant.

For various  $\gamma_s$  values,  $K_{\phi_M}/ET^3$  is plotted as function of  $\beta$  in Figure 6.16.

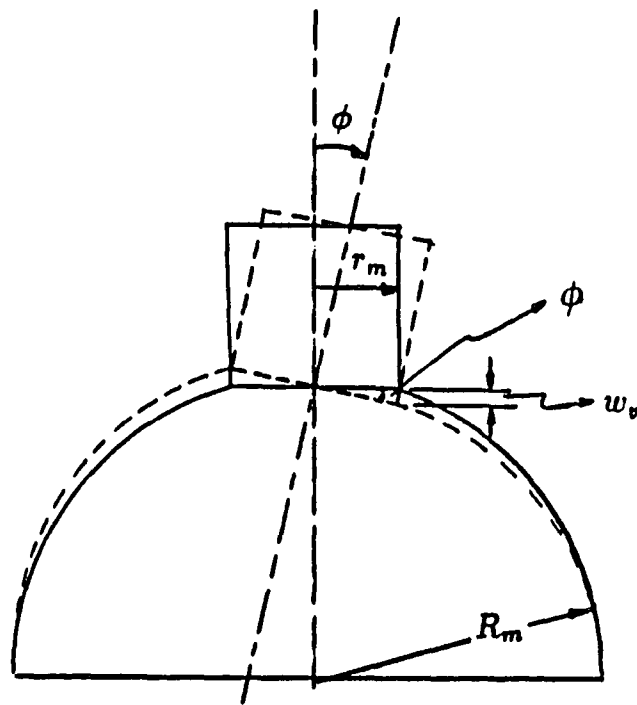


Figure 5.3: Angular Displacement by Overturning Moment

### 5.2.4 Comparison of Rotational Spring Constant due to Overturning Moment

Identical  $\gamma_s$  and  $\beta$  combinations are utilized in comparing the rotational spring constant results from Batra & Sun's work with the results from the finite element method. These comparisons are shown in Table 5.6. It is noted that the results are in very good agreement, however, the finite element method yields a more flexible rotational spring constant than the theoretical method.

	Finite Element Method <i>in-lb/rad</i>	Batra & Sun Work <i>in-lb/rad</i>
$T = 0.4 \text{ in}$ $\gamma_s = 25 \beta = 0.2$	$1.4 \times 10^7$	$1.47 \times 10^7$
$T = 0.4 \text{ in}$ $\gamma_s = 50 \beta = 0.1$	$7.09 \times 10^6$	$7.3 \times 10^6$
$T = 0.2 \text{ in}$ $\gamma_s = 50 \beta = 0.1$	$8.86 \times 10^5$	$9.13 \times 10^5$
$T = 0.4 \text{ in}$ $\gamma_s = 75 \beta = 0.2$	$5.29 \times 10^7$	$5.54 \times 10^7$

Table 5.6: Comparison of  $K_{\phi_M}$  due to the Overturning Moment with Batra & Sun's Work [15] (based on the Theoretical Solution from Bijlaard)

## 5.3 Torsional Moment

### 5.3.1 Local Stress

It is known that the torsional moment induces pure shear. The torsional shear stress is given by

$$\tau = K_{ts} \cdot M_T \quad (5.26)$$

where the stress coefficient,  $K_{ts}$ , is shear stress per unit torsional moment. From numerical data, this shear stress coefficient can be defined as:

$$K_{ts} T^3 = H_{11} \quad (5.27)$$

where  $H_{11}$  is dimensionless, and  $K_{ts} T^3$  is a shear stress factor due to torsional moment, which is plotted for various  $\gamma_s, \beta$  combinations in Figure 6.9.

### 5.3.2 Comparison of the Shear Stress

Bijlaard employed the condition of static equilibrium to derive the average shear stress in the shell at the juncture as  $\tau = M_T / (2\pi r_m^2 T)$ . Figure 5.4 shows the comparison of FEM shear stress results with the above equation. It shows that the FEM results are in very good agreement with the average shear stress mentioned above.

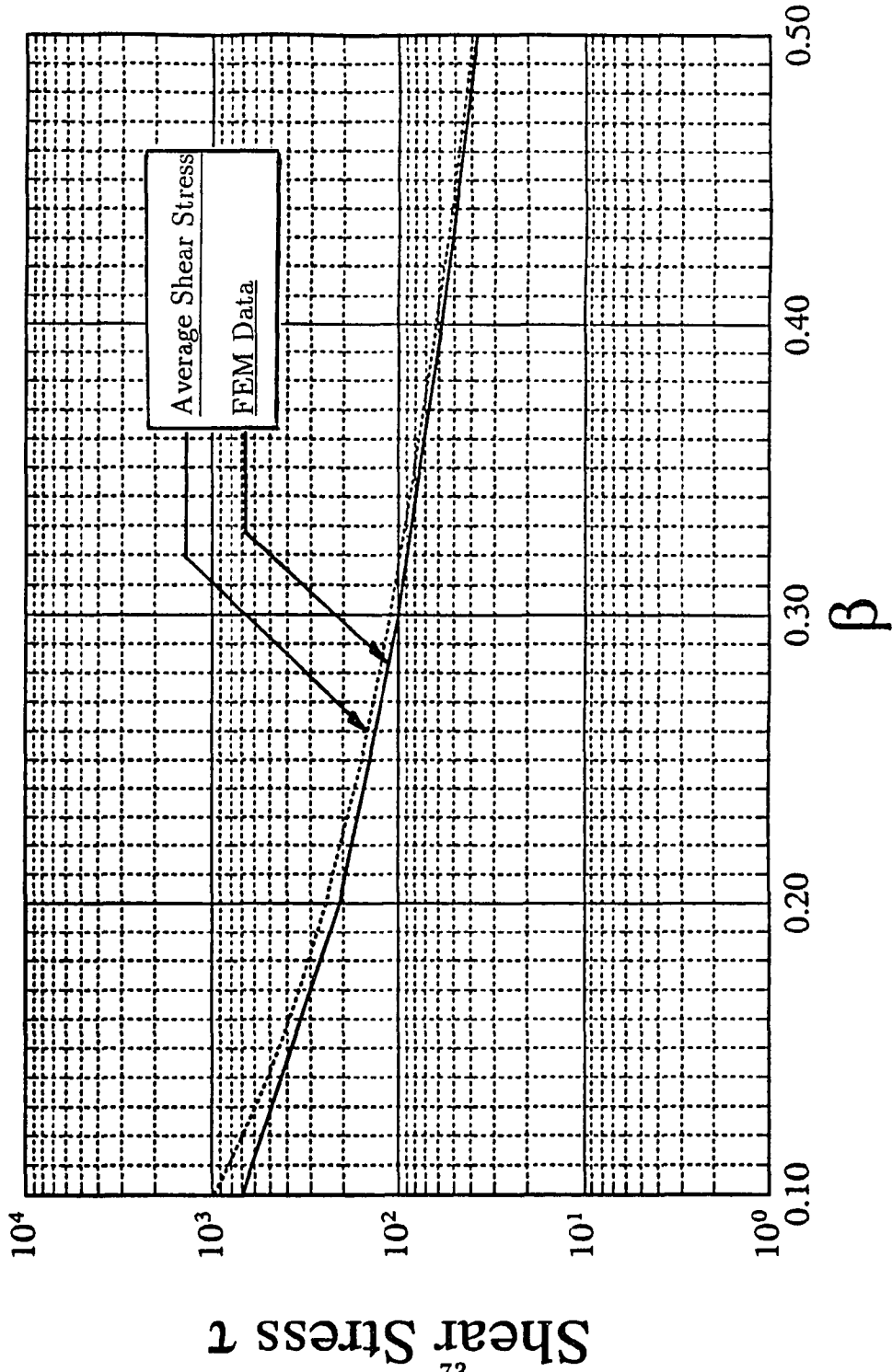


Figure 5.4 - Comparison of Shear Stress due to Torsional Moment with Average Shear Stress  
 ( $\gamma_s = 50$ ,  $M_T = 10000 \text{ in-lb}$ ,  $T = 0.4 \text{ in}$ )

### 5.3.3 Torsional Spring Constant

Again, the average value of  $\theta_T$  across the thickness of the model is used to define the torsional spring constant:

$$K_{\theta_T} = \frac{M_T}{\theta_T} \quad (5.28)$$

Referring to Figure 4.12, with

$$\theta_T = \frac{u_x \sin \theta_i - u_z \cos \theta_i}{r_m} \quad (5.29)$$

where  $u_x$  and  $u_z$  are normal displacements in  $x$  and  $z$  direction respectively. Again, one may define:

$$\frac{K_{\theta_T}}{ET^3} = H_{12} \quad (5.30)$$

$K_{\theta_T}/ET^3$  is a normalized torsional spring constant which is plotted with various  $\gamma_s$  and  $\beta$  combinations in Figure 6.17

### 5.3.4 Comparison of the Torsional Spring Constant

For the case of  $\beta = 0.1$ , this study adopted the similar model as that of the nozzle-pipe connection developed by Chiou & Sun [29]. When  $\beta$  is very small, the juncture of the piping-nozzle model remains practically on the same plane, hence the curvature effect is not significant. A comparison of the torsional spring constants for each combination for 6 special values of  $\gamma_s$  (10, 15, 20, 25, 30, 50) with  $\beta$  of 0.1 is shown in Table 5.7. The torsional spring constants calculated by the finite element method are also compared with the theoretical data derived from Eqs.(3.92) to (3.97) as shown in Table 5.8. It shows that the FEM results are in agreement with the theoretical results, however, the FEM values are more flexible.

	Nozzle-Sphere Model <i>in-lb/rad</i>	Nozzle-Piping Model <i>in-lb/rad</i>
$T = 0.4 \text{ in}$ $\gamma_s = 10 \beta = 0.1$	$1.18 \times 10^7$	$1.10 \times 10^7$
$T = 0.4 \text{ in}$ $\gamma_s = 15 \beta = 0.1$	$2.52 \times 10^7$	$2.04 \times 10^7$
$T = 0.4 \text{ in}$ $\gamma_s = 20 \beta = 0.1$	$4.26 \times 10^7$	$3.62 \times 10^7$
$T = 0.4 \text{ in}$ $\gamma_s = 25 \beta = 0.1$	$6.31 \times 10^7$	$5.71 \times 10^7$
$T = 0.4 \text{ in}$ $\gamma_s = 30 \beta = 0.1$	$8.87 \times 10^7$	$8.15 \times 10^7$
$T = 0.4 \text{ in}$ $\gamma_s = 50 \beta = 0.1$	$2.2 \times 10^8$	$1.45 \times 10^8$

Table 5.7: Comparison of Torsional Spring Constant with Pipe-Nozzle Connection Solution from Chiou and Sun (when the nozzle is very small) [29]

	Finite Element Method <i>in-lb/rad</i>	Theoretical Method <i>in-lb/rad</i>
T = 0.4 in $\gamma_s = 50 \beta = 0.1$	$2.26 \times 10^8$	$2.36 \times 10^8$
T = 0.4 in $\gamma_s = 50 \beta = 0.2$	$8.66 \times 10^8$	$10.2 \times 10^8$
T = 0.4 in $\gamma_s = 75 \beta = 0.1$	$5.09 \times 10^8$	$5.37 \times 10^8$
T = 0.4 in $\gamma_s = 75 \beta = 0.2$	$1.95 \times 10^9$	$2.35 \times 10^9$
T = 0.4 in $\gamma_s = 100 \beta = 0.1$	$9.05 \times 10^8$	$9.50 \times 10^8$
T = 0.4 in $\gamma_s = 100 \beta = 0.2$	$3.46 \times 10^9$	$4.21 \times 10^9$

Table 5.8: Comparison of Torsional Spring Constant with Theoretical Solution

## 5.4 Horizontal Shear Force

In the horizontal shear force model, the nodal shear forces are uniformly applied in the negative  $z$  direction on the juncture as shown in Figure 4.13. The resulting normal stresses (circumferential and meridional) are larger as the angular position  $\theta$  increases. Thus the maximum normal stress occurs at point  $C_U$  or  $C_L$  as shown in Fig.5.1. The shear stress  $\tau$  at point  $B_U$  and point  $B_L$  is maximum. Due to the thin thickness, the difference of the shear stresses between outside surface and inside surface are insignificant. Thus the mean value of the shear stress across the thickness is recorded.

### 5.4.1 Local Stress

The numerical results also show a biaxial state of stress in both circumferential and meridional directions. In this study the distributed load is acting horizontally on the shell in the negative  $z$  direction. This load causes a tensile meridional membrane stress and compressive circumferential membrane stress across the thickness of the juncture. Also, local bending stress occurs linearly across the thickness. Again the normal stress coefficient,  $K$ , *psi* per unit horizontal shear force is used to define these normal stresses. The circumferential stress is given by:

$$\sigma_c = K_c \cdot V_Z \quad (5.31)$$

where  $K_c$  has both bending and membrane components, i.e.

$$K_c = K_{c,m} \pm K_{c,b} \quad (5.32)$$

where the "+" sign is used for the outside surface, and the "-" sign used for the inside surface as shown in Appendix C. The subscript  $m$  stands for membrane, and

$b$  stands for bending, respectively. The meridional stress is given by:

$$\sigma_m = K_m \cdot V_Z \quad (5.33)$$

where again,

$$K_m = K_{m,m} \pm K_{m,b} \quad (5.34)$$

For the numerical results, one defines:

$$K_{c,b} \cdot T^2 = H_{12} \quad (5.35)$$

$$K_{m,b} \cdot T^2 = H_{13} \quad (5.36)$$

$$K_{c,m} \cdot T^2 = H_{14} \quad (5.37)$$

$$K_{m,m} \cdot T^2 = H_{15} \quad (5.38)$$

where  $H_{12}$ ,  $H_{13}$ ,  $H_{14}$ , and  $H_{15}$  are again dimensionless, and  $K_{c,b}T^2$ ,  $K_{m,b}T^2$ ,  $K_{c,m}T^2$ , and  $K_{m,m}T^2$  are stress factors, which are plotted as functions of  $\gamma_s$  and  $\beta$  as shown in Figures 6.10-6.13.

From section 2.3.4.1 of WRC bulletin 107 [28], the shear stress coefficient can be defined as:

$$K_{vs} = \frac{\tau}{V_Z} = \frac{1}{r_m T \pi} \quad (5.39)$$

Substituting  $r_m = \gamma_s T \beta$  into Eq.(5.39), one obtains

$$K_{v_s} T^2 = \frac{1}{\pi \gamma_s \beta} \quad (5.40)$$

From Eq.(5.40), one may plot  $K_{v_s} T^2$ , the shear stress factor, as a function of  $\gamma_s$  and  $\beta$  as shown in Figure 6.14.

### 5.4.2 Comparison of Stresses

Bijlaard employed the condition of static equilibrium to derive the Average shear stress of the shell at the juncture as:

$$\tau = \frac{V_Z}{\pi r_m T} \quad (5.41)$$

However, the finite element method results show that shear force induces a significant amount of normal stress around the juncture. Bijlaard's solution did not provide for such normal stresses. Furthermore, the shear stress calculated by bijlaard's formula is larger than the shear stress calculated by the finite element method. For a given  $\gamma_s$ , the induced shear stress is relatively large when  $\beta$  value is small. The deviation of the shear stress between the theoretical formula and the finite element method decreases as the  $\beta$  value increases as shown in Figure 5.5.

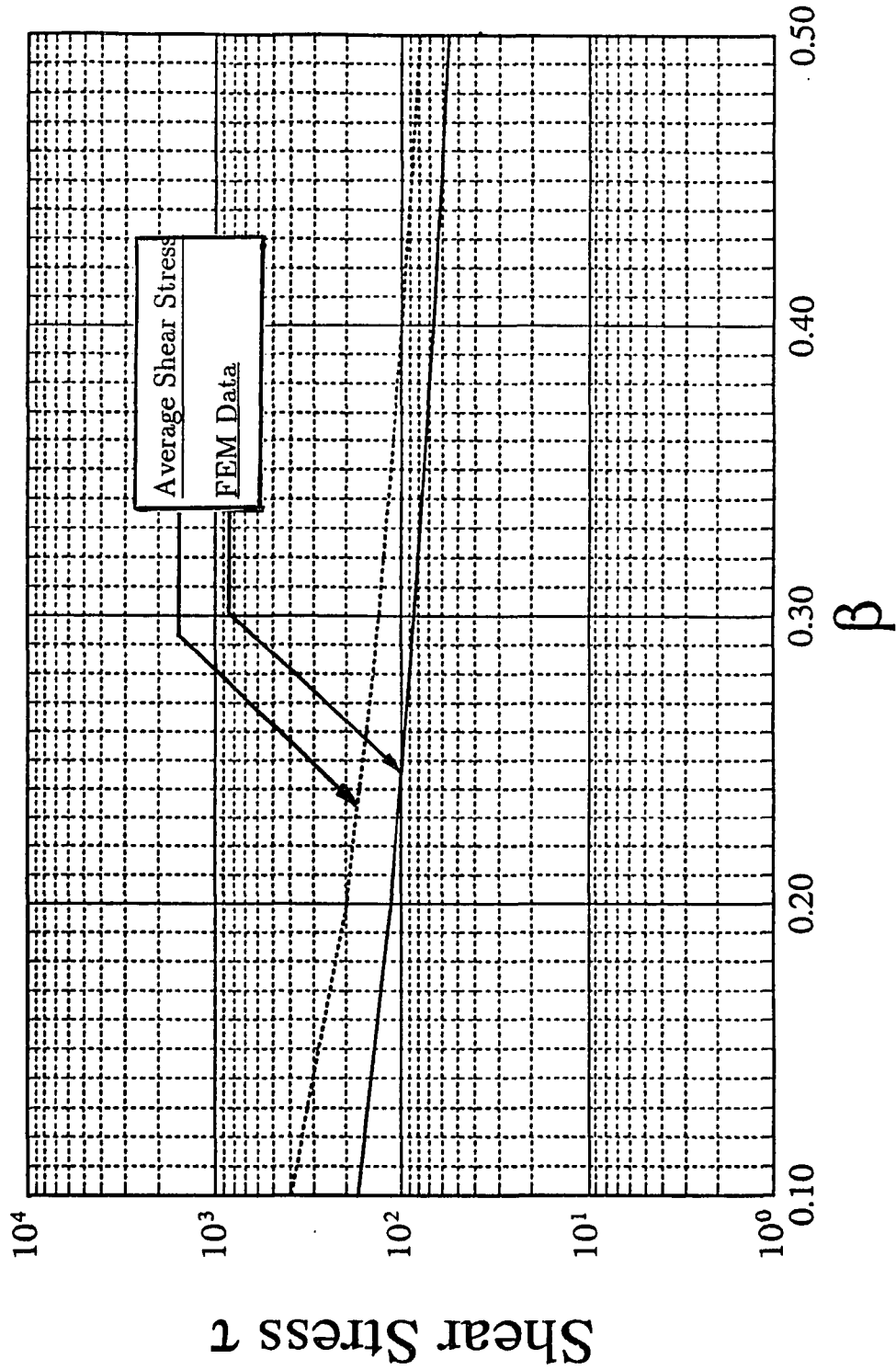


Figure 5.5 - Comparison of Shear Stress due to Horizontal Shear Force with Average Shear Stress  
 ( $\gamma_s = 75$ ,  $V_z = 1570 \text{ lb}$ ,  $T = 0.4 \text{ in}$ )

### 5.4.3 Shear Spring Constant

Again, the geometrical parameters  $\gamma_s$  and  $\beta$  are used to evaluate the shear spring constant,  $K_V$ . Referring to Figure 4.13, the  $z$ -deflection  $\delta_z$  increases as the angular position  $\theta$  increases. The average value of  $\delta_z$  at nodal point  $C$  between the outside and inside surfaces of the juncture is used. The shear spring constant can be defined as:

$$K_V = \frac{V_Z}{\delta_z} \quad (5.42)$$

Applying the same reasoning used in developing Eq.(5.11) for the radial spring constant, we can define for the spring constant:

$$\frac{K_V}{ET} = H_{16} \quad (5.43)$$

where  $H_{16}$  is dimensionless and  $K_V/ET$  is a normalized shear spring constant. This constant is plotted as function of  $\gamma_s$  and  $\beta$  in the Figure 6.18.

# Chapter 6

## Conclusion

Since the finite element method simulates both the real geometry of sphere-nozzle connections and the actual external loading conditions, it represents a major improvement over previous methods in calculating local stresses and spring constants due to external loading. One may conclude that:

1. For external radial force, the induced normal stresses shown in Figures 6.1-6.4 and the radial spring constants shown in Figure 6.15 indicate:
  - For given  $\gamma_s$  values, the normal stresses,  $\sigma_c$  and  $\sigma_m$ , decrease as  $\beta$  values increase.
  - For a given value of  $\beta$ , the normal stresses,  $\sigma_c$  and  $\sigma_m$  decrease as  $\gamma_s$  values increase.
  - For given  $\gamma_s$  values, the radial spring constant,  $K_y$ , increases as  $\beta$  values increase.
  - For a given value of  $\beta$ , the radial spring constant,  $K_y$  decreases as  $\gamma_s$  values increase.
2. For overturning moment, the induced normal stresses shown in Figures 6.5-6.8 and the rotational spring constants shown in Figure 6.16 indicate:

- For a given value of  $\gamma_s$ , the normal stresses,  $\sigma_c$  and  $\sigma_m$ , decrease as  $\beta$  values increase.
  - For a given value of  $\beta$ , all local stresses decrease as  $\gamma_s$  values increase.
  - For a given value of  $\gamma_s$ , the rotational spring constant,  $K_{\phi_M}$ , increases as the  $\beta$  values increase.
  - For a given value of  $\beta$ , the rotational spring constant,  $K_{\phi_M}$  increases as  $\gamma_s$  values increase.
3. For torsional moment, the induced shear stresses shown in Figure 6.9 and the torsional spring constants shown in Figure 6.17 indicate:
- For given  $\gamma_s$  values, the shear stress,  $\tau$ , decreases as  $\beta$  values increase.
  - For a given value of  $\beta$ , the shear stress,  $\tau$ , decreases as  $\gamma_s$  values increase.
  - For given  $\gamma_s$  values, the torsional spring constant,  $K_{\theta_T}$ , increases as  $\beta$  values increase.
  - For a given value of  $\beta$ , the torsional spring constant,  $K_{\theta_T}$ , increases as  $\gamma_s$  values increase.
4. For horizontal shear force, the induced local normal stresses shown in the Figures 6.10 - 6.13, the induced shear stresses shown in Figure 6.14 and the shear spring constants shown in Figure 6.18 indicate:
- For given  $\gamma_s$  values, all the local stresses ( $\sigma_c$ ,  $\sigma_m$ , and  $\tau$ ) decrease as  $\beta$  values increase.
  - For a given value of  $\beta$ , all the local stresses ( $\sigma_c$ ,  $\sigma_m$ , and  $\tau$ ) decrease as  $\gamma_s$  values increase.
  - For given  $\gamma_s$  values, the shear spring constant,  $K_V$ , increases as  $\beta$  values increase.

- For a given value of  $\beta$ , the shear spring constant,  $K_V$ , decreases as  $\gamma_s$  values increase.

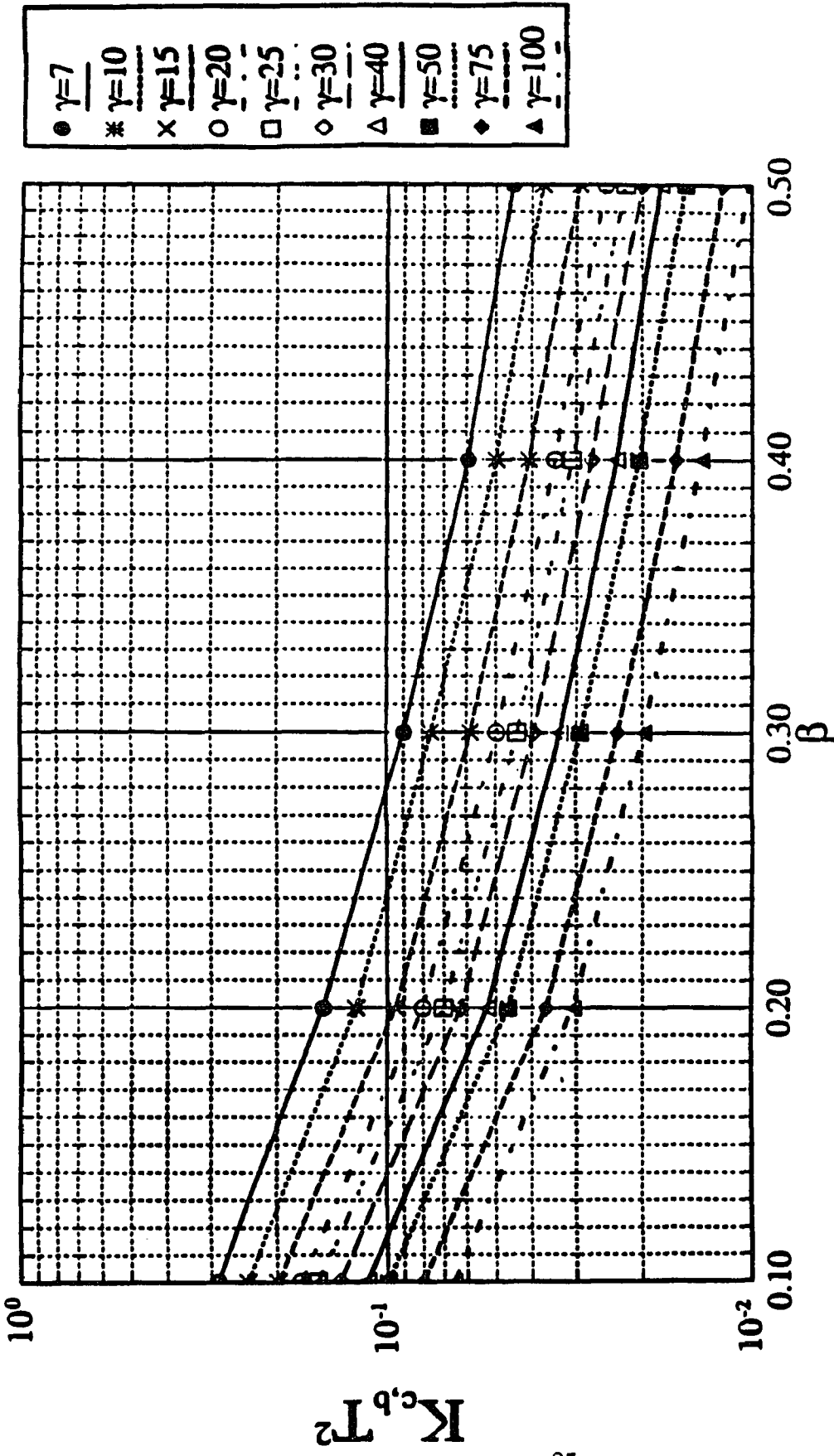


Figure 6.1 - Circumferential Bending Stress Factor due to Radial Force P

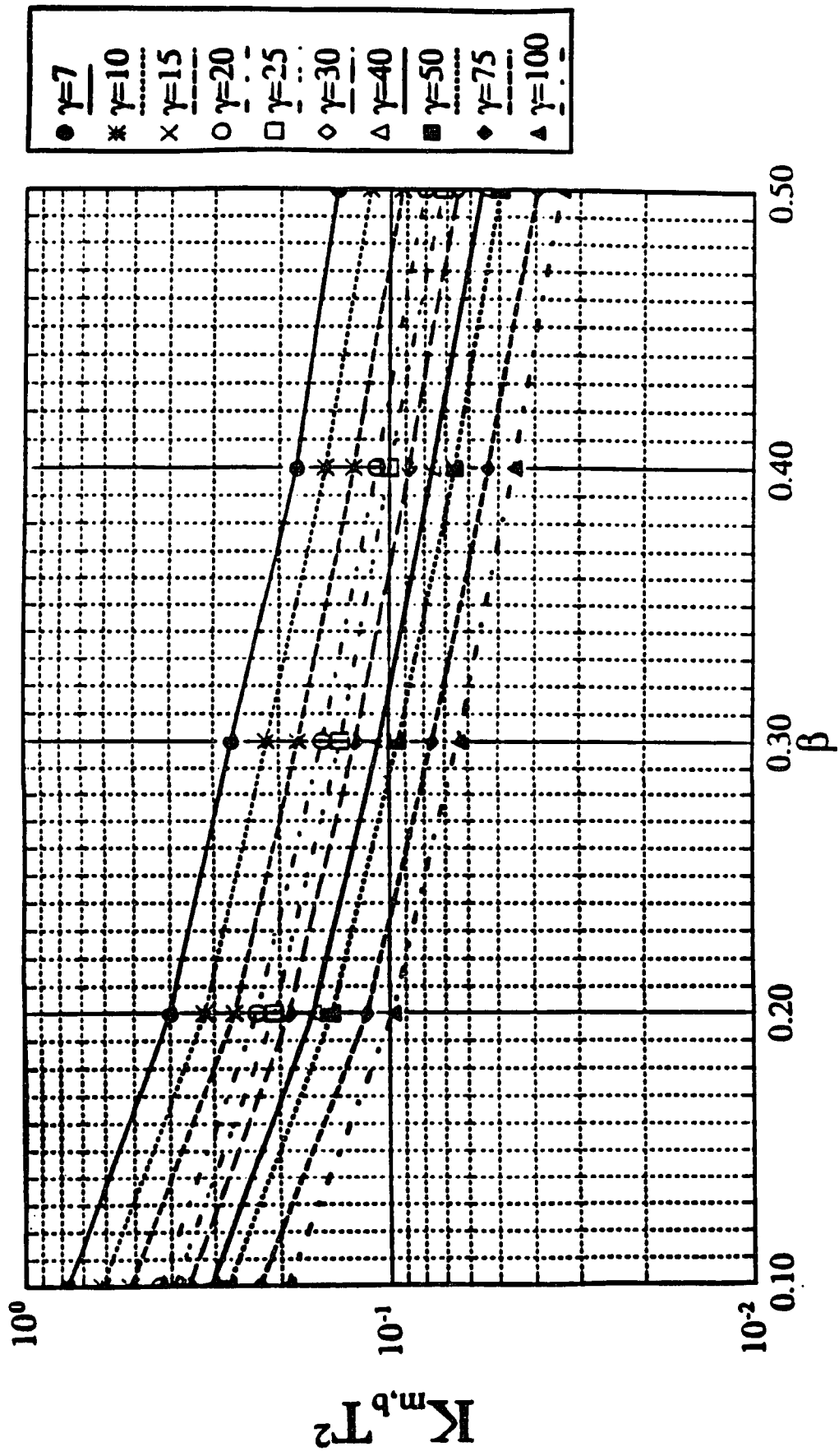


Figure 6.2 – Meridional Bending Stress Factor due to Radial Force P

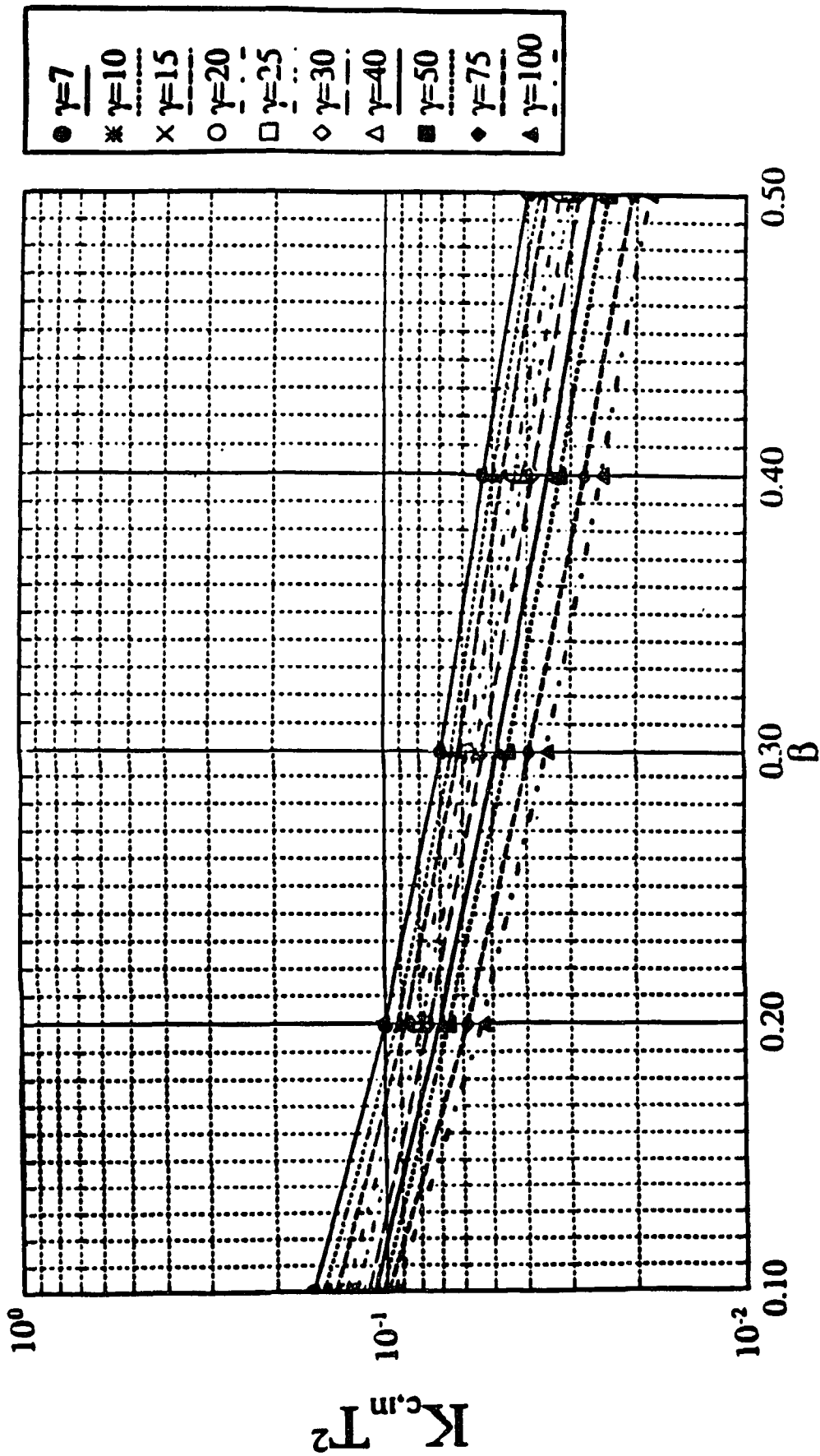


Figure 6.3 - Circumferential Membrane Stress Factor due to Radial Force P

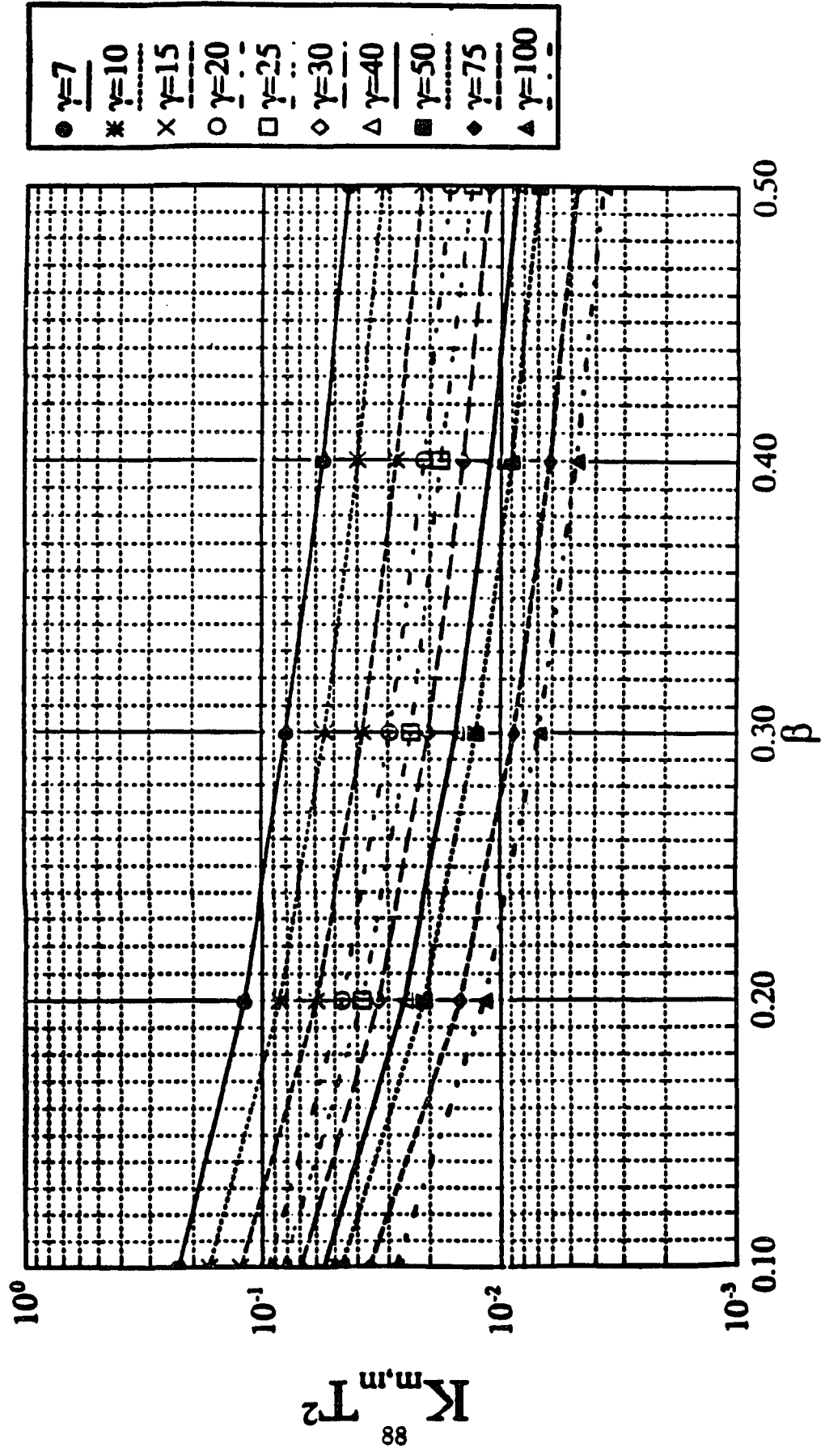


Figure 6.4 - Meridional Membrane Stress Factor due to Radial Force P

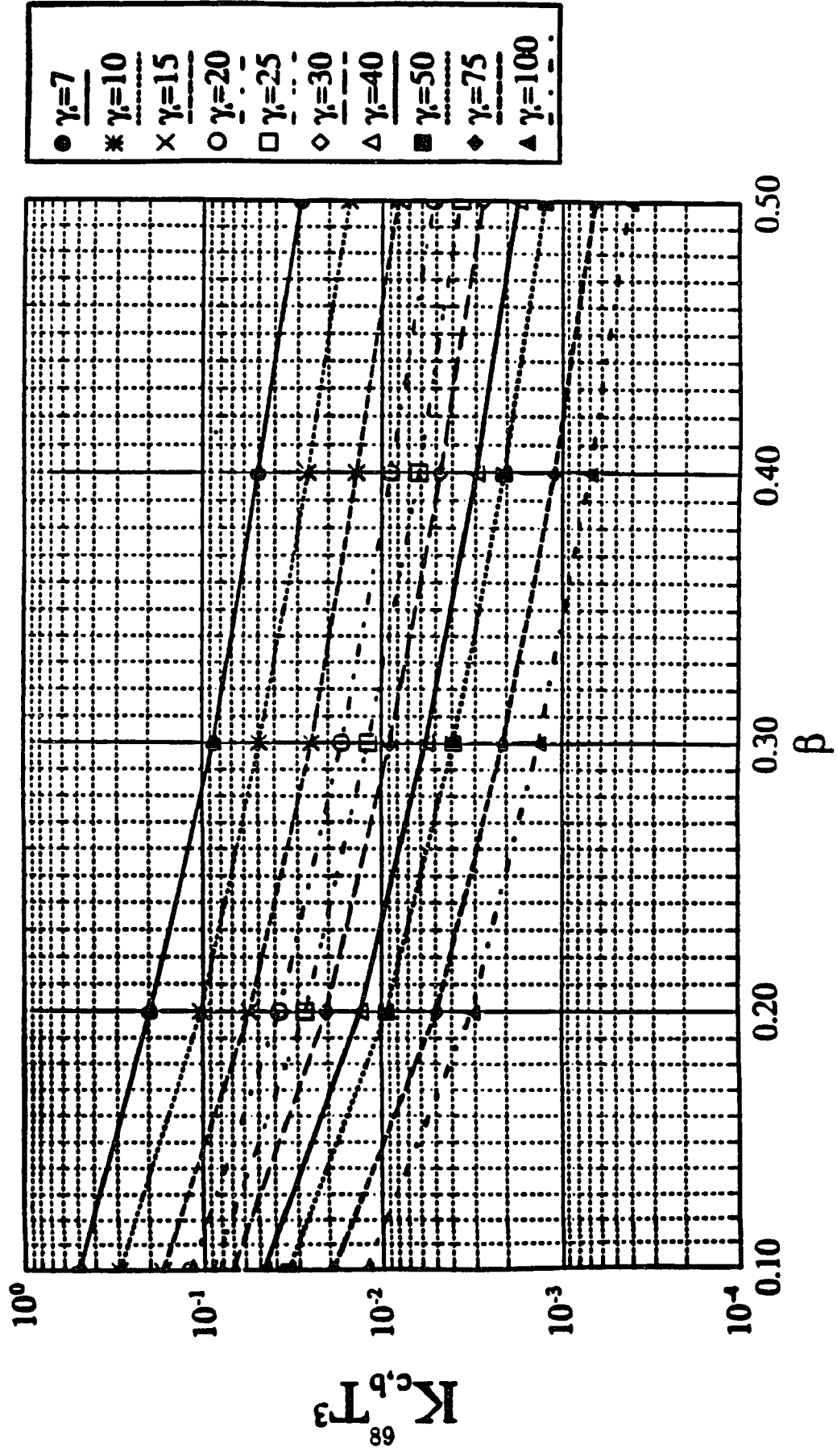


Figure 6.5 - Circumferential Bending Stress Factor due to Overturning Moment  $M_x$  or  $M_z$

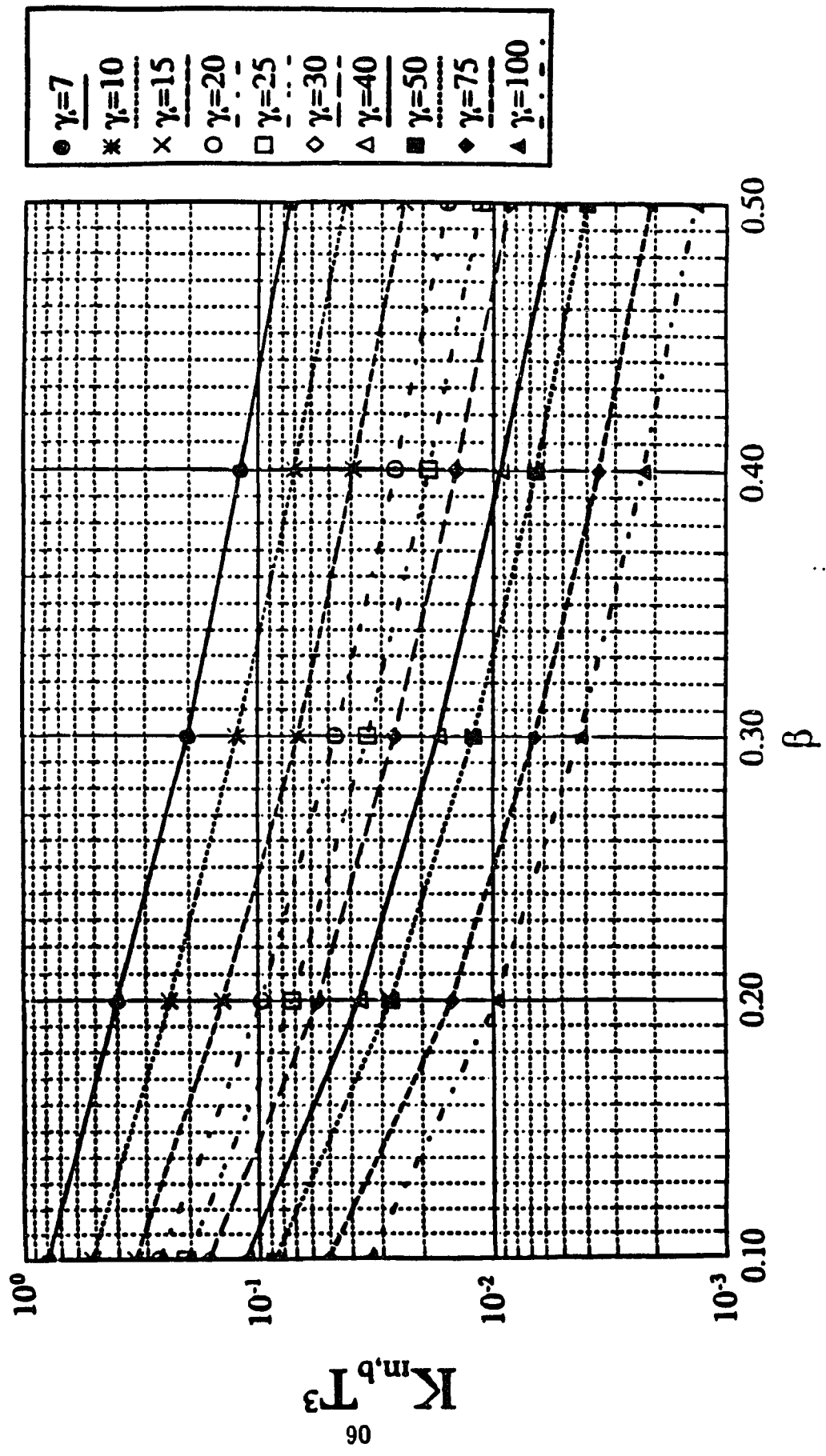


Figure 6.6 - Meridional Bending Stress Factor due to Overturning Moment  $M_x$  or  $M_z$

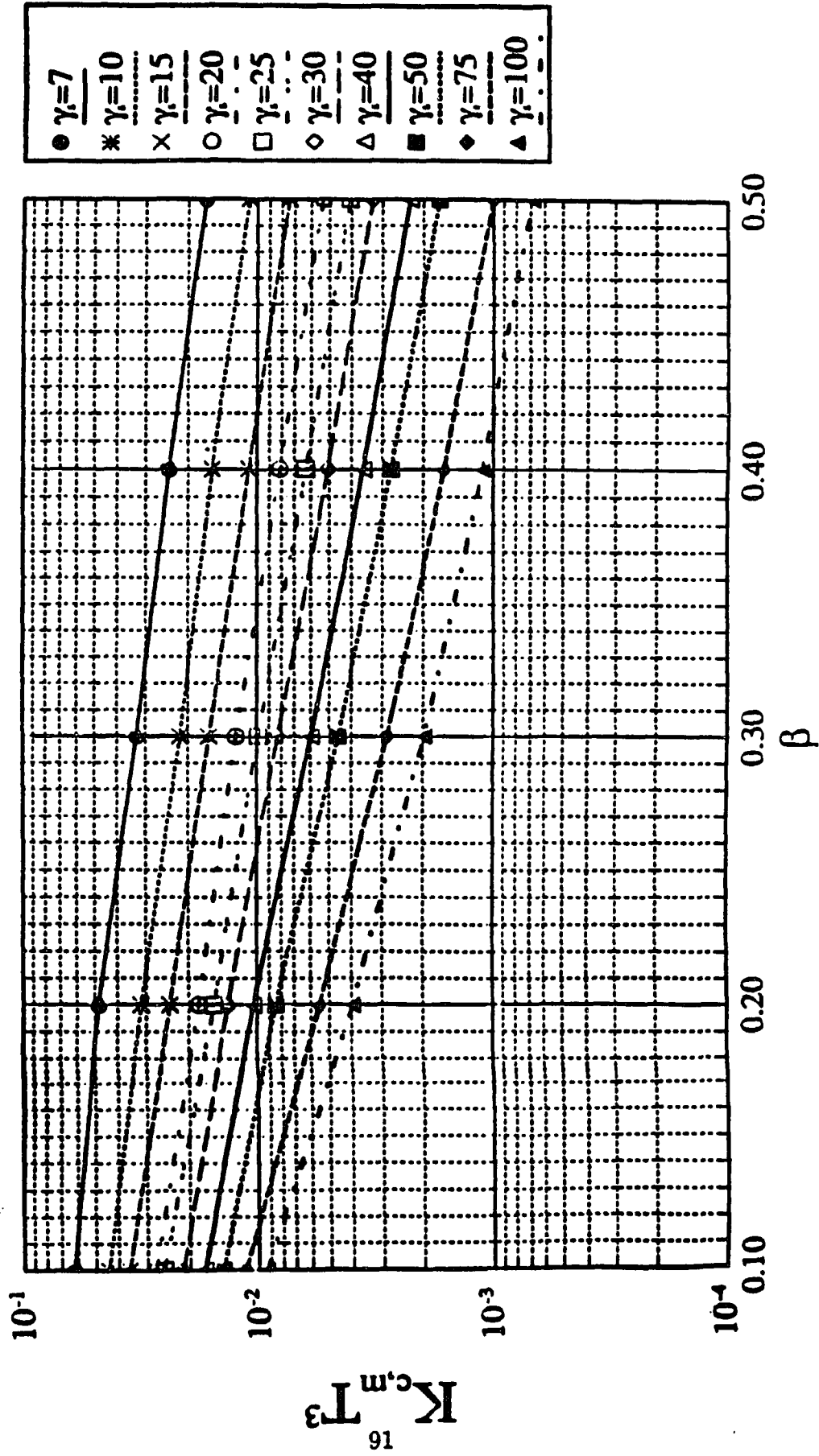


Figure 6.7 - Circumferential Membrane Stress Factor due to Overturning Moment  $M_x$  or  $M_z$

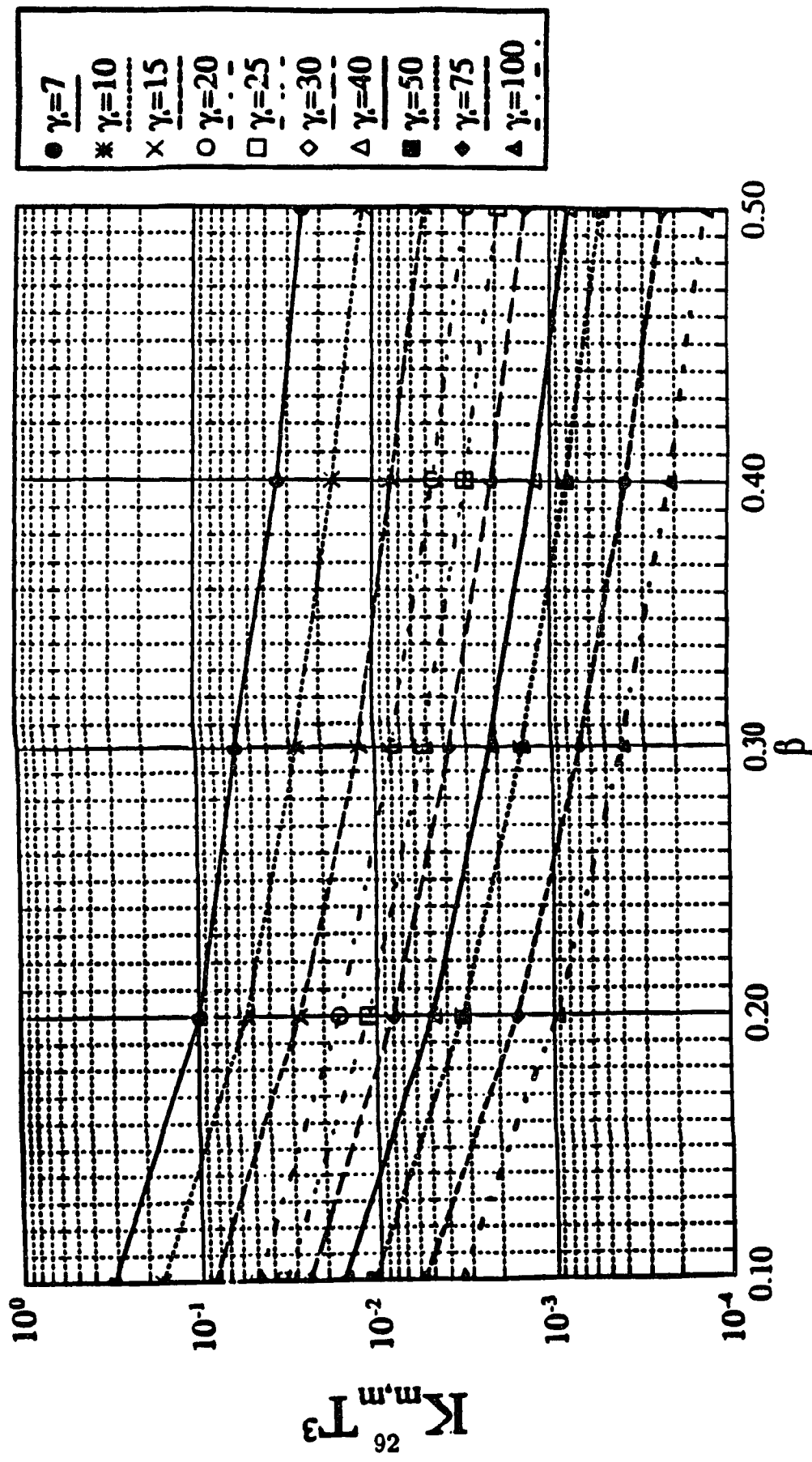


Figure 6.8 - Meridional Membrane Stress Factor due to Overturning Moment  $M_x$  or  $M_z$

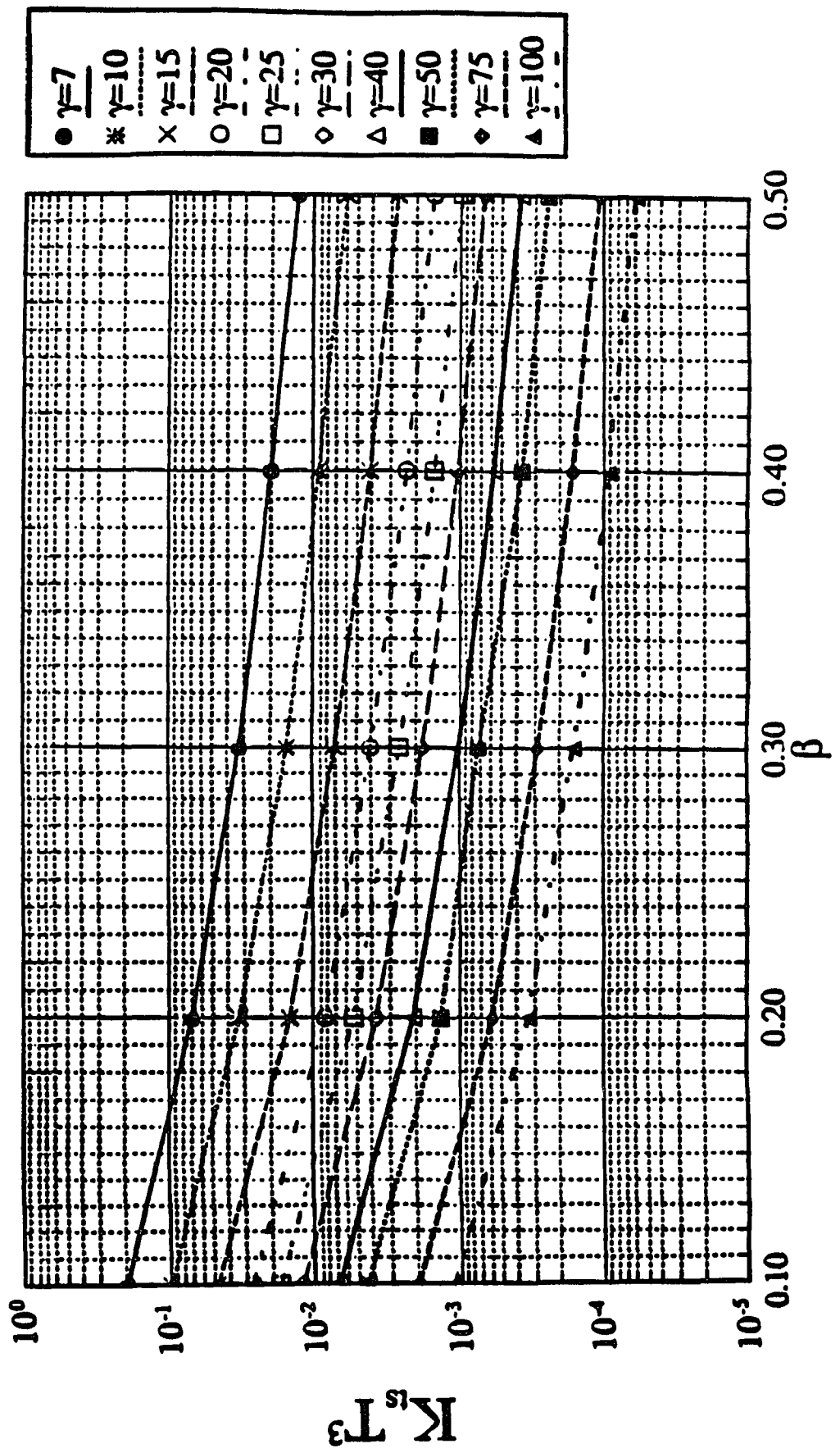


Figure 6.9 - Shear Stress Factor due to Torsional Moment  $M_T$

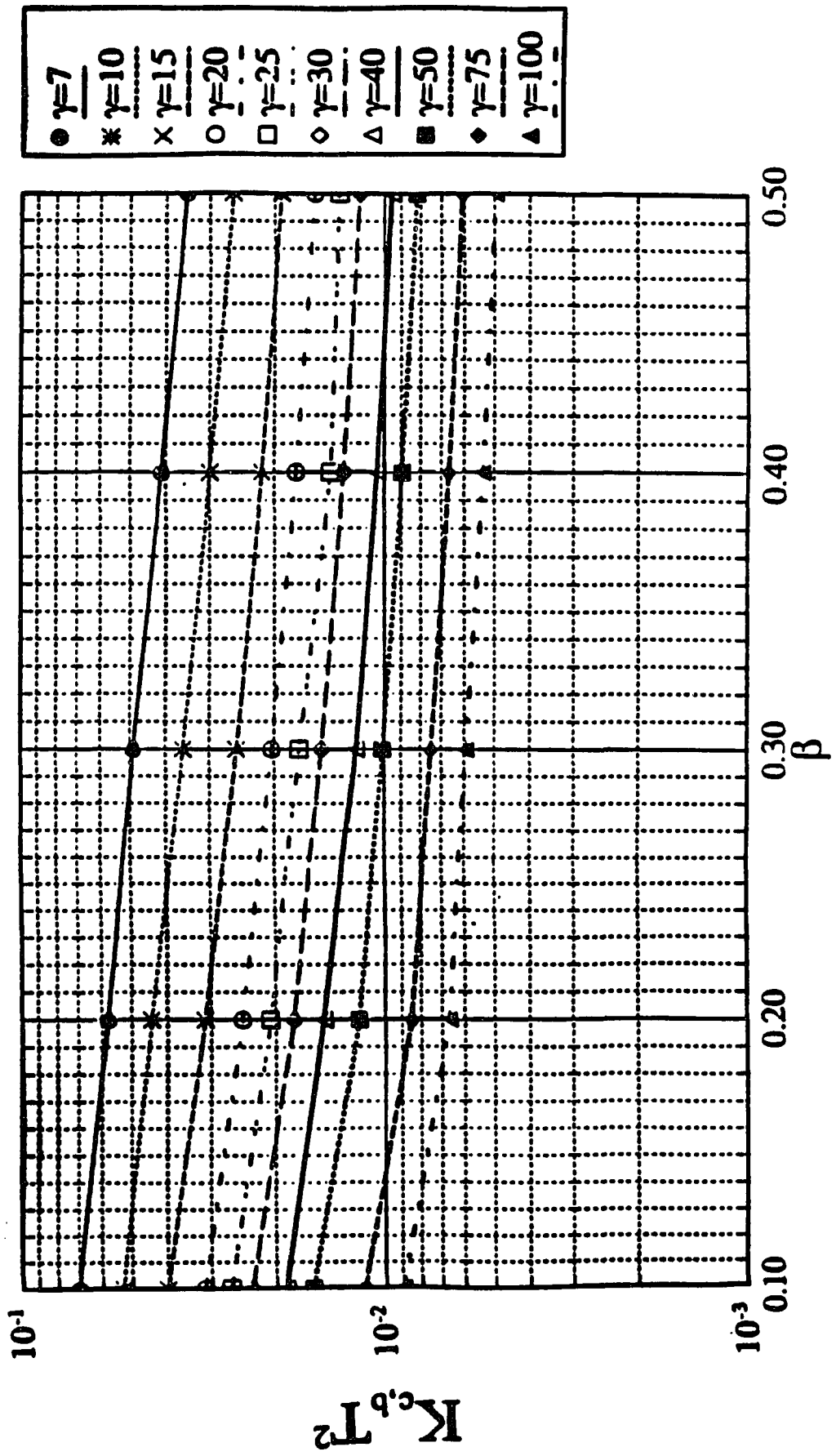


Figure 6.10 - Circumferential Bending Stress Factor due to Horizontal Shear Force  $V_x$  or  $V_z$

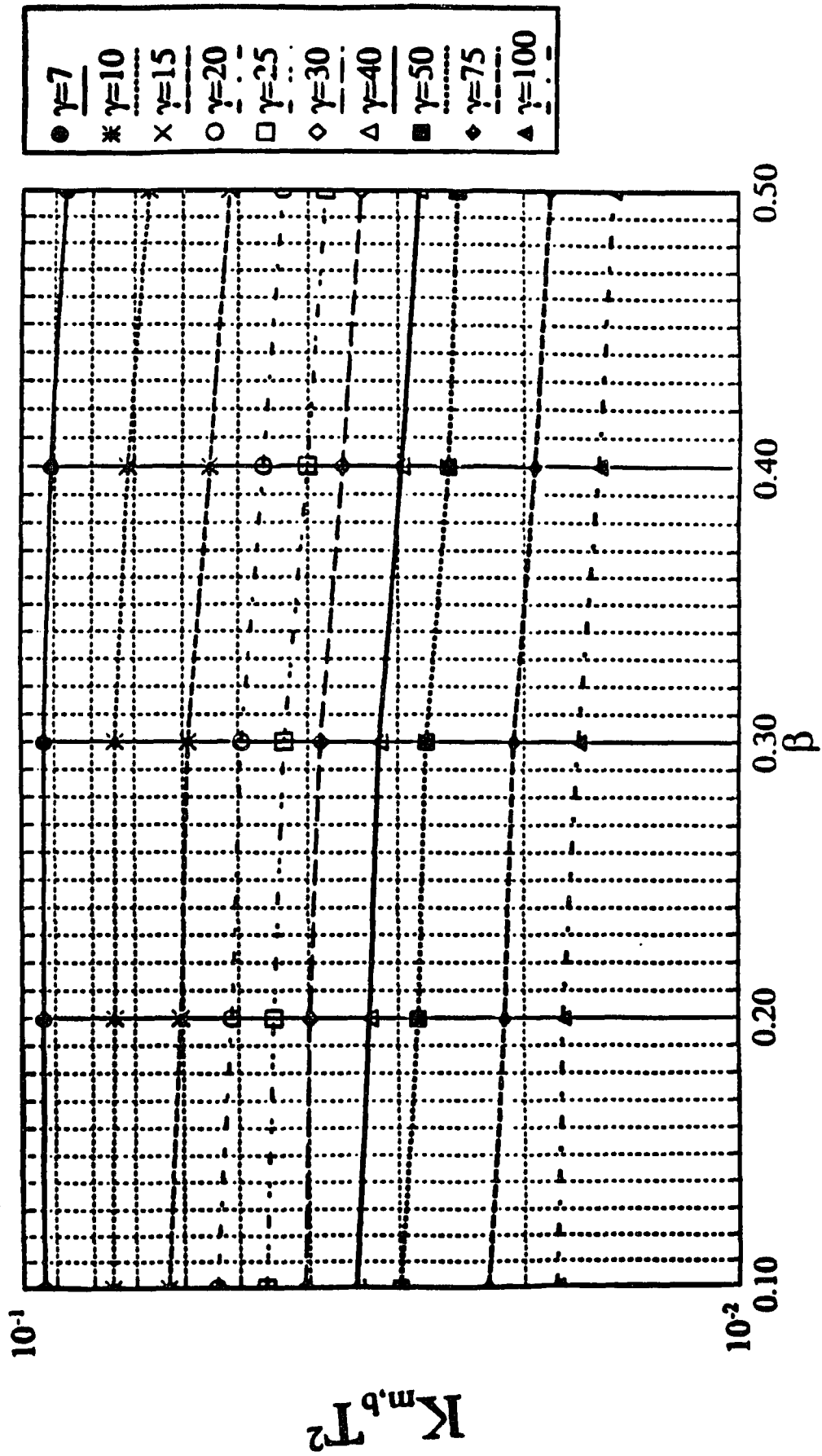


Figure 6.11 - Meridional Bending Stress Factor due to Horizontal Shear Force  $V_x$  or  $V_z$

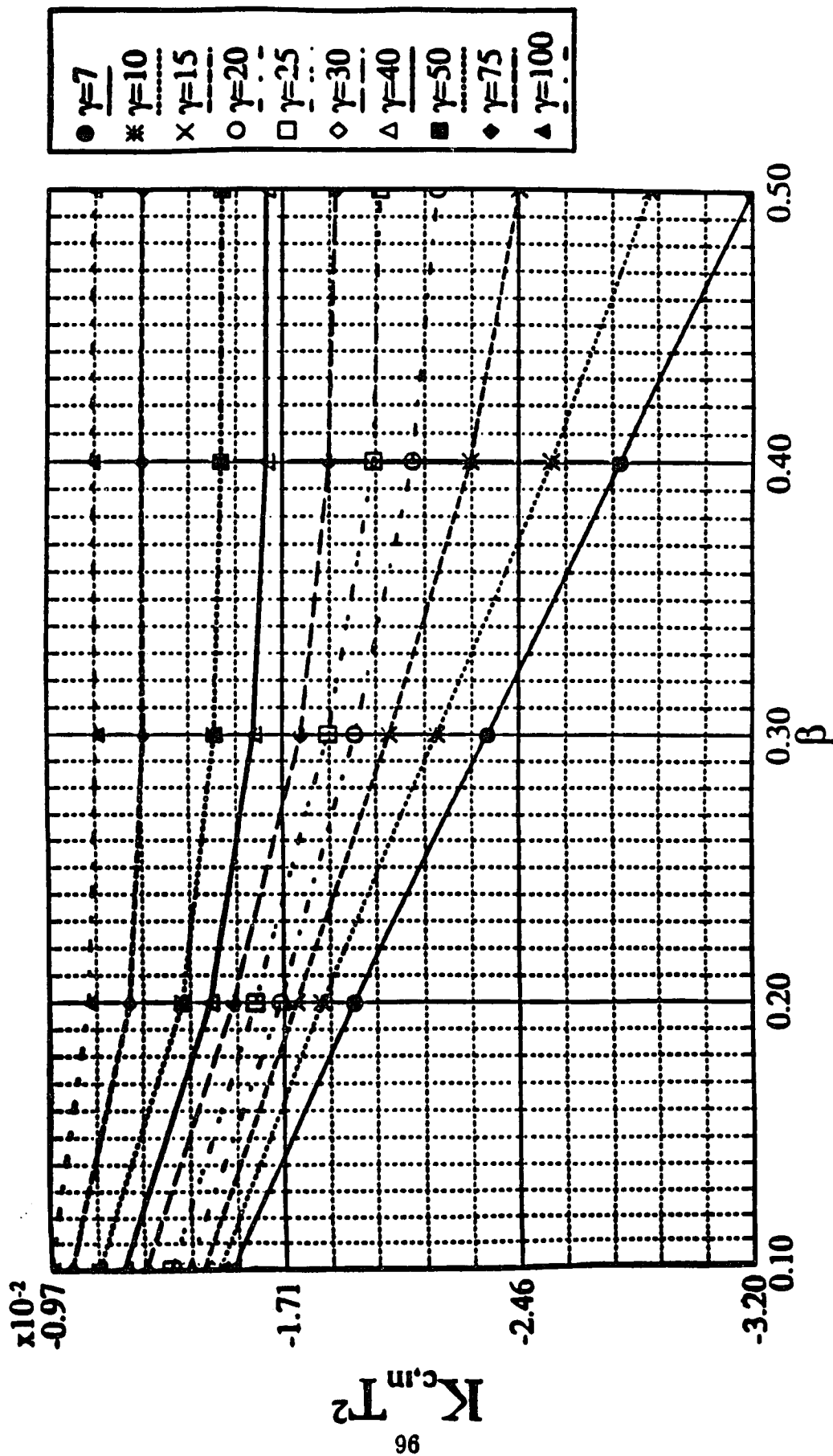


Figure 6.12 - Circumferential Membrane Stress Factor due to Horizontal Shear Force  $V_x$  or  $V_z$

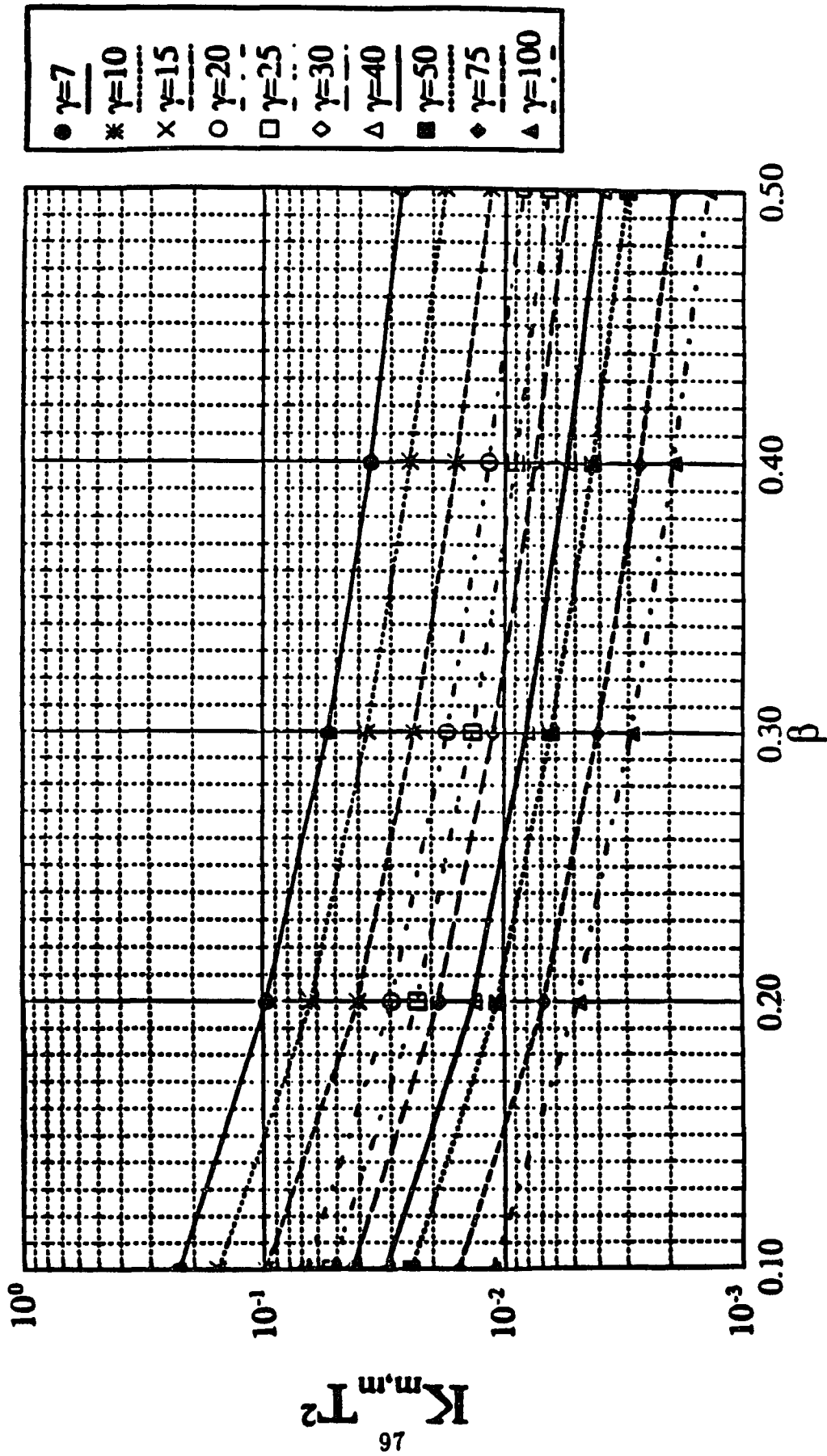


Figure 6.13 - Meridional Membrane Stress Factor due to Horizontal Shear Force  $V_x$  or  $V_z$

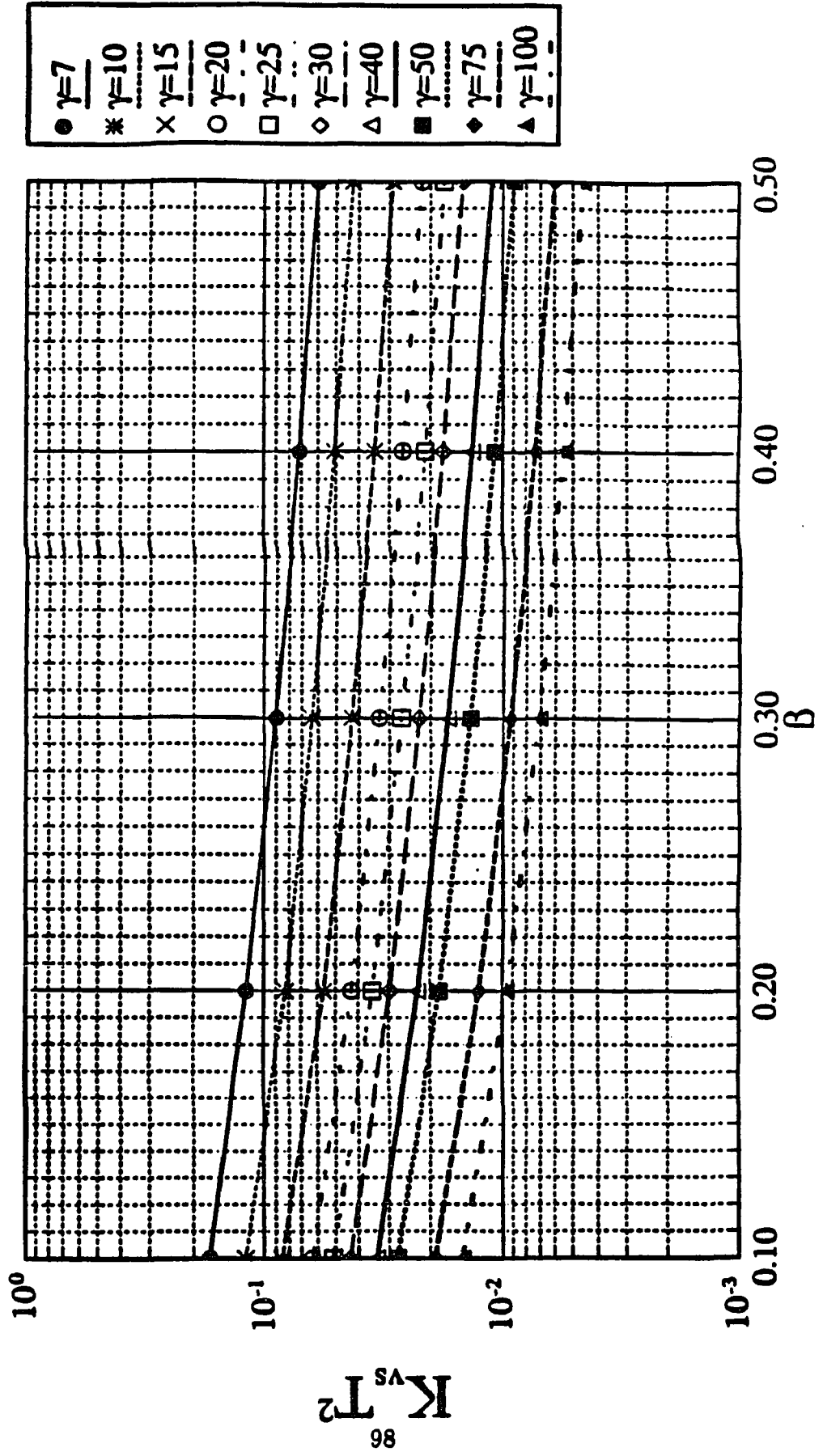


Figure 6.14 - Shear Stress Factor due to Horizontal Shear Force  $V_x$  or  $V_z$

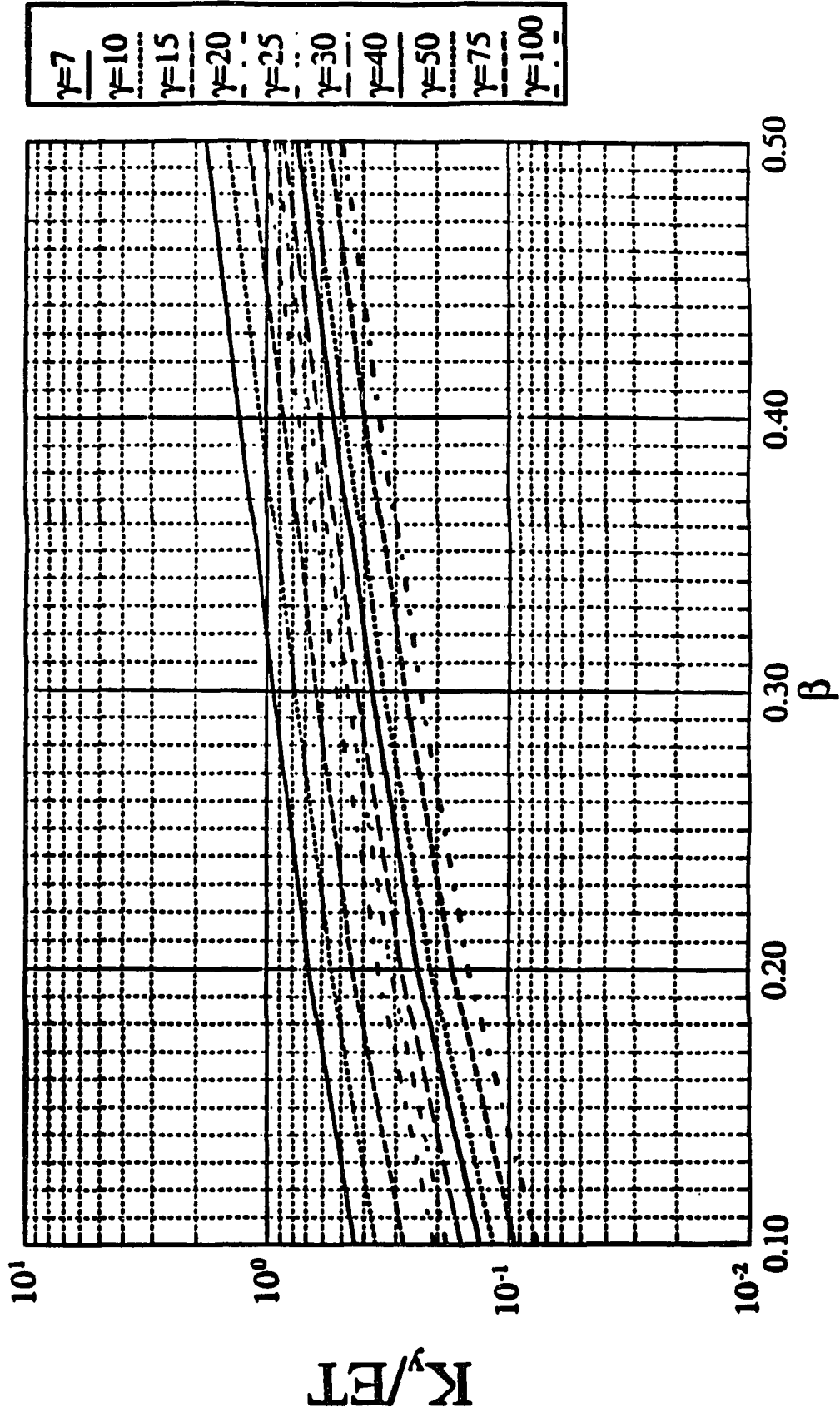


Figure 6.15 - Normalized Radial Spring Constant due to Radial Force P

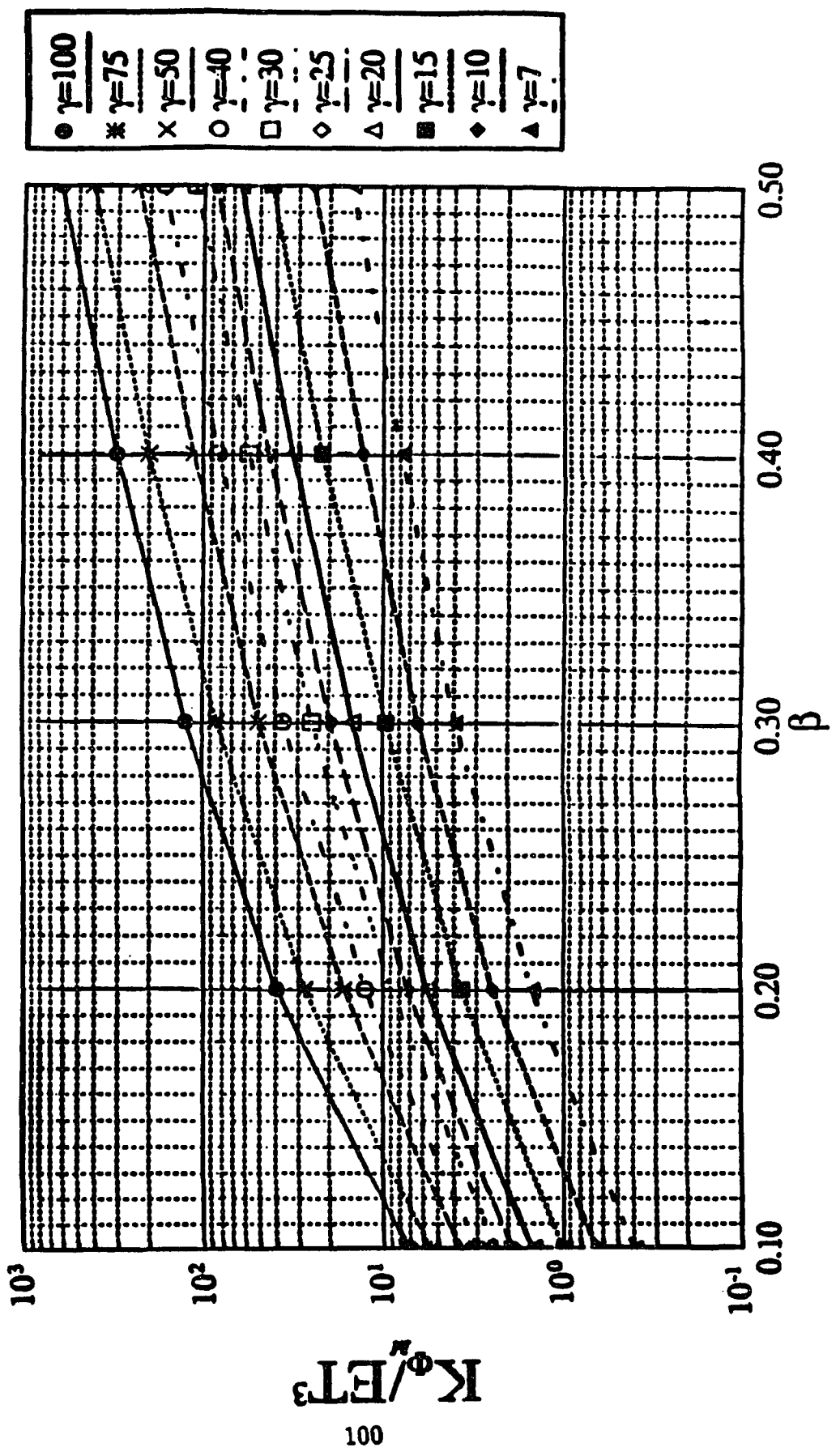


Figure 6.16 - Normalized Rotational Spring Constant due to Overturning Moment  $M_x$  or  $M_z$

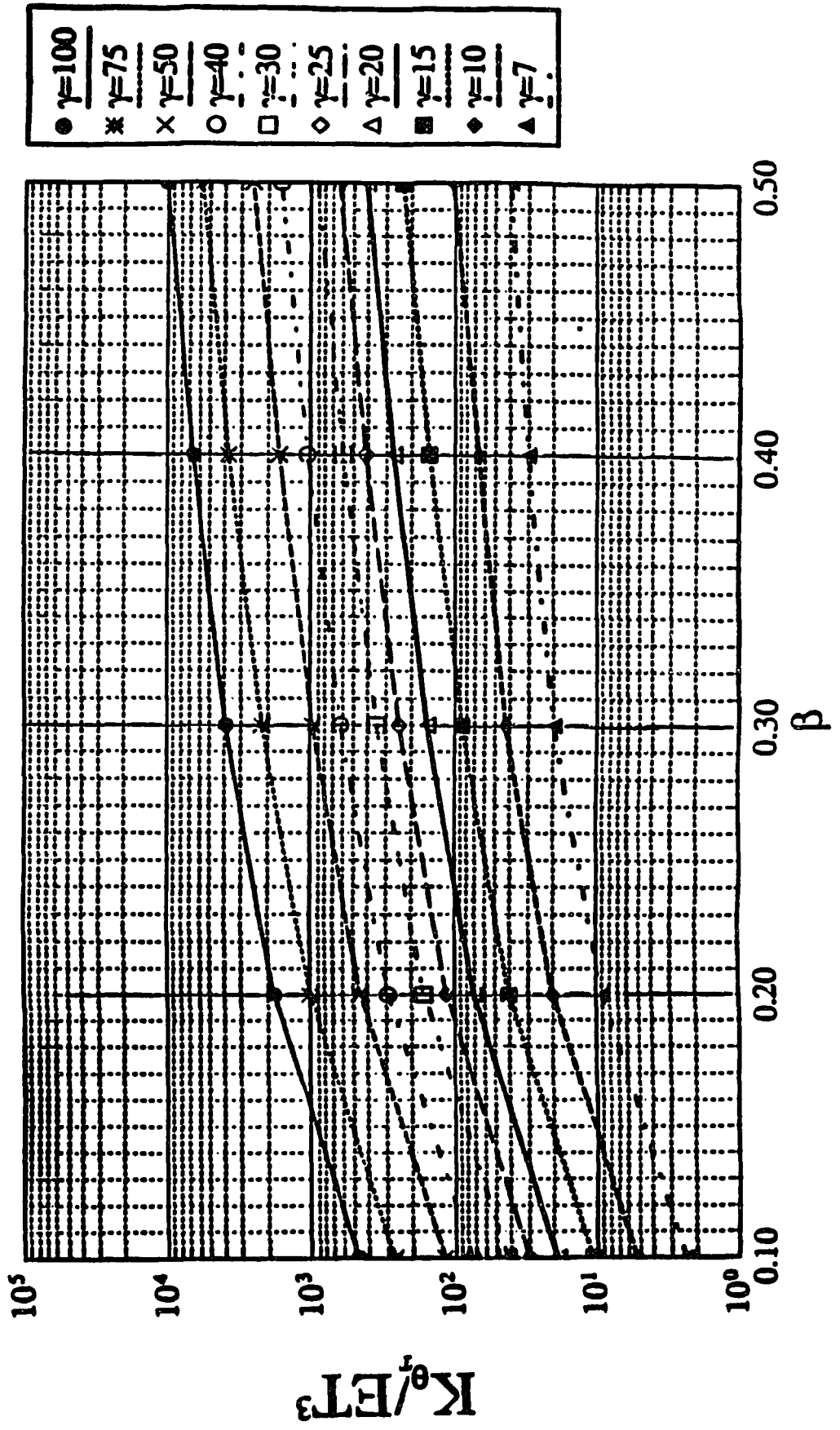


Figure 6.17 - Normalized Torsional Spring Constant due to Torsional Moment  $M_T$

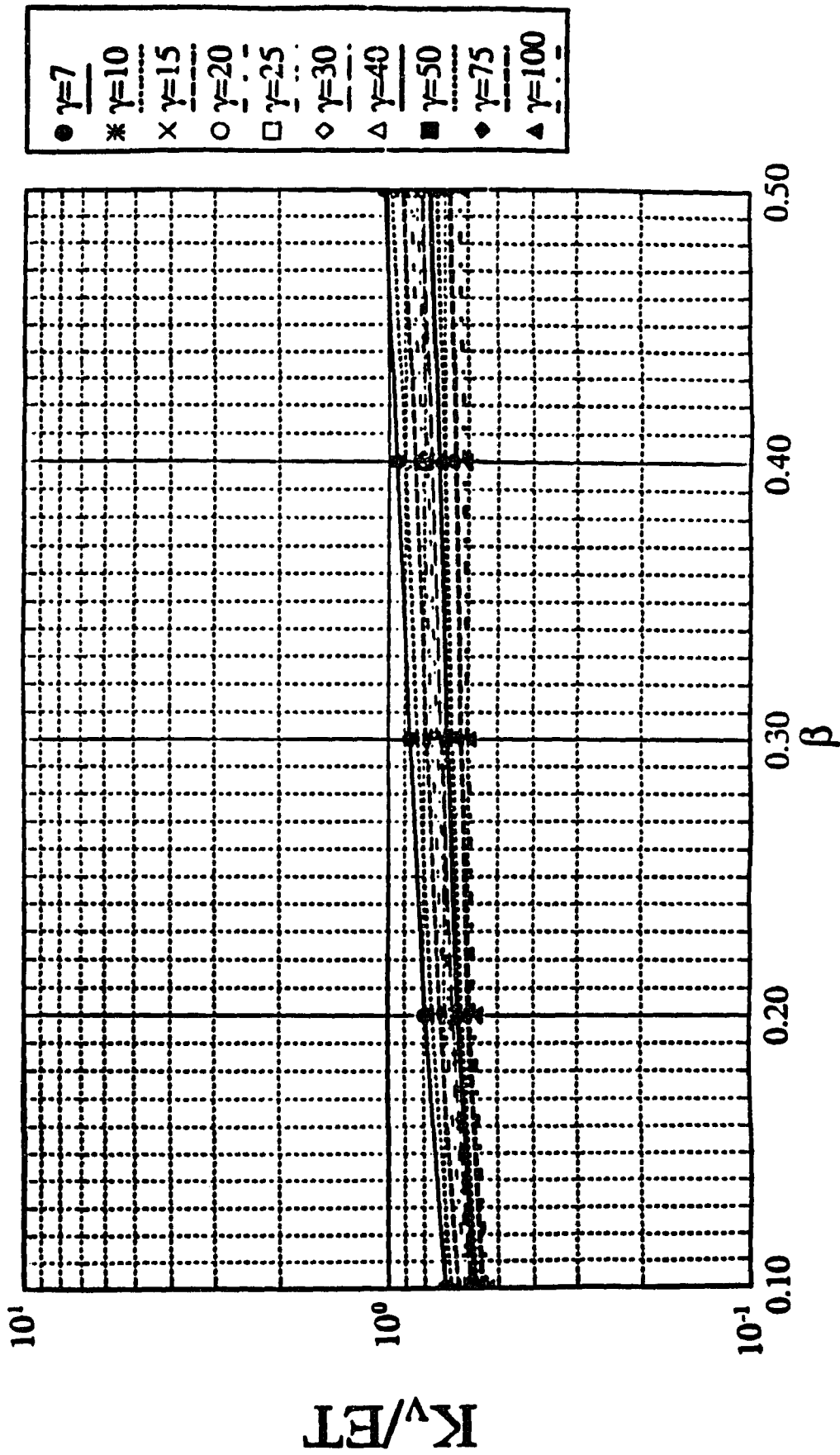


Figure 6.18 - Normalized Shear Spring Constant due to Shear Force  $V_x$  or  $V_z$

# Appendix

## Appendix A ANSYS Program

### A.1 Quadrilateral Shell Element Model due to Radial Force

```
/prep7  
/title  
/show  
c***mesh module
```

Define Constants
------------------

*set,thc,0.4	c**thickness of the nozzle
*set,ths,0.4	c**thickness of the sphere
*set,beta,0.4	c** $\beta$ value
*set,gama,75	c** $\gamma_s$ value
*set,rs,gama*ths	c**radius of the sphere
*set,rc,rs*beta	c**radius of the sphere
*set,hoc,rs*0.5	c**height of the nozzle
*set,radi,asin(beta)	c**half opening of the juncture with respect to the symmetry axis
*set,quot,(180.0)/3.14159	
*set,mult,quot*radi	
*set,four,(90.0)-(mult+15)	
*set,thir,0	
*set,ang,rc/rs	
*set,func,asin(ang)	
*set,hi,rs*cos(func)	c**y-coordinate of the juncture
*set,high,hi+hoc	c**y-coordinate of the top of the nozzle
*set,low,hi+(hoc*0.3)	
*set,foc,11.3636	c**nodal force

## Set Material Properties

et,1,63	c**define element type of the sphere
nuxy,1,0.3	c** $\mu$ value of the sphere
et,2,63	c**define element type of the nozzle
ex,1,30e6	c**elastic modulus of the sphere
ex,2,30e6	c**elastic modulus of the nozzle
nuxy,2,0.3	c** $\mu$ value of the nozzle
r,1,ths	
r,2,thc	

## Define Constants

k,1	
k,2,1	c**global coordinate system
k,3,,1	
cskp,11,2,1,3,2	c**cylindrical coordinate system
cskp,12,1,1,ew,,1,1,1	c**spherical coordinate system

## Mesh Finite Element Model

csys,11	
a,1,2,12,11	
a,11,12,5,4	
real,1	
elsize,2.25,,2	c**element size
amesh,1,2,1	c**element mesh
a,2,3,13,12	
a,12,13,6,5	
real,1	
elsize,0.9375,,2	
amesh,3,4,1	
csys,12	

```

real,2
a,3,9,14,13
a,13,14,10,6
elsize,1.125,,2
amesh,5,6,1
real,2
a,9,7,15,14
a,14,15,8,10
elsize,1.5,,2
amesh,7,8,1
eplot                                c**element plot
nall
eall
arall
dsys
/angle
/pnum,elem,0
csys,0
wfront
wsort,y
symbc,0,1,0,0.05
symbc,0,3,0,0.05

```

<b>Apply Nodal Forces</b>
---------------------------

```

nall
eall
nselect,y,high                        c**select nodes on the top of the nozzle
f,599,fy,-foc*0.5,,683,84
f,606,fy,-foc,,616,1
f,684,fy,-foc,,693,1
nall
eall
arall
nselect,y,0                            c**select nodes located at the equator
d,all,all                               c**selected nodes to be constrained
nall
eall
arall
/plot,forc,1                           c**plot nodal forces
/plot,tdis,1                            c**plot boundary conditions

```

```
/type,,2
/view,,1,1,1
nplot
eplot
iter,1,1,1
afwrite,,1
finish
/check
/exec
/input,27
finish
/post1
store,stres,disp
set
set,1,1
finish
/eof
```

c\*\*end of the file

## A.2 Quadrilateral Shell Element Model due to Overturning Moment

```
/prep7
/title
/show
c***mesh module
```

<b>Define Constant</b>
------------------------

```
*set,thc,0.4          c**thickness of the nozle
*set,ths,0.4          c**thickness of the sphere
*set,beta,0.4         c** $\beta$  value
*set,gama,75          c** $\gamma_s$  value
*set,rs,gama*ths      c**mean radius of the sphere
*set,rc,rs*beta       c**mean radius of the nozzle
*set,hoc,rs*0.5       c**height of the nozzle
*set,radi,asin(beta)  c**half opening angle of the sphere
                      with respect to the symmetry axis

*set,quot,(180.0)/3.14159
*set,mult,quot*radi
*set,four,(90.0)-(mult+15)
*set,thir,0
*set,ang,rc/rs
*set,func,asin(ang)
*set,hi,rs*cos(func)  c**y coordinate of the juncture
*set,high,hi+hoc      c**y coordinate of the top of the nozzle
*set,low,hi+(hoc*0.3)
*set,para,0.16675
*set,foc,para*17.858  c**nozzle force
*set,col,0.99475      c**cos(4.09)
*set,co2,0.9898       c**cos(9.18)
*set,co3,0.977
*set,co4,0.9595
*set,co5,0.9369
*set,co6,0.9096
*set,co7,0.8777
*set,co8,0.8413
*set,co9,0.8006
*set,co10,0.7558
*set,co11,0.7072
```

```

*set,co12,0.655
*set,co13,0.5994
*set,co14,0.5408
*set,co15,0.4796
*set,co16,0.4156
*set,co17,0.3497
*set,co18,0.282
*set,co19,0.2128
*set,co20,0.1426
*set,co21,0.07167
*set,co22,0.00035

```

### Define Material Properties

```

et,1,63          c**define the element type of the sphere
nuxy,1,0.3      c** $\mu$  value of the sphere
et,2,63          c**define the element type of the nozzle
                ex,2,30e6      c**elastic modulus of the nozzle,  $ex=ey=ez$ 
nuxy,2,0.3      c** $\mu$  value of the nozzle
r,1,ths
r,2,thc
k,1
k,2,1           c**define the global coordinate system
k,3,,1
cskp,11,2,1,3,2 c**define the cylindrical coordinate system
cskp,12,1,1,3,2 c**define the spherical coordinate system

```

### Define Keypoints

```

csys,11          c**the spherical coordinate system
k,1,rs
k,2,rs,,four
k,3,rs,,50
k,4,rs,90
k,5,rs,90,four
k,6,rs,90,50

```

```

k,11,rs,45
k,12,rs,45,four
k,13,rs,45,50
kmove,3,11,rs,,999,12,rc,999,999
kmove,6,11,rs,90,999,12,rc,999,999
kmove,13,11,rs,45,999,12,rc,999,999
csys,12
k,7,rc,,high
k,8,rc,90,high
k,9,rc,,low
k,10,rc,90,low
k,14,rc,45,low
k,15,rc,45,high
/view,,1,1,1
kplot                                c**plot keypoints

```

<b>Define Keyareas</b>
------------------------

```

csys,11
a,1,2,12,11
a,11,12,5,4
a,2,3,13,12
a,12,13,6,5
csys,12
a,3,9,14,13
a,13,14,10,6
a,9,7,15,14
a,14,15,8,10
/mdiv,3
/pnum,area,1
/view,,1,1,1
aplot                                c**plot area made up of the keypoints
lplot                                c**plot line made up of the keypoints
aral
alist
klist
/pnum,line,-1
/view,,1,1,1
lplot
c***et,1,63

```

## Mesh Finite Element Model

```
csys,11
a,1,2,12,11
a,11,12,5,4
real,1
elsize,2.25,,2
amesh,1,2,1
a,2,3,13,12
a,12,13,6,5
real,1
elsize,0.9375,,2
amesh,3,4,1
csys,12
real,2
a,3,9,14,13
a,13,14,10,6
elsize,1.125,,2
amesh,5,6,1
real,2
a,9,7,15,14
a,14,15,8,10
elsize,1.5,,2
amesh,7,8,1
eplot
eall
dsys
/angle
/pnum,elem,0
csys,0
wfront
wsort,y
/view,,1,1,1
symsbc,0,1,0,0.05
asymsbc,0,3,0,0.05
```

c\*\*define element size  
c\*\*element mesh

c\*\*element plot

## Apply Nodal Force

```

nall
eall
nselect,y,high
f,599,fy,-foc*0.5
f,607,fy,-foc*co1
f,608,fy,-foc*co2
f,609,fy,-foc*co3
f,610,fy,-foc*co4
f,611,fy,-foc*co5
f,612,fy,-foc*co6
f,613,fy,-foc*co7
f,614,fy,-foc*co8
f,615,fy,-foc*co9
f,616,fy,-foc*co10
f,606,fy,-foc*co11
f,684,fy,-foc*co12
f,685,fy,-foc*co13
f,686,fy,-foc*co14
f,687,fy,-foc*co15
f,688,fy,-foc*co16
f,689,fy,-foc*co17
f,690,fy,-foc*co18
f,691,fy,-foc*co19
f,692,fy,-foc*co20
f,693,fy,-foc*co21
nall
eall
arall
nselect,y,0
d,all,all
nlist,all
nall
eall
arall
/plot,forc,1
/plot,tdis,1
/plot,type,,2
/plot/view,,1,1,1
nplot
eplot
iter,1,1,1
afwrite,,1
finish
/check
/exec

```

```
c**select nodes to be constrained
```

```
c**plot nodal forces
c**plot boundary conditions
```

```
/input,27  
finish  
/post1  
set  
nall  
eall  
set,1,1  
finish  
/eof
```

```
c**end of the file
```

### A.3 Quadrilateral Shell Element Model due to Torsional Moment

```
/prep7
/title
/show
c***mesh module
*set,thc,0.4          c**thickness of the nozzle
*set,ths,0.4          c**thickness of the sphere
*set,beta,0.4         c** $\beta$  value
*set,gama,75          c** $\gamma_s$  value
*set,rs,gama*ths      c**radius of the sphere
*set,rc,rs*beta       c**radius of the nozzle
*set,hoc,rs*0.5       c**hight of the nozzle
*set,radi,asin(beta)  c**half opening of the juncture
                      with respect to the symmetry axis

*set,quot,(180.0)/3.14159
*set,mult,quot*radi
*set,four,(90.0)-(mult+15)
*set,thir,0
*set,ang,rc/rs
*set,func,asin(ang)
*set,hi,rs*cos(func)  c**y coordinate of the juncture
*set,high,hi+hoc     c**y coordinate of the top of the nozzle
*set,low,hi+(hoc*0.3)
*set,para,0.16675
*set,foc,para*17.858  c**nodal force
*set,col,0.99475      c**cos(4.09)
*set,co2,0.9898      c**cos(9.18)
*set,co3,0.977
*set,co4,0.9595
*set,co5,0.9369
*set,co6,0.9096
*set,co7,0.8777
*set,co8,0.8413
*set,co9,0.8006
*set,co10,0.7558
*set,co11,0.7072
*set,co12,0.655
*set,co13,0.5994
*set,co14,0.5408
*set,co15,0.4796
*set,co16,0.4156
*set,co17,0.3497
*set,co18,0.282
```

```

*set,co19,0.2128
*set,co20,0.1426
*set,co21,0.07167
*set,co22,0.00035
*set,sn1,0.0713          c**sin(4.09)
*set,sn2,0.14228        c**sin(9.18)
*set,sn3,0.21252
*set,sn4,0.28167
*set,sn5,0.3494
*set,sn6,0.415328
*set,sn7,0.47915
*set,sn8,0.54053
*set,sn9,0.59916
*set,sn10,0.6547
*set,sn11,0.70698
*set,sn12,0.75562
*set,sn13,0.8004
*set,sn14,0.8411
*set,sn15,0.87756
*set,sn16,0.9095
*set,sn17,0.93685
*set,sn18,0.9594
*set,sn19,0.97708
*set,sn20,0.98977
*set,sn21,0.99743
*set,sn22,0.99984
et,1,63                  c**define the element type of the sphere
nuxy,1,0.3               c** $\mu$  value of the sphere
et,2,63                  c**define element type of the nozzle
ex,1,30e6                c**elastic modulus of the sphere
ex,2,30e6                c**elastic modulus of the nozzle
nuxy,2,0.3              c** $\mu$  value of the nozzle
r,1,ths
r,2,thc

```

<b>Define the Positions of Keypoints</b>
--

```

k,1
k,2,1                    c**define the global coordinate system
k,3,,,1
cskp,11,2,1,3,2

```

```

cscp,12,1,1,3,2
csys,11
k,1,rs
k,2,rs,,four
k,3,rs,,50
k,4,rs,90
k,5,rs,90,four
k,6,rs,90,50
k,11,rs,45
k,12,rs,45,four
k,13,rs,45.50
kmove,3,11,rs,,999,12,rc,999,999
kmove,6,11,rs,90,999,12,rc,999,999
kmove,13,11,rs,45,999,12,rc,999,999
csys,12
k,7,rc,,high
k,8,rc,90,high
k,9,rc,,low
k,10,rc,90,low
k,14,rc,45,low
k,15,rc,45,high
/view,,1,1,1
kplot

```

<b>Define Keyareas</b>
------------------------

```

csys,11
a,1,2,12,11
a,11,12,5,4
a,2,3,13,12
a,12,13,6,5
csys,12
a,3,9,14,13
a,13,14,10,6
a,9,7,15,14
a,14,15,8,10
/mdiv,3
/pnum,area,1
/view,,1,1,1
aplot
lplot

```

```
aral
alist
klist
/pnum,line,-1
/view,,1,1,1
lplot
```

## Mesh Finite Element Model

```
csys,11
a,1,2,12,11
a.11,12,5,4
real,1
elsize,2.25,,2          c**define element size
amesh,1,2,1             c**element mesh
a,2,3,13,12
a,12,13,6,5
real,1
elsize,0.9375,,2
amesh,3,4,1
csys,12
real,2
a,3,9,14,13
a,13,14,10,6
elsize,1.125,,2
amesh,5,6,1
real,2
a,9,7,15,14
a,14,15,8,10
elsize,1.5,,2
amesh,7,8,1
eplot
eall
dsys
/angle
/pnum,elem,0
csys,0
wfront
wsort,y
/view,,1,1,1
asymbc,0,1,0,0.05
```

asymbc,0,3,0,0.05  
eplot

**Apply Nodal Forces**

```
nall
eall
nselect,y,hi
f,300,fx,foc*0.5
f,310,fx,foc*co1
f,311,fx,foc*co2
f,312,fx,foc*co3
f,313,fx,foc*co4
f,314,fx,foc*co5
f,315,fx,foc*co6
f,316,fx,foc*co7
f,317,fx,foc*co8
f,318,fx,foc*co9
f,319,fx,foc*co10
f,309,fx,foc*co11
f,409,fx,foc*co12
f,410,fx,foc*co13
f,411,fx,foc*co14
f,412,fx,foc*co15
f,413,fx,foc*co16
f,414,fx,foc*co17
f,415,fx,foc*co18
f,416,fx,foc*co19
f,417,fx,foc*co20
f,418,fx,foc*co21
f,408,fz,-foc*0.5
f,310,fz,-foc*sn1
f,311,fz,-foc*sn2
f,312,fz,-foc*sn3
f,313,fz,-foc*sn4
f,314,fz,-foc*sn5
f,315,fz,-foc*sn6
f,316,fz,-foc*sn7
f,317,fz,-foc*sn8
f,318,fz,-foc*sn9
f,319,fz,-foc*sn10
```

```

f,309,fz,-foc*sn11
f,409,fz,-foc*sn12
f,410,fz,-foc*sn13
f,411,fz,-foc*sn14
f,412,fz,-foc*sn15
f,413,fz,-foc*sn16
f,414,fz,-foc*sn17
f,415,fz,-foc*sn18
f,416,fz,-foc*sn19
f,417,fz,-foc*sn20
f,418,fz,-foc*sn21
nall
eall
arall
nsel,y,0
d,all,all
nlist,all
nall
eall
arall
/pcb,forc,1
/pcb,tdis,1
/type,,2
/view,,1,1,1
nplot
eplot
iter,1,1,1
afwrite,,1
finish
/check
/exec
/input,27
finish
/post1
store,stres,disp
set
nall
eall
set,1,1
finish
/eof

```

c\*\*selected nodes to be constrained

c\*\*plot nodal forces  
c\*\*plot boundary conditions

c\*\*end of the file

## A.4 Quadrilateral Shell Element Model due to Horizontal Shear Force

```
/prep7  
/title  
/show  
c***mesh module
```

### Define Constants

```
*set,thc,0.4          c**thickness of the nozzle  
*set,ths,0.4          c**thickness of the sphere  
*set,beta,0.4         c** $\beta$  value  
*set,gama,75          c** $\gamma_s$  value  
*set,rs,gama*ths      c**radius of the sphere  
*set,rc,rs*beta       c**radius of the nozzle  
*set,hoc,rs*0.5       c**height of the nozzle  
*set,radi,asin(beta)  c**half opening of the juncture  
                      with respect to the symmetry axis  
  
*set,quot,(180.0)/3.14159  
*set,mult,quot*radi  
*set,four,(90.0)-(mult+15)  
*set,thir,0  
*set,ang,rc/rs  
*set,func,asin(ang)  
*set,hi,rs*cos(func)  c** $y$  coordinate of the juncture  
*set,high,hi+hoc      c** $y$  coordinate of the top of the nozzle  
*set,low,hi+(hoc*0.3)  
*set,para,1  
*set,foc,para*17.858  c**nodal force
```

### Set Material Properties

```
et,1,63               c**define element type of the sphere  
nuxy,1,0.3           c** $\mu$  value of the sphere  
et,2,63               c**define element type of the nozzle
```

ex,1,30e6	c**elastic modulus of the sphere
ex,2,30e6	c**elastic modulus of the nozzle
nuxy,2,0.3	c** $\mu$ value of the nozzle
r,1,ths	
r,2,thc	

**Set Positions of Keypoints**

k,1	
k,2,1	c**define the global coordinate system
k,3,,1	
cskp,11,2,1,3,2	
cskp,12,1,1,3,2	
csys,11	
k,1,rs	
k,2,rs,,four	
k,3,rs,,50	
k,4,rs,90	
k,5,rs,90,four	
k,6,rs,90,50	
k,11,rs,45	
k,12,rs,45,four	
k,13,rs,45,50	
kmove,3,11,rs,,999,12,rc,999,999	
kmove,6,11,rs,90,999,12,rc,999,999	
kmove,13,11,rs,45,999,12,rc,999,999	
csys,12	
k,7,rc,,high	
k,8,rc,90,high	
k,9,rc,,low	
k,10,rc,90,low	
k,14,rc,45,low	
k,15,rc,45,high	
/view,,1,1,1	
kplot	

**Define Keyareas**

```

csys,11
a,1,2,12,11
a,11,12,5,4
a,2,3,13,12
a,12,13,6,5
csys,12
a,3,9,14,13
a,13,14,10,6
a,9,7,15,14
a,14,15,8,10
/mdiv,3
/pnum,area,1
/view,,1,1,1
aplot
lplot
aral
alist
klist
/pnum,line,-1
/view,,1,1,1
lplot

```

<b>Mesh Finite Element Model</b>
----------------------------------

```

csys,11
a,1,2,12,11
a,11,12,5,4
real,1
elsize,2.25,,2          c**define element size
amesh,1,2,1             c**element mesh
a,2,3,13,12
a,12,13,6,5
real,1
elsize,0.9375,,2
amesh,3,4,1
csys,12
real,2
a,3,9,14,13
a,13,14,10,6
elsize,1.125,,2
amesh,5,6,1

```

```

real,2
a,9,7,15,14
a,14,15,8,10
elsize,1.5,,2
amesh,7,8,1
eplot
eall
dsys
/angle
/pnum,elem,0
csys,0
wfront
wsort,y
/view,,1,1,1
symbc,0,1,0,0.05
asymbc,0,3,0,0.05
eplot

```

<h3>Apply Nodal Forces</h3>
-----------------------------

```

nall
eall
nselect,y,hi                                c**select nodes located at the juncture
f,300,fz,-foc*0.5,,408,108
f,309,fz,-foc,,319,1
f,409,fz,-foc,,418,1
nall
eall
arall
nselect,y,0                                c**select nodes located at the equator
d,all,all                                  c**selected nodes to be constrained
nlist,all
nall
eall
arall
/plot,forc,1                               c**plot nodal forces
/plot,tdis,1                               c**plot boundary conditions
/type,,2
/view,,1,1,1
nplot
eplot

```

```
iter,1,1,1
afwrite,,1
finish
/check
/exec
/input,27
finish
/post1
store,stres,disp
set
nall
eall
set,1,1
finish
/eof
```

c\*\*end of the file

## A.5 Isoparametric Solid Element Model due to Radial Force

```
/prep7
/title
/show
c*** mesh module
```

### Define Constants

```
*set,thc,0.4          c**thickness of the nozzle
*set,ths,0.4          c**thickness of the sphere
*set,beta,0.4         c** $\beta$  value
*set,gama,7           c** $\gamma$ , value
*set,mid,gama*ths     c**mean rdadius of the sphere
*set,irs,mid-(0.5*ths) c**inside radius of the sphere
*set,ors,mid+(0.5*ths) c**outside radius of the sphere
*set,midd,mid*beta    c**mean radius of the nozzle
*set,hoc,irs*0.5      c**height of the nozzle
*set,radi,asin(beta)  c**half opening of the juncture
                      with respect to the symmetry axis

*set,quot,(180.0)/3.14159
*set,mult,quot*radi
*set,four,(90.0)-(mult+15)
*set,firs,-89
*set,seco,-45
*set,thir,0
*set,irc,midd-(0.5*thc) c**inside radius of the nozzle
*set,ang,irc/irs
*set,func,asin(ang)
*set,high,irs*cos(func) c**y coordinate of the juncture
*set,five,(hoc*0.3)+high
*set,six,(hoc*0.6)+high
*set,seve,(hoc+high)   c**y coordinate of the top of the nozzle
*set,foc,6.944         c**nodal forces
c****set,mid,irs+(0.5*ths)
c****set,midd,irc+(0.5*thc)
*set,mido,mid+(0.25*ths) c**radius of the sphere between
                        c**mean radius and outside radius
*set,midi,mid-(0.25*ths) c**radius of the sphere between
                        c**mean radius and inside radius
*set,orc,midd+(0.5*thc) c**outside radius of the nozzle
```

<code>*set,mddo,midd+(0.25*thc)</code>	radius of the nozzle between c**mean radius and outside radius
<code>*set,mddi,midd-(0.25*thc)</code>	c**radius of the nozzle bedteen c**mean radius and inside radius
<code>*set,a,orc/ors</code>	
<code>*set,nul,asin(a)</code>	
<code>*set,b,irc/irs</code>	
<code>*set,nu2,asin(b)</code>	

**Set Material Properties**

<code>ex,1,30e6</code>	c**elastic moduls of the sphere
<code>nuxy,1,0.3</code>	c** $\mu$ value of the sphere
<code>et,2,45,,,,,2</code>	c**define element type of the nozzle
<code>ex,2,30e6</code>	c**elastic modulus of the nozzle
<code>nuxy,2,0.3</code>	c** $\mu$ value of the nozzle
<code>r,2,ths</code>	
<code>r,1,thc</code>	

**Set Positions of the Keypoints**

<code>k,1</code>	
<code>k,2,1</code>	c**define the global coordinate system
<code>k,3,,1</code>	
<code>cskp,11,2,1,3,2</code>	
<code>cskp,12,1,1,3,2</code>	
<code>csys,11</code>	
<code>k,1,ors,,firs</code>	
<code>k,2,irs,,firs</code>	
<code>k,3,ors,,seco</code>	
<code>k,4,irs,,seco</code>	
<code>k,5,ors</code>	
<code>k,6,irs</code>	
<code>k,7,ors,,four</code>	
<code>k,8,irs,,four</code>	
<code>k,9,ors,,50</code>	

k,10,irs,,50  
k,15,mid,,firs  
k,16,mid,,seco  
k,17,mid  
k,18,mid,,four  
k,19,mid,,50  
k,22,ors,90,firs  
k,23,irs,90,firs  
k,24,ors,90,seco  
k,25,irs,90,seco  
k,26,ors,90  
k,27,irs,90  
k,28,ors,90,four  
k,29,irs,90,four  
k,30,ors,90,50  
k,31,irs,90,50  
k,36,mid,90,firs  
k,37,mid,90,seco  
k,38,mid,90  
k,39,mid,90,four  
k,40,mid,90,50  
k,43,mido,,firs  
k,44,midi,,firs  
k,45,mido,,seco  
k,46,midi,,seco  
k,47,mido  
k,48,midi  
k,49,mido,,four  
k,50,midi,,four  
k,51,mido,,50  
k,52,midi,,50  
k,57,mido,90,firs  
k,58,midi,90,firs  
k,59,mido,90,seco  
k,60,midi,90,seco  
k,61,mido,90  
k,62,midi,90  
k,63,mido,90,four  
k,64,midi,90,four  
k,65,mido,90,50  
k,66,midi,90,50  
kmove,9,11,ors,,999,12,orc,999,999  
kmove,10,11,irs,,999,12,irc,999,999  
kmove,19,11,mid,,999,12,midd,999,999  
kmove,30,11,ors,90,999,12,orc,999,999

kmove,31,11,irs,90,999,12,irc,999,999  
kmove,40,11,mid,90,999,12,midd,999,999  
kmove,51,11,mido,,999,12,mddo,999,999  
kmove,52,11,midi,,999,12,mddi,999,999  
kmove,65,11,mido,90,999,12,mddo,999,999  
kmove,66,11,midi,90,999,12,mddi,999,999  
csys,12  
k,11,orc,,five  
k,12,irc,,five  
k,13,orc,,seve  
k,14,irc,,seve  
c\*\*\*k,15,orc,,seve  
c\*\*\*k,16,irc,,seve  
k,20,midd,,five  
k,21,midd,,seve  
k,32,orc,90,five  
k,33,irc,90.five  
k,34,orc,90,seve  
k,35,irc,90,seve  
k,41,midd,90,five  
k,42,midd,90,seve  
k,53,mddo,,five  
k,54,mddi,,five  
k,55,mddo,,seve  
k,56,mddi,,seve  
k,67,mddo,90,five  
k,68,mddi,90,five  
k,69,mddo,90,seve  
k,70,mddi,90,seve  
/view,,1,1,1  
kplot

<b>Define Keyareas</b>
------------------------

csys,11  
a,44,2,4,46  
a,15,44,46,16  
a,43,15,16,45  
a,1,43,45,3  
a,46,4,6,48  
a,16,46,48,17

a,45,16,17,47  
a,3,45,47,5  
a,48,6,8,50  
a,17,48,50,18  
a,47,17,18,49  
a,5,47,49,7  
a,50,8,10,52  
a,18,50,52,19  
a,49,18,19,51  
a,7,49,51,9  
a,58,23,25,60  
a,36,58,60,37  
a,57,36,37,59  
a,22,57,59,24  
a,60,25,27,62  
a,37,60,62,38  
a,59,37,38,61  
a,24,59,61,26  
a,62,27,29,64  
a,38,62,64,39  
a,61,38,39,63  
a,26,61,63,28  
a,64,29,31,66  
a,39,64,66,40  
a,63,39,40,65  
a,28,63,65,30  
r,1  
csys,12  
a,52,10,12,54  
a,19,52,54,20  
a,51,19,20,53  
a,9,51,53,11  
a,54,12,14,56  
a,20,54,56,21  
a,53,20,21,55  
a,11,53,55,13  
a,66,31,33,68  
a,40,66,68,41  
a,65,40,41,67  
a,30,65,67,32  
a,68,33,35,70  
a,41,68,70,42  
a,67,41,42,69  
a,32,67,69,34  
r,2

```

/mdiv,3
/pnum,area,1
/view,,1,1,1
aplot
lplot
aral
alist
klist
/pnum,line,-1
/view,,1,1,1

```

<b>Mesh Finite Element Model</b>
----------------------------------

```

lplot
et,1,45
csys,11
v,6,27,62,48,8,29,64,50          c**define keyvolume
v,48,62,38,17,50,64,39,18
v,17,38,61,47,18,39,63,49
v,47,61,26,5,49,63,28,7
elsize,0.525,,2                  c**element size
vmesh,1,4,1                       c**element mesh
v,8,29,64,50,10,31,66,52
v,50,64,39,18,52,66,40,19
v,18,39,63,49,19,40,65,51
v,49,63,28,7,51,65,30,9
elsize,0.175,,2
vmesh,5,8,1
csys,12
v,10,31,66,52,12,33,68,54
v,52,66,40,19,54,68,41,20
v,19,40,65,51,20,41,67,53
v,51,65,30,9,53,67,32,11
elsize,0.175,,2
vmesh,9,12,1
v,12,33,68,54,14,35,70,56
v,54,68,41,20,56,70,42,21
v,20,41,67,53,21,42,69,55
v,53,67,32,11,55,69,34,13
elsize,0.21,,2
vmesh,13,16,1

```

```

symbc,0,1,0,0.05
symbc,0,3,0,0.05
/view,,1,1,1
/type,,2
/view,,1,1,1
eplot

```

<b>Apply Nodal Forces</b>
---------------------------

```

csys,0
nall
eall
c***nselect,y,seve
c***f,all,fy,-foc
f,907,fy,-foc*0.5,,914,1
f,707,fy,-foc*0.5,,714,1
f,751,fy,-foc*0.5,,851,50
f,756,fy,-foc*0.5,,856,50
f,857,fy,-foc,,864,1
f,807,fy,-foc,,814,1
f,757,fy,-foc,,764,1
f,901,fy,-foc*0.25,,906,5
f,701,fy,-foc*0.25,,706,5
nall
eall
arall
c***nselect,y,0
nselect,node,241,250,1

d,all,all
nlist,all
nall
eall
arall
/plot,forc,1
/plot,tdis,1
/type,,2
/view,,1,1,1
nplot
eplot
iter,1,1,1

```

selected nodes located at the  
outer layer of the equator  
c\*\*selected nodes to be constrained

c\*\*plot nodal forces  
c\*\*plot boundary conditions

```
afwrite,,1
finish
/check
/exec
/input,27
finish
/post1
c***/output,40
store,stres,disp
set
/view,,1,1,1
pldisp,1
set,1,1
save
finish
/eof
```

c\*\*end of the file

## A.6 Isoparametric Solid Element Model due to Overturning Moment

```
/prep7
/title
/show
c*** mesh module
```

<b>Define Constants</b>
-------------------------

<pre>*set,thc,0.4 *set,ths,0.4 *set,beta,0.4 *set,gama,7 *set,mid,gama*ths *set,irs,mid-(0.5*ths) *set,ors,mid+(0.5*ths) *set,midd,mid*beta *set,hoc,irs*0.5 *set,radi,asin(beta)  *set,quot,(180.0)/3.14159 *set,mult,quot*radi *set,four,(90.0)-(mult+15) *set,firs,-89 *set,seco,-45 *set,thir,0 *set,irc,midd-(0.5*thc) *set,ang,irc/irs *set,func,asin(ang) *set,high,irs*cos(func) *set,five,(hoc*0.3)+high *set,six,(hoc*0.6)+high *set,seve,(hoc+high) *set,co1,0.9848 *set,co2,0.93969 *set,co3,0.866 *set,co4,0.766 *set,co5,0.6427 *set,co6,0.5 *set,co7,0.342</pre>	<pre>c**thickness of the nozzle c**thickness of the sphere c**<math>\beta</math> value c**<math>\gamma</math>, value c**mean radius of the sphere c**inside radius of the sphere c**outside radius of the sphere c**mean radius of the nozzle c**height of the nozzle c**half opening of the nozzle with respect to the symmetry axis  c**inside radius of the nozzle  c**y coordinate of the juncture  c**y coordinate of the top of the nozzle c**cos(10) value c**cos(20) value</pre>
---	--

*set,co8,0.1736	
*set,par,0.84112	
*set,tep1,ths/(2*midd)	
*set,tep2,ths/(4*midd)	
*set,fm,21.1576*par	c**nodal force applied at the mean radius of the nozzle, see Fig
*set,fi,(1-tep1)*fm	c**nodal force see Fig.
*set,fm,(1-tep2)*fm	c**nodal force see Fig.
*set,fmo,(1+tep2)*fm	c**nodal force see Fig.
*set,fo,(1+tep1)*fm	c**nodal force see Fig.
c****set,mid,irs+(0.5*ths)	
c****set,midd,irc+(0.5*thc)	
*set,mido,mid+(0.25*ths)	c**radius of the sphere between mean radius and outside radius
*set,midi,mid-(0.25*ths)	c**radius of the sphere between mean radius and inside radius
*set,orc,midd+(0.5*thc)	c**outside radius of the nozzle
*set,mddo,midd+(0.25*thc)	c**radius of the nozzle between mean radius and outside radius
*set,mddi,midd-(0.25*thc)	c**radius of radius between mean radius and inside radius
*set,a,orc/ors	
*set,nul,asin(a)	
*set,b,irc/irs	
*set,nu2,asin(b)	

<b>Set Material Properties</b>
--------------------------------

et,1,45,,,,,1	c**define element type of the sphere
ex,1,30e6	c**elastic modulus of the sphere
nuxy,1,0.3	c** $\mu$ value of the sphere
et,2,45,,,,,2	c**element type of the nozzle
ex,2,30e6	c**elastic modulus of the nozzle
nuxy,2,0.3	c** $\mu$ value of the nozzle

<b>Set positions of the Keypoints</b>
---------------------------------------

k,1  
k,2,1  
k,3,,1  
cskp,11,2,1,3,2  
cskp,12,1,1,3,2  
csys,11  
k,1,ors,,firs  
k,2,irs,,firs  
k,3,ors,,seco  
k,4,irs,,seco  
k,5,ors  
k,6,irs  
k,7,ors,,four  
k,8,irs,,four  
k,9,ors,,50  
k,10,irs,,50  
k,15,mid,,firs  
k,16,mid,,seco  
k,17,mid  
k,18,mid,,four  
k,19,mid,,50  
k,22,ors,90,firs  
k,23,irs,90,firs  
k,24,ors,90,seco  
k,25,irs,90,seco  
k,26,ors,90  
k,27,irs,90  
k,28,ors,90,four  
k,29,irs,90,four  
k,30,ors,90,50  
k,31,irs,90,50  
k,36,mid,90,firs  
k,37,mid,90,seco  
k,38,mid,90  
k,39,mid,90,four  
k,40,mid,90,50  
k,43,mido,,firs  
k,44,midi,,firs  
k,45,mido,,seco  
k,46,midi,,seco  
k,47,mido  
k,48,midi  
k,49,mido,,four  
k,50,midi,,four  
k,51,mido,,50

c\*\*define the global coordinate system

k,52,midi,,50  
k,57,mido,90,firs  
k,58,midi,90,firs  
k,59,mido,90,seco  
k,60,midi,90,seco  
k,61,mido,90  
k,62,midi,90  
k,63,mido,90,four  
k,64,midi,90,four  
k,65,mido,90,50  
k,66,midi,90,50  
kmove,9,11,ors,,999,12,orc,999,999  
kmove,10,11,irs,,999,12,irc,999,999  
kmove,19,11,mid,,999,12,midd,999,999  
kmove,30,11,ors,90,999,12,orc,999,999  
kmove,31,11,irs,90,999,12,irc,999,999  
kmove,40,11,mid,90,999,12,midd,999,999  
kmove,51,11,mido,,999,12,mddo,999,999  
kmove,52,11,midi,,999,12,mddi,999,999  
kmove,65,11,mido,90,999,12,mddo,999,999  
kmove,66,11,midi,90,999,12,mddi,999,999  
csys,12  
k,11,orc,,five  
k,12,irc,,five  
k,13,orc,,seve  
k,14,irc,,seve  
c\*\*\*k,15,orc,,seve  
c\*\*\*k,16,irc,,seve  
k,20,midd,,five  
k,21,midd,,seve  
k,32,orc,90,five  
k,33,irc,90,five  
k,34,orc,90,seve  
k,35,irc,90,seve  
k,41,midd,90,five  
k,42,midd,90,seve  
k,53,mddo,,five  
k,54,mddi,,five  
k,55,mddo,,seve  
k,56,mddi,,seve  
k,67,mddo,90,five  
k,68,mddi,90,five  
k,69,mddo,90,seve  
k,70,mddi,90,seve  
/view,,1,1,1

kplot

<b>Define Keyareas</b>
------------------------

csys,11  
a,44,2,4,46  
a,15,44,46,16  
a,43,15,16,45  
a,1,43,45,3  
a,46,4,6,48  
a,16,46,48,17  
a,45,16,17,47  
a,3,45,47,5  
a,48,6,8,50  
a,17,48,50,18  
a,47,17,18,49  
a,5,47,49,7  
a,50,8,10,52  
a,18,50,52,19  
a,49,18,19,51  
a,7,49,51,9  
a,58,23,25,60  
a,36,58,60,37  
a,57,36,37,59  
a,22,57,59,24  
a,60,25,27,62  
a,37,60,62,38  
a,59,37,38,61  
a,24,59,61,26  
a,62,27,29,64  
a,38,62,64,39  
a,61,38,39,63  
a,26,61,63,28  
a,64,29,31,66  
a,39,64,66,40  
a,63,39,40,65  
a,28,63,65,30  
r,1  
csys,12  
a,52,10,12,54  
a,19,52,54,20

```

a,51,19,20,53
a,9,51,53,11
a,54,12,14,56
a,20,54,56,21
a,53,20,21,55
a,11,53,55,13
a,66,31,33,68
a,40,66,68,41
a,65,40,41,67
a,30,65,67,32
a,68,33,35,70
a,41,68,70,42
a,67,41,42,69
a,32,67,69,34
r,2
/mdiv,3
/pnum,area,1
/view,,1,1,1
aplot
lplot
aral
/pnum,line,-1
/view,,1,1,1
lplot

```

<b>Mesh Finite Element Model</b>
----------------------------------

```

et,1,45
csys,11
v,6,27,62,48,8,29,64,50          c**define keyvolume
v,48,62,38,17,50,64,39,18
v,17,38,61,47,18,39,63,49
v,47,61,26,5,49,63,28,7
elsize,0.525,,2                  c**element size
vmesh,1,4,1                       c**element mesh
v,8,29,64,50,10,31,66,52
v,50,64,39,18,52,66,40,19
v,18,39,63,49,19,40,65,51
v,49,63,28,7,51,65,30,9
elsize,0.175,,2
vmesh,5,8,1

```

```

csys,12
v,10,31,66,52,12,33,68,54
v,52,66,40,19,54,68,41,20
v,19,40,65,51,20,41,67,53
v,51,65,30,9,53,67,32,11
elsize,0.175,,2
vmesh,9,12,1
v,12,33,68,54,14,35,70,56
v,54,68,41,20,56,70,42,21
v,20,41,67,53,21,42,69,55
v,53,67,32,11,55,69,34,13
elsize,0.21,,2
vmesh,13,16,1
symbc,0,1,0,0.05
asymbc,0,3,0,0.05
/view,,1,1,1
/type,,2
/view,,1,1,1
epplot

```

<b>Apply Nodal Forces</b>
---------------------------

```

csys,0
nall
eall
f,906,fy,fo*0.5
f,914,fy,fo*co1
f,913,fy,fo*co2
f,912,fy,fo*co3
f,911,fy,fo*co4
f,910,fy,fo*co5
f,909,fy,fo*co6
f,908,fy,fo*co7
f,907,fy,fo*co8
f,856,fy,fmo*0.5
f,864,fy,fmo*co1
f,863,fy,fmo*co2
f,862,fy,fmo*co3
f,861,fy,fmo*co4
f,860,fy,fmo*co5
f,859,fy,fmo*co6

```

```

f,858,fy,fmo*co7
f,857,fy,fmo*co8
f,806,fy,fm*0.5
f,814,fy,fm*co1
f,813,fy,fm*co2
f,812,fy,fm*co3
f,811,fy,fm*co4
f,810,fy,fm*co5
f,809,fy,fm*co6
f,808,fy,fm*co7
f,807,fy,fm*co8
f,756,fy,fm*0.5
f,764,fy,fm*co1
f,763,fy,fm*co2
f,762,fy,fm*co3
f,761,fy,fm*co4
f,760,fy,fm*co5
f,759,fy,fm*co6
f,758,fy,fm*co7
f,757,fy,fm*co8
f,706,fy,fi*0.5
f,714,fy,fi*co1
f,713,fy,fi*co2
f,712,fy,fi*co3
f,711,fy,fi*co4
f,710,fy,fi*co5
f,709,fy,fi*co6
f,708,fy,fi*co7
f,707,fy,fi*co8
nall
eall
arall
nsel,node,281,290,1

d,all,all
nall
eall
arall
/plot,forc,1
/plot,tdis,1
/type,2
/view,1,1,1
nplot
eplot
iter,1,1,1

```

```

c**selected nodes at the
    outer layer of the equator
c**selected nodes to be constrained

c**plot nodal forces
c**plot boundary conditions

```

```
afwrite,,1
finish
/check
/exec
/input,27
finish
/post1
store,stres,disp
set
csys,0
set,1,1
save
finish
/eof
```

c\*\*end of the file

## A.7 Isoparametric Solid Element Model due to Torsional Moment

```
/prep7
/title
/show
c*** mesh module
```

Define Constants
------------------

```
*set,thc,0.4          c**thickness of the sphere
*set,ths,0.4          c**thickness of the nozzle
*set,beta,0.4         c** $\beta$  value
*set,gama,7           c** $\gamma_s$  value
*set,mid,gama*ths     c**mean radius of the sphere
*set,irs,mid-(0.5*ths) c**inside radius of the sphere
*set,ors,mid+(0.5*ths) c**outside radius of the sphere
*set,midd,mid*beta    c**mean radius of the nozzle
*set,hoc,irs*0.5      c**height of the nozzle
*set,radi,asin(beta)  c**half opening of the juncture
                      with respect to the symmetry axis

*set,quot,(180.0)/3.14159
*set,mult,quot*radi
*set,four,(90.0)-(mult+15)
*set,firs,-89
*set,seco,-45
*set,thir,0
*set,irc,midd-(0.5*thc) c**inside radius of the nozzle
*set,ang,irc/irs
*set,func,asin(ang)
*set,high,irs*cos(func)
*set,five,(hoc*0.3)+high
*set,six,(hoc*0.6)+high
*set,seve,(hoc+high)  c**y coordinate of the top of the nozzle
*set,co1,0.9848        c**cos(10) value
*set,co2,0.93969       c**cos(20) value
*set,co3,0.866
*set,co4,0.766
*set,co5,0.6427
*set,co6,0.5
*set,co7,0.342
```

*set,co8,0.1736	
*set,sn1,0.1736	c**sin(10) value
*set,sn2,0.342	c**sin(20) value
*set,sn3,0.5	
*set,sn4,0.64278	
*set,sn5,0.766	
*set,sn6,0.866	
*set,sn7,0.9397	
*set,sn8,0.9848	
*set,f,59.526	
*set,par,0.84112	
*set,tep1,ths/(2*midd)	
*set,tep2,ths/(4*midd)	
*set,fm,21.1576*par	
*set,fi,(1-tep1)*fm	
*set,fim,(1-tep2)*fm	
*set,fmo,(1+tep2)*fm	
*set,fo,(1+tep1)*fm	
c****set,mid,irs+(0.5*ths)	
c****set,midd,irc+(0.5*thc)	
*set,mido,mid+(0.25*ths)	c**radius of the sphere between mean radius and outside radius
*set,midi,mid-(0.25*ths)	c**radius of the sphere between mean radius and inside radius
*set,orc,midd+(0.5*thc)	c**outside radius of the nozzle
*set,mddo,midd+(0.25*thc)	c**radius of the nozzle between mean radius and outside radius
*set,mddi,midd-(0.25*thc)	c**radius of the nozzle between mean radius and inside radius
*set,a,orc/ors	
*set,nul,asin(a)	
*set,b,irc/irs	
*set,nu2,asin(b)	
et,1,45,,,,,1	c**define element type of the sphere
ex,1,30e6	c**elastic modulus of the sphere
nuxy,1,0.3	c** $\mu$ value of the sphere
et,2,45,,,,,2	c**define element type of the nozzle
ex,2,30e6	c**elastic modulus of the nozzle
nuxy,2,0.3	c** $\mu$ value of the nozzle

<b>Set Positions of Keypoints</b>
-----------------------------------

k,1  
k,2,1  
k,3,,,1  
cskp,11,2,1,3,2  
cskp,12,1,1,3,2  
csys,11  
k,1,ors,,firs  
k,2,irs,,firs  
k,3,ors,,seco  
k,4,irs,,seco  
k,5,ors  
k,6,irs  
k,7,ors,,four  
k,8,irs,,four  
k,9,ors,,50  
k,10,irs,,50  
k,15,mid,,firs  
k,16,mid,,seco  
k,17,mid  
k,18,mid,,four  
k,19,mid,,50  
k,22,ors,90,firs  
k,23,irs,90,firs  
k,24,ors,90,seco  
k,25,irs,90,seco  
k,26,ors,90  
k,27,irs,90  
k,28,ors,90,four  
k,29,irs,90,four  
k,30,ors,90,50  
k,31,irs,90,50  
k,36,mid,90,firs  
k,37,mid,90,seco  
k,38,mid,90  
k,39,mid,90,four  
k,40,mid,90,50  
k,43,mido,,firs  
k,44,midi,,firs  
k,45,mido,,seco  
k,46,midi,,seco  
k,47,mido  
k,48,midi  
k,49,mido,,four  
k,50,midi,,four  
k,51,mido,,50

c\*\*define the global coordinate system

k,52,midi,,50  
k,57,mido,90,firs  
k,58,midi,90,firs  
k,59,mido,90,seco  
k,60,midi,90,seco  
k,61,mido,90  
k,62,midi,90  
k,63,mido,90,four  
k,64,midi,90,four  
k,65,mido,90,50  
k,66,midi,90,50  
kmove,9,11,ors,,999,12,orc,999,999  
kmove,10,11,irs,,999,12,irc,999,999  
kmove,19,11,mid,,999,12,midd,999,999  
kmove,30,11,ors,90,999,12,orc,999,999  
kmove,31,11,irs,90,999,12,irc,999,999  
kmove,40,11,mid,90,999,12,midd,999,999  
kmove,51,11,mido,,999,12,mddo,999,999  
kmove,52,11,midi,,999,12,mddi,999,999  
kmove,65,11,mido,90,999,12,mddo,999,999  
kmove,66,11,midi,90,999,12,mddi,999,999  
csys,12  
k,11,orc,,five  
k,12,irc,,five  
k,13,orc,,seve  
k,14,irc,,seve  
c\*\*\*k,15,orc,,seve  
c\*\*\*k,16,irc,,seve  
k,20,midd,,five  
k,21,midd,,seve  
k,32,orc,90,five  
k,33,irc,90,five  
k,34,orc,90,seve  
k,35,irc,90,seve  
k,41,midd,90,five  
k,42,midd,90,seve  
k,53,mddo,,five  
k,54,mddi,,five  
k,55,mddo,,seve  
k,56,mddi,,seve  
k,67,mddo,90,five  
k,68,mddi,90,five  
k,69,mddo,90,seve  
k,70,mddi,90,seve  
/view,,1,1,1

kplot

<b>Define Keyareas</b>
------------------------

csys,11  
a,44,2,4,46  
a,15,44,46,16  
a,43,15,16,45  
a,1,43,45,3  
a,46,4,6,48  
a,16,46,48,17  
a,45,16,17,47  
a,3,45,47,5  
a,48,6,8,50  
a,17,48,50,18  
a,47,17,18,49  
a,5,47,49,7  
a,50,8,10,52  
a,18,50,52,19  
a,49,18,19,51  
a,7,49,51,9  
a,58,23,25,60  
a,36,58,60,37  
a,57,36,37,59  
a,22,57,59,24  
a,60,25,27,62  
a,37,60,62,38  
a,59,37,38,61  
a,24,59,61,26  
a,62,27,29,64  
a,38,62,64,39  
a,61,38,39,63  
a,26,61,63,28  
a,64,29,31,66  
a,39,64,66,40  
a,63,39,40,65  
a,28,63,65,30  
r,1  
csys,12  
a,52,10,12,54  
a,19,52,54,20

```

a,51,19,20,53
a,9,51,53,11
a,54,12,14,56
a,20,54,56,21
a,53,20,21,55
a,11,53,55,13
a,66,31,33,68
a,40,66,68,41
a,65,40,41,67
a,30,65,67,32
a,68,33,35,70
a,41,68,70,42
a,67,41,42,69
a,32,67,69,34
r,2
/mdiv,3
/pnum,area,1
/view,,1,1,1
aplot
lplot
aral
/pnum,line,-1
/view,,1,1,1
lplot

```

<b>Mesh Finite Element Model</b>
----------------------------------

```

et,1,45
csys,11
v,6,27,62,48,8,29,64,50          c**define keyvolume
v,48,62,38,17,50,64,39,18
v,17,38,61,47,18,39,63,49
v,47,61,26,5,49,63,28,7
elsize,0.525,,2                  c**element size
vmesh,1,4,1                       c**element mesh
v,8,29,64,50,10,31,66,52
v,50,64,39,18,52,66,40,19
v,18,39,63,49,19,40,65,51
v,49,63,28,7,51,65,30,9
elsize,0.175,,2
vmesh,5,8,1

```

```

csys,12
v,10,31,66,52,12,33,68,54
v,52,66,40,19,54,68,41,20
v,19,40,65,51,20,41,67,53
v,51,65,30,9,53,67,32,11
elsize,0.175,,2
vmesh,9,12,1
v,12,33,68,54,14,35,70,56
v,54,68,41,20,56,70,42,21
v,20,41,67,53,21,42,69,55
v,53,67,32,11,55,69,34,13
elsize,0.21,,2
vmesh,13,16,1
symbc,0,1,0,0.05
asymbc,0,3,0,0.05
/view,,1,1,1
/type,,2
/view,,1,1,1
eplot

```

c\*\*element plot

<b>Apply Nodal Forces</b>
---------------------------

```

csys,0
nall
eall
f,501,fz,-f*0.5
f,507,fz,-f*co1
f,507,fx,f*sn1
f,508,fz,-f*co2
f,508,fx,f*sn2
f,509,fz,-f*co3
f,509,fx,f*sn3
f,510,fz,-f*co4
f,510,fx,f*sn4
f,511,fz,-f*co5
f,511,fx,f*sn5
f,512,fz,-f*co6
f,512,fx,f*sn6
f,513,fz,-f*co7
f,513,fx,f*sn7
f,514,fz,-f*co8

```

```

f,514,fx,f*sn8
f,506,fx,f*0.5
nall
eall
arall
nset,node,281,290,1
c**select nodes located at
    the outside layer of the equator
c**selected nodes to be constrained

d,all,all
nall
eall
arall
c**plot nodal forces
c**plot boundary conditions
/pbc,forc,1
/pbc,tdis,1
/type,,2
/view,,1,1,1
nplot
eplot
iter,1,1,1
afwrite,,1
finish
/check
/exec
/input,27
finish
/post1
store,stres,disp
set
csys,0
type,,2
/view,,1,1,1
set,1,1
save
finish
/eof
c**end of the file

```

## A.8 Isoparametric solid Element Model due to Horizontal Shear Force

```
/prep7
/title
/show
c*** mesh module
```

<b>Define Constants</b>
-------------------------

<pre>*set,ths,0.4 *set,thc,0.4 *set,beta,0.4 *set,gama,7 *set,mid,gama*ths *set,irs,mid-(0.5*ths) *set,ors,mid+(0.5*ths) *set,midd,mid*beta *set,hoc,irs*0.5 *set,radi,asin(beta)  *set,quot,(180.0)/3.14159 *set,mult,quot*radi *set,four,(90.0)-(mult+15) *set,firs,-89 *set,seco,-45 *set,thir,0 *set,irc,midd-(0.5*thc) *set,ang,irc/irs *set,func,asin(ang) *set,high,irs*cos(func) *set,five,(hoc*0.3)+high *set,six,(hoc*0.6)+high *set,seve,(hoc+high) *set,col,0.9848 *set,co2,0.93969 *set,co3,0.866 *set,co4,0.766 *set,co5,0.6427 *set,co6,0.5 *set,co7,0.342</pre>	<pre>c**thickness of the sphere c**thickness of the nozzle c**<math>\beta</math> value c**<math>\gamma</math>, value c**mean radius of the sphere c**inside radius of the sphere c**outside radius of the sphere c**mean radius of the nozzle c**height of the nozzle c**half opening of the juncture     with respect to the symmetry axis  c**inside radius of the nozzle  c**y coordinate of the juncture  c**y coordinate of the top of the nozzle c**cos(10) value c**cos(10) value</pre>
---	--

```

*set,co8,0.1736
*set,par,0.84112
*set,tep1,ths/(2*midd)
*set,tep2,ths/(4*midd)
*set,fm,21.1576*par
*set,fi,(1-tep1)*fm
*set,fi,(1-tep2)*fm
*set,fmo,(1+tep2)*fm
*set,fo,(1+tep1)*fm
c****set,mid,irs+(0.5*ths)
c****set,midd,irc+(0.5*thc)
*set,mido,mid+(0.25*ths)
*set,midi,mid-(0.25*ths)
*set,orc,midd+(0.5*thc)
*set,mddo,midd+(0.25*thc)
*set,mddi,midd-(0.25*thc)
*set,a,orc/ors
*set,nu1,asin(a)
*set,b,irc/irs
*set,nu2,asin(b)

```

c\*\*radius of the sphere between  
mean radius and outside radius  
c\*\*radius of the sphere between  
mean radius and inside radius  
c\*\*outside radius of the nozzle  
c\*\*radius of the nozzle between  
mean radius and outside radius  
c\*\*radius of the nozzle between  
c\*\*mean radius and inside radius

### Set Material Properties

```

et,1,45,,,,,1
ex,1,30e6
nuxy,1,0.3
et,2,45,,,,,2
ex,2,30e6
nuxy,2,0.3

```

c\*\*define element type of the sphere  
c\*\*elastic modulus of the sphere  
c\*\* $\mu$  value of the sphere  
c\*\*define element type of the nozzle  
c\*\*elastic modulus of the nozzle  
c\*\* $\mu$  value of the nozzle

### Define Keypoints

k,1  
 k,2,1  
 k,3,,1  
 cskp,11,2,1,3,2  
 cskp,12,1,1,3,2  
 csys,11  
 k,1,ors,,firs  
 k,2,irs,,firs  
 k,3,ors,,seco  
 k,4,irs,,seco  
 k,5,ors  
 k,6,irs  
 k,7,ors,,four  
 k,8,irs,,four  
 k,9,ors,,50  
 k,10,irs,,50  
 k,15,mid,,firs  
 k,16,mid,,seco  
 k,17,mid  
 k,18,mid,,four  
 k,19,mid,,50  
 k,22,ors,90,firs  
 k,23,irs,90,firs  
 k,24,ors,90,seco  
 k,25,irs,90,seco  
 k,26,ors,90  
 k,27,irs,90  
 k,28,ors,90,four  
 k,29,irs,90,four  
 k,30,ors,90,50  
 k,31,irs,90,50  
 k,36,mid,90,firs  
 k,37,mid,90,seco  
 k,38,mid,90  
 k,39,mid,90,four  
 k,40,mid,90,50  
 k,43,mido,,firs  
 k,44,midi,,firs  
 k,45,mido,,seco  
 k,46,midi,,seco  
 k,47,mido  
 k,48,midi  
 k,49,mido,,four  
 k,50,midi,,four  
 k,51,mido,,50

c\*\*define the global coordinate system

k,52,midi,,50  
k,57,mido,90,firs  
k,58,midi,90,firs  
k,59,mido,90,seco  
k,60,midi,90,seco  
k,61,mido,90  
k,62,midi,90  
k,63,mido,90,four  
k,64,midi,90,four  
k,65,mido,90,50  
k,66,midi,90,50  
kmove,9,11,ors,,999,12,orc,999,999  
kmove,10,11,irs,,999,12,irc,999,999  
kmove,19,11,mid,,999,12,midd,999,999  
kmove,30,11,ors,90,999,12,orc,999,999  
kmove,31,11,irs,90,999,12,irc,999,999  
kmove,40,11,mid,90,999,12,midd,999,999  
kmove,51,11,mido,,999,12,mddo,999,999  
kmove,52,11,midi,,999,12,mddi,999,999  
kmove,65,11,mido,90,999,12,mddo,999,999  
kmove,66,11,midi,90,999,12,mddi,999,999  
csys,12  
k,11,orc,,five  
k,12,irc,,five  
k,13,orc,,seve  
k,14,irc,,seve  
c\*\*\*k,15,orc,,seve  
c\*\*\*k,16,irc,,seve  
k,20,midd,,five  
k,21,midd,,seve  
k,32,orc,90,five  
k,33,irc,90,five  
k,34,orc,90,seve  
k,35,irc,90,seve  
k,41,midd,90,five  
k,42,midd,90,seve  
k,53,mddo,,five  
k,54,mddi,,five  
k,55,mddo,,seve  
k,56,mddi,,seve  
k,67,mddo,90,five  
k,68,mddi,90,five  
k,69,mddo,90,seve  
k,70,mddi,90,seve  
/view,,1,1,1

kplot

<b>Define Keyareas</b>
------------------------

csys,11  
a,44,2,4,46  
a,15,44,46,16  
a,43,15,16,45  
a,1,43,45,3  
a,46,4,6,48  
a,16,46,48,17  
a,45,16,17,47  
a,3,45,47,5  
a,48,6,8,50  
a,17,48,50,18  
a,47,17,18,49  
a,5,47,49,7  
a,50,8,10,52  
a,18,50,52,19  
a,49,18,19,51  
a,7,49,51,9  
a,58,23,25,60  
a,36,58,60,37  
a,57,36,37,59  
a,22,57,59,24  
a,60,25,27,62  
a,37,60,62,38  
a,59,37,38,61  
a,24,59,61,26  
a,62,27,29,64  
a,38,62,64,39  
a,61,38,39,63  
a,26,61,63,28  
a,64,29,31,66  
a,39,64,66,40  
a,63,39,40,65  
a,28,63,65,30  
r,1  
csys,12  
a,52,10,12,54  
a,19,52,54,20

```

a,51,19,20,53
a,9,51,53,11
a,54,12,14,56
a,20,54,56,21
a,53,20,21,55
a,11,53,55,13
a,66,31,33,68
a,40,66,68,41
a,65,40,41,67
a,30,65,67,32
a,68,33,35,70
a,41,68,70,42
a,67,41,42,69
a,32,67,69,34
r,2
/ndiv,3
/pnum,area,1
/view,,1,1,1
aplot
lplot
aral
/pnum.line,-1
/view,,1,1,1
lplot

```

<b>Mesh Finite Element Model</b>
----------------------------------

```

et,1,45
csys,11
v,6,27,62,48,8,29,64,50          c**define keyvolume
v,48,62,38,17,50,64,39,18
v,17,38,61,47,18,39,63,49
v,47,61,26,5,49,63,28,7
elsize,0.525,,2                  c**element size
vmesh,1,4,1                       c**element mesh
v,8,29,64,50,10,31,66,52
v,50,64,39,18,52,66,40,19
v,18,39,63,49,19,40,65,51
v,49,63,28,7,51,65,30,9
elsize,0.175,,2
vmesh,5,8,1

```

```

csys,12
v,10,31,66,52,12,33,68,54
v,52,66,40,19,54,68,41,20
v,19,40,65,51,20,41,67,53
v,51,65,30,9,53,67,32,11
elsize,0.175,,2
vmesh,9,12,1
v,12,33,68,54,14,35,70,56
v,54,68,41,20,56,70,42,21
v,20,41,67,53,21,42,69,55
v,53,67,32,11,55,69,34,13
elsize,0.21,,2
vmesh,13,16,1
symbc,0,1,0,0.05
asymbc,0,3,0,0.05
/view,,1,1,1
/type,,2
/view,,1,1,1
eplot

```

<b>Apply Nodal Forces</b>
---------------------------

<pre> csys,0 nall eall f,501,fz,-f*0.5,,506,5 f,507,fz,-f,,514,1 nall eall arall nsel,node,281,290,1  d,all,all nall eall arall /pcb,forc,1 /pcb,tdis,1 /type,,2 /view,,1,1,1 nplot </pre>	<pre> c**select nodes located at the     outside layer of the equator c**selected nodes to be constrained  c**plot nodal forces c**plot boundary conditions </pre>
--	--

```
eplot
iter,1,1,1
afwrite,,1
finish
/check
/exec
/input,27
finish
/post1
store,stres,disp
set
csys,0
set,1,1
finish
/eof
```

```
c**end of the file
```

## Appendix B: Kelvin Functions and their Derivatives

The real and imaginary parts of  $J_\nu(xe^{3\pi i/4})$  are denoted by  $Ber_\nu x$  and  $Bei_\nu x$  and are given as follows:

$$Ber_\nu x = \left(\frac{x}{2}\right)^\nu \sum_{k=0}^{\infty} \frac{\cos\left[\left(\frac{3\nu}{4} + \frac{k}{2}\right)\pi\right]}{k!\Gamma(\nu + k + 1)} \left(\frac{x^2}{4}\right)^k$$

$$Bei_\nu x = \left(\frac{x}{2}\right)^\nu \sum_{k=0}^{\infty} \frac{\sin\left[\left(\frac{3\nu}{4} + \frac{k}{2}\right)\pi\right]}{k!\Gamma(\nu + k + 1)} \left(\frac{x^2}{4}\right)^k$$

where

$$\Gamma(\nu + k + 1) = (k + 1)!$$

The functions  $Berx$  and  $Beix$  (i.e. functions of zero order) are given as follows:

$$Berx = 1 - \frac{(x^2/4)^2}{(2!)^2} + \frac{(x^2/4)^4}{(4!)^2} - \dots$$

$$Beix = \frac{x^2}{4} - \frac{(x^2/4)^3}{(3!)^2} + \frac{(x^2/4)^5}{(5!)^2} - \dots$$

The real and imaginary parts of  $e^{-n\pi i/2} K_n(xe^{\pi i/4})$  are denoted by  $ker_n x$  and  $kei_n x$  and are given as follows:

$$\begin{aligned} ker_n x &= \frac{1}{2} \left(\frac{x}{2}\right)^{-n} \sum_{k=0}^{n-1} \cos\left[\left(\frac{3n}{4} + \frac{k}{2}\right)\pi\right] \frac{(n-k-1)!}{k!} \left(\frac{x^2}{4}\right)^k - \ln\left(\frac{x}{2}\right) Ber_n x + \frac{\pi}{4} Bei_n x \\ &\quad + \frac{1}{2} \left(\frac{x}{2}\right)^n \sum_{k=0}^{\infty} \cos\left[\left(\frac{3n}{4} + \frac{k}{2}\right)\pi\right] \frac{(\Psi(k+1) + \Psi(n+k+1))}{k!(n+k)!} \left(\frac{x^2}{4}\right)^k \end{aligned}$$

$$kei_n x = -\frac{1}{2} \left(\frac{x}{2}\right)^{-n} \sum_{k=0}^{n-1} \sin\left[\left(\frac{3n}{4} + \frac{k}{2}\right)\pi\right] \frac{(n-k-1)!}{k!} \left(\frac{x^2}{4}\right)^k - \ln\left(\frac{x}{2}\right) Bei_n x - \frac{\pi}{4} Ber_n x$$

$$+ \frac{1}{2} \left(\frac{x}{2}\right)^n \sum_{k=0}^{\infty} \sin\left[\left(\frac{3n}{4} + \frac{k}{2}\right)\pi\right] \frac{\Phi(k+1) + \Phi(n+k+1)}{k!(n+k)!} \left(\frac{x^2}{4}\right)^k$$

where  $\Phi(n)$  is given as follows:

For  $n = 1$ :

$$\Phi(1) = -\gamma$$

For  $n \geq 2$ :

$$\Phi(n) = -\gamma + \sum_{k=1}^{n-1} (k^{-1})$$

where  $\gamma = 0.5772156649 = \text{Euler's Constant}$

The functions  $kerx$  and  $keix$  (i.e. functions of zero order) are given as follows:

$$kerx = -\ln\left(\frac{x}{2}\right)Berx + \frac{\pi}{4}Beix + \sum_{k=0}^{\infty} (-1)^k \frac{\Psi(2k+1)}{((2k)!)^2} \left(\frac{x^2}{4}\right)^{2k}$$

$$keix = -\ln\left(\frac{x}{2}\right)Berx - \frac{\pi}{4}Beix + \sum_{k=0}^{\infty} (-1)^k \frac{\Psi(2k+2)}{((2k+1)!)^2} \left(\frac{x^2}{4}\right)^{2k+1}$$

The functions  $kerx$  and  $keix$  (i.e. Kelvin functions of first order) can be obtained by substituting  $n = 1$  in expressions for  $ker_n x$  and  $kei_n x$ . The derivatives of Kelvin functions ( $ker'x$  and  $kei'x$ ) are obtained as follows

$$ker'x = \frac{ker_1 x + kei_1 x}{\sqrt{2}}$$

$$kei'x = \frac{-ker_1 x + kei_1 x}{\sqrt{2}}$$

## Appendix C Superposition of all Loads

Fig. No.	Read curves for	Calculate absolute values of stress and enter result	STRESS: if load is opposite that shown, reverse signs shown							
			$A_U$	$A_L$	$B_U$	$B_L$	$C_U$	$C_L$	$D_U$	$D_L$
6.3	$K_{c,m}T^2$	$(K_{c,m}T^2)P/T^2$	-	-	-	-	-	-	-	-
6.1	$K_{c,b}T^2$	$(K_{c,b}T^2)P/T^2$	-	+	-	+	-	+	-	+
6.7	$K_{c,m}T^3$	$(K_{c,m}T^3)M_X/T^3$					-	-	+	+
6.5	$K_{c,b}T^3$	$(K_{c,b}T^3)M_X/T^3$					-	+	+	-
6.7	$K_{c,m}T^3$	$(K_{c,m}T^3)M_Z/T^3$	-	-	+	+				
6.5	$K_{c,b}T^3$	$(K_{c,b}T^3)M_Z/T^3$	-	+	+	-				
6.12	$K_{c,m}T^2$	$(K_{c,m}T^2)V_X/T^2$	+	+	-	-				
6.10	$K_{c,b}T^2$	$(K_{c,b}T^2)V_X/T^2$	-	+	-	+	-	+	-	+
6.12	$K_{c,m}T^2$	$(K_{c,m}T^2)V_Z/T^2$					-	-	+	+
6.10	$K_{c,b}T^2$	$(K_{c,b}T^2)V_Z/T^2$					-	+	+	-
Algebraical summation of $\sigma_c =$										
6.4	$K_{m,m}T^2$	$(K_{m,m}T^2)P/T^2$	-	-	-	-	-	-	-	-
6.2	$K_{m,b}T^2$	$(K_{m,b}T^2)P/T^2$	-	+	-	+	-	+	-	+
6.8	$K_{m,m}T^3$	$(K_{m,m}T^3)M_X/T^3$					-	-	+	+
6.6	$K_{m,b}T^3$	$(K_{m,b}T^3)M_X/T^3$					-	+	+	-
6.8	$K_{m,m}T^3$	$(K_{m,m}T^3)M_Z/T^3$	-	-	+	+				
6.6	$K_{m,b}T^3$	$(K_{m,b}T^3)M_Z/T^3$	-	+	+	-				
6.13	$K_{m,m}T^2$	$(K_{m,m}T^2)V_X/T^2$	-	-	+	+				
6.11	$K_{m,b}T^2$	$(K_{m,b}T^2)V_X/T^2$	-	+	-	+	-	+	-	+
6.13	$K_{m,m}T^2$	$(K_{m,m}T^2)V_Z/T^2$					+	+	-	-
6.11	$K_{m,b}T^2$	$(K_{m,b}T^2)V_Z/T^2$					-	+	+	-
Algebraical summation of $\sigma_m =$										

Fig. No.	Read curves for	Calculate absolute values of stress and enter result	STRESS: if load is opposite that shown, reverse signs shown							
			$A_U$	$A_L$	$B_U$	$B_L$	$C_U$	$C_L$	$D_U$	$D_L$
6.14	$K_{vs}T^2$	$(K_sT^2)V_X/T^2$					-	-	+	+
6.14	$K_{vs}T^2$	$(K_{vs}T^2)V_Z/T^2$	+	+	-	-				
6.9	$K_{ts}T^2$	$(K_{ts}T^2)M_T/T^2$	+	+	+	+	+	+	+	+
Algebraical summation of $\tau =$										
Combined stress intensity $S.I. =$										
When $\sigma_c$ and $\sigma_m$ have like signs: $S.I. = [\sigma_c + \sigma_m + \sqrt{(\sigma_c - \sigma_m)^2 + 4\tau^2}]/2$										
When $\tau = 0$ : $S.I. = \text{largest of } \sigma_c, \sigma_m \text{ or }  \sigma_c - \sigma_m $										
When $\sigma_c$ and $\sigma_m$ have unlike signs: $S.I. = \sqrt{(\sigma_c - \sigma_m)^2 + 4\tau^2}$										

# Bibliography

- [1] "ANSYS user's manual I", Swanson Analysis Systems, Inc., Rev. 4.3, 1987.
- [2] "ANSYS user's manual II", Swanson Analysis System, Inc., Rev. 4.3, 1987.
- [3] Novozhilov, V. V., "Thin Shell Theory", P. Noordhoff, Ltd., Groningen, The Netherlands, p 2, 1964.
- [4] Rose, R. T., "New Design Method for Pressure Vessel Nozzles", The Engineer, 214, 5556, July 20, 1962 and Welding Res. Abroad, IX, pp 43-47, Feb. 1963.
- [5] Taylor, C. E., Lind, N. C., and Schweiker, J. W., "A Three Dimensional Photoelastic Study of Stresses Around Reinforced Outlets in Pressure Vessel", Welding Research Council Bulletin No. 51, June 1959.
- [6] "Uniform Notation System for Pressure Vessel Shell Theory", Mech. Eng., 77(6) pp 505-507, 1955, and The Welding Journal, 34(8), Research Suppl., pp 393s-395s, 1955.
- [7] Bijlaard, P. P., "Local Stresses in Spherical Shells from Radial or Moment Loadings", The Welding Journal, 36(5), pp 240s-243s, Research Suppl., pp 608s-617s, 1955.
- [8] Bijlaard, P. P., "Computation of the stresses from Local Loads in Spherical Pressure Vessels or Pressure Vessel Heads", Welding Research Council Bulletin No. 34, pp 1-8, March 1957.

- [9] Bijlaard, P. P., "Stresses in Spherical Vessel from Radial Loads Acting on a Pipe", Welding Research Council Bulletin Series No. 49, pp 1-9 April, 1959.
- [10] Bijlaard, P. P., "Stresses in Spherical Vessel from External Moments Acting on a Pipe", Welding Research Council Bulletin Series No. 49, pp 31-62, April, 1959.
- [11] Bijlaard, P. P., "stresses in spherical vessels from local loads transferred by a pipe, Additional Data on Stresses in Cylindrical Shells under Local Loading", Welding Research Council Bulletin No. 50, pp 1-9, May, 1959.
- [12] Leckie, F. A. and Penny, R. K., "a Critical Study of the Solutions for the Asymmetric Bending of Spherical Shells", Welding Research Council Bulletin No. 90, September, 1963.
- [13] Penny, R. K. and Leckie, F. A., "Solutions for the Stresses at Nozzles in Pressure Vessels", Welding Research Council Bulletin No. 90, September, 1963.
- [14] Batra, B. and Sun, B. C., "On radial Spring Constants at the juncture of a radial nozzle and a spherical shell", pp. 490-504, Fifth International Conference, on Pressure Vessel Technology, San Francisco, Ca., Sept., 1984.
- [15] Batra, B. and Sun, B. C., "On Rotational Spring Constants at the juncture of a radial nozzle and a spherical shell", ASME Pressure Vessel Conference New Orleans, La., June, 1985.
- [16] Prakash, P. and Rao, K. P., "Stresses in a Spherical Shell with a Circular Elastic Inclusion", Transaction of the ASME, pp 228-233, August, 1974.
- [17] Waters, E. O., "Stresses Near a Cylindrical Outlet in Spherical Vessel", Welding Research Council No. 96, pp 1-9, May, 1964.

- [18] Dally, J. W., "an Experimental Investigation of the Stresses Produced in Spherical Vessels by External Loads Transferred by a Nozzle", pp 1-29, Ibid., No. 84, Jan., 1963.
- [19] Riley, W. F., "Experimental determination of stress distributions in thin-walled cylindrical and spherical pressure vessel with circular nozzle", IITRI Final Report, Project No. M6053, March, 15, 1965. (published in Welding Research Council Bulletin No. 108, September, 1965)
- [20] Witt, F. J., Gwaltney, R. C., Maxwell, R. L., and Holland, R. W., "A Comparison of Theoretical and Experimental Results from Spherical Shells with a Single Radially Attached Nozzle", Journal of Engineering for Power, Transactions of the ASME, pp 333-340 July, 1967
- [21] Calladine, C.R., "On the Design of Reinforcement for Openings and Nozzles in Thin Spherical Pressure Vessels", Journal of Mechanical Engineering Science, Vol. 8, No. 1, pp 1-14, 1966.
- [22] Bailey, R. and Hicks, R., "Localized Loads Applied to a Spherical Pressure Vessel Through a Cylindrical Insert", Journal of Mechanical Engineering Science, Vol. 2, No. 4, p 302, 1960.
- [23] Chao, T. L., "Stresses in Spherical Shells due to Local Loading over a Rectangular Area", ASME Journal of Pressure Vessel Technology, Vol 107, No. 2, 1985.
- [24] Brooks, G. N., "Loaded Rectangular Attachments to Spherical Shells", in Proceedings of the 1987 ASME Pressure Vessel and Piping Conference, San Diego, California, PVP-Vol. 124, pp.27-31, 1987.

- [25] Brooks, G. N., "Spring Constants for Rectangular Attachment to Spherical Shells", in Proceedings of 1990 ASME Pressure Vessel and Piping Conference, Nashville, Tennessee, PVP-Vol. 194, pp.9-13, 1990.
- [26] Reissner, E., "Stresses and Small Displacements of Shallow Spherical Shells", International Journal of Mathematical Physics, 25, pp. 80-85, 1946.
- [27] Timoshenko S., and S. Woinowsky-krieger, "Theory of plates and shells", 2nd edition, *M<sub>c</sub>*Graw-Hill Book Co., Inc., 1970.
- [28] Wichman, K. R., Hopper, A. G., Mershon, J. L., "Local Stresses in Spherical and Cylindrical Shells due to External Loadings", Welding Research Council Bulletin 107, pp 975-985, 1968.
- [29] Chiou, S. C., and Sun, B. C., 1987, "On Torsional Spring Constant at the Juncture of Piping-Nozzle", Vol. 120, ASME, Pressure Vessel and Piping Design Conference, San Diego, California, pp.83-86.